

# Micromilling of hardened tool steels

## Proefschrift

ter verkrijging van de graad van doctor  
aan de Technische Universiteit Delft,  
op gezag van de Rector Magnificus prof. dr. ir. J.T. Fokkema,  
voorzitter van het College voor Promoties,  
in het openbaar te verdedigen

op donderdag 22 oktober 2009 om 10.00 uur

door

Peiyuan LI

werktuigkundig ingenieur  
geboren te Jilin, China

Dit proefschrift is goedgekeurd door de promotor:  
Prof. ir. R.H. Munnig Schmidt

Copromotor: dr. ir. H.H. Langen

Samenstelling promotiecommissie:

Rector Magnificus,	voorzitter
Prof. ir. R.H. Munnig Schmidt,	Technische Universiteit Delft, promotor
Dr. ir. H.H. Langen,	Technische Universiteit Delft, copromotor
Prof. dr. U. Staufer,	Technische Universiteit Delft
Prof. dr. -ing. habil. B. Karpuschewski,	Otto-von-Guericke-Universität Magdeburg, Duitsland
Prof. dr. D.M. Allen,	Cranfield University, Verenigd Koninkrijk
Prof. dr. K. Cheng,	Brunel University, Verenigd Koninkrijk
Ir. J.A.J. Oosterling,	TNO Industrie & Techniek
Prof. dr. ir. A. van Keulen,	Technische Universiteit Delft, reservelid

Dr. ir. A.M. Hoogstrate heeft als begeleider in belangrijke mate aan de totstandkoming van het proefschrift bijgedragen.



The research presented in this thesis was financially supported by the Innovation Research Programme (IOP) of the Dutch government in the field of Precision Engineering (project number IPT 04010A).

ISBN: 978-90-9024640-6

Printed in the Netherlands  
Copyright © 2009 by Peiyuan Li  
All rights reserved.

# Acknowledgement

If I have to use one word to describe my PhD experience, it will be dynamic. When I look back the four-year journey, it is full of changes. This can be proved by some simple facts: I have studied/worked in 2 departments, 3 different sections; there are altogether 4 project leaders (daily supervisors) involved successively; I used 4 different machine tools at 3 different locations; I had to adapt my working plan frequently according to the practical situation. I am very glad that this project is finished on time in the end. However, I deeply realize that without the help of others it would be impossible for me to achieve all these.

First of all, I would like to show my gratitude to my promoter prof. R.H. Munnig Schmidt for his interest, guidance, enjoyable discussions and full support all the time. I want to thank my copromoter dr. Hans Langen for his devoted supervision and valuable remarks. Special thanks to Han Oosterling (TNO), from whom I always got encouragement and support. I also want to thank two previous project leaders for their contributions to this project: dr. Andre Hoogstrate, and dr. Marcel Achtsnick.

I would like to thank all the members of the examination committee for their serious review of my thesis and precious comments for improvement: prof. Stauffer, prof. Karpuschewski, prof. Allen, and prof. Cheng. Special thanks to prof. Allen for offering me the opportunity to do a visiting research at Cranfield University, from which I have learned a lot.

This research project was sponsored by the Innovation Research Program (IOP) of the Dutch government. I want to thank all the members of the user committee for their cooperation and contributions: Lex Westland, Eddy Schipper, Edwin Fierkens, Guido Gubbels, Harmen Altena, Viktoria Bana, Jaco Saurwalt, Jos van den Biggelaar, Jos Weterings, Pierre van den Hurk, Stefan van Weert, Frits van der Pol, and Etienne Catoire. Special thanks to van Hoorn Carbide Company for their close cooperation during this research.

I would like to thanks people from Mondragon University in Spain for accepting me to do some experiments there: Patxi Aristimuño, Pedro Jose

Arrazola, Javier Aperribay, Endika Gandarias, Eneritz and Javi. I also want to thank people from Cranfield University in UK: Daniel Zdebski, John Hedge, Tan Jin, and all the PhDs in the Precision Engineering Office for their hospitality, which made my stay as a visiting researcher so pleasant. Special thanks to Daniel for the assistance during experiments and interesting talks about work and life.

I want to thank all the colleagues in the PME department at TU Delft for their cooperation and help in the last four years, especially colleagues from former PMA, MSD, MNE, the Microfactory research group, and MicroNed. Special thanks to Harry Jansen for his technical support on the experimental setup, Jos van Driel for his assistant in teaching activities, and Vincent Henneken, Rogier Blom, and Frans Leenders for their help with the translation of some thesis materials. I would like to thank dr. Guiming Song from the Department of Materials Science and Engineering for his comments on the content of my thesis. I like to thank all the students who contributed on this project.

I also want to thank all the colleagues in the group of machining processes at TNO Industrie & Techniek for their kindness to me. Special thanks to Douwe Jan IJlst for his support in conducting experiments.

Furthermore, I would like to thank all my friends for their companion and support which made my life here enjoyable.

Finally I want to thank my parents and sister. They give me everything I need and never ask for anything back. I cannot say thank you enough!

Peiyuan Li

Delft, July 2009

# Summary

Miniaturized parts are increasingly demanded in different fields like medical, transportation, environmental, and communication industries. In order to manufacture these parts in an economical way, mass replication methods, such as micro injection molding, have to be applied. Currently, Electro Discharge Machining (EDM) process is mainly used to manufacture the needed moulds for micro injection molding in industries. In order to achieve the final shape, several electrodes have to be made by milling with different levels of geometrical accuracy. Besides, the material removal rate of EDM is relatively low. This results in a long throughput-time and high manufacturing cost. Therefore, industries are looking for alternative technologies to overcome these drawbacks; micromilling is one of the promising technologies.

The advantages of the micromilling technology include the applicability of a broad range of materials including hardened tool steels, the capability of manufacturing three dimensional geometries, accurate machining of complex features, and it is economical for small and medium lot sizes, etc. However, although micromilling in principle is a good alternative for the EDM process, it is found in research that some challenges have to be overcome before this technology is ready to be adopted in industrial applications.

The literature survey shows that the fundamental micro cutting mechanism has been well investigated and understood through the study of micro orthogonal cutting and ultraprecision machining. Issues related to the application of micromilling have however not yet been well studied. Besides, inconsistent observations are commonly seen in literature. This is because observed results in micromilling are highly dependent on the experimental conditions.

Based on the literature survey and initial micromilling tests, the general goal of this research has been defined as to develop and describe a reliable micromilling process for precision machining of hardened tool steels. It was decided to first improve lives of micro endmills to achieve a reliable cutting, and then to improve the performance of the process through process planning. In this research, experiments were mainly done with  $\varnothing 0.5$  mm square endmills

on hardened tool steels (AISI H11, H13, etc.).

Experimental investigations were done to identify the main problems in micromilling. It was observed that the used commercial micro tools suffered severe wear, the tool life was too short to conduct a successful task, and the workpiece quality was not achieving the requirements. Investigations were conducted to understand tool wear types and mechanism. The factors which influence the tool performance were analyzed. It was found that the geometry of commercial tools is mainly derived from macro endmills, with which the cutting edge corners have the highest stress level. The machining parameters and tool paths are two factors that have significant effect on the tool performance; however, there was no good method available for the planning of the micromilling process.

The geometry of micro endmills was studied theoretically by means of analytical modeling and FEA method. Having understood the relationship between geometrical features of the cutting tool and their influence on the tool performance (stiffness and strength of the cutting edge corners), the geometry of the micro endmill can be designed specifically for a given application to achieve the desired performance. This method was demonstrated by designing the micro square endmill especially for hard milling applications. The newly designed tools were manufactured and validated through experiments in comparison with the commercial tools. The experimental results have shown that the new designs have improved the tool performance as expected.

The planning of the micromilling process has been divided into two parts. In the first part, design of experiments has been used to understand the relationship between input variables (machining parameters and tool paths) and process response (tool wear and surface finish). With this method, the significant variables can be identified by means of ANOVA analysis, and the cutting conditions can be planned accordingly to optimize the process output. For example, to have a long tool life is important for the roughing operation, and to achieve a good surface finish is of interest for the finishing operation.

In the second part of the process planning, a knowledge-based method is used to plan cutting conditions for the machining of micro features with high aspect ratios. The selection of machining parameters was done by means of a force model, which describes the relation between machining parameters and average forces. The tool paths were tested by a FEM model. An improved tool path was proposed to overcome the disadvantage of the conventional tool path. Experiments were done with conditions chosen by the theoretical analysis, and the results proved the validity of the developed method. Micro ribs with aspect ratios higher than 50 could be machined successfully.

# Samenvatting

Er is een groeiende vraag naar geminiaturiseerde onderdelen in verschillende gebieden van industrie, zoals gezondheidszorg, transport, milieu en communicatie. Teneinde deze onderdelen op een kostenefficiënte wijze te produceren, is het noodzakelijk deze via massareplicatietechnieken zoals micro-spuitsieten te produceren. Momenteel wordt voornamelijk het proces van vonkverspaning ('Electro Discharge Machining - EDM') gebruikt om de matrijzen te fabriceren die nodig zijn voor het micro-spuitsieten. Om de uiteindelijke vorm te verkrijgen moeten verscheidene elektrodes gefreesd worden met verschillende eisen ten aanzien van geometrische nauwkeurigheid. Dit resulteert in een lange doorlooptijd en hoge fabricagekosten. Om die reden is men op zoek naar alternatieve technologieën om deze nadelen te omzeilen. Microfreen is één van de veelbelovende technologieën.

Micro-freestecnologie heeft een aantal voordelen. Het is toepasbaar op een breed scala van materialen, waaronder gehard gereedschapsstaal, het is mogelijk driedimensionale geometrieën te produceren, complexe details kunnen nauwkeurig bewerkt worden, en het proces is kostenefficiënt voor kleine en middelgrote oplagen. Hoewel, ondanks dat micro-freen in principe een goed alternatief voor het EDM proces is, blijkt uit onderzoek dat er nog enige uitdagingen te nemen zijn alvorens deze techniek klaar is om in een industriële omgeving te worden toegepast.

De literatuurstudie laat zien dat het fundamentele micro-verspaningsmechanisme grondig onderzocht en begrepen is door studie van orthogonale verspaning op micro-schaal en ultraprecisie bewerking. Daarentegen, zaken gerelateerd aan de toepassing van micro-freen zijn nog niet volledig onderzocht. Daarnaast treft men in de literatuur geregeld tegenstrijdige observaties aan. Dit hangt samen met de sterke afhankelijkheid van de resultaten met de experimentele condities.

Gebaseerd op literatuurstudie en initiële micro-freestesten is de algemene doelstelling van dit onderzoek geformuleerd als het ontwikkelen en beschrijven van een betrouwbaar micro-freesproces voor precisiebewerking van gehard gereedschapsstaal. Er is besloten om eerst de levensduur van de micro-

eindfrezes te verbeteren om een betrouwbaar verspaningsproces te bereiken, om vervolgens de prestaties van het proces te verbeteren door procesplanning. In dit onderzoek zijn voornamelijk freesexperimenten gedaan met  $\varnothing$  0.5 mm rechthoekige micro-eindfrezes in gehard gereedschapsstaal (AISI H11, H13, enz.).

Experimenteel onderzoek is verricht om de belangrijkste problemen bij het micro-frezes van gehard gereedschapsstaal te identificeren. Er is vastgesteld dat de commercieel beschikbare micro-eindfrezes onderhevig zijn aan ernstige slijtage, dat de levensduur van de gereedschappen te kort was om een micro-frees taak succesvol af te ronden en dat de werkstukqualiteit niet binnen de specificaties was. Er is onderzoek gedaan naar de aard en het mechanisme van gereedschapslijtage. De factoren die de prestaties van het gereedschap beïnvloeden zijn eveneens geanalyseerd. Dit toonde aan dat de geometrie van commercieel beschikbare gereedschappen voornamelijk zijn afgeleid van macro-eindfrezes, waarbij de hoeken van de snijkanten de hoogste spanningen ondervinden. Daarnaast hebben de bewerkingsparameters en het bewerkingspad een significant effect op de prestaties van microfrezes, en is er geen goede methode beschikbaar voor de planning van het micro-freesproces.

Om die reden is ervoor gekozen de prestaties van het micro-freesproces op twee aspecten te verbeteren: geometrie van het gereedschap en procesplanning.

De geometrische kenmerken van micro-eindfrezes zijn bestudeerd met behulp van een cantilever balk model en een eindige elementen model van de frees om de invloed van deze kenmerken te bestuderen op de prestaties van het gereedschap (stijfheid en sterkte van de hoeken van de snijkanten). Met inzicht in deze relatie kan de geometrie naar gelang de toepassing worden aangepast om de gewenste prestaties te verkrijgen. Deze aanpak is gedemonstreerd door geminiaturiseerde rechthoekige eindfrezes te ontwerpen speciaal voor de toepassing hardfrezes. De nieuw ontworpen gereedschappen zijn gefabriceerd en gevalideerd door experimenten, waarbij resultaten zijn vergeleken met die verkregen met commercieel beschikbare gereedschappen.

De planning van het micro-freesproces is in twee delen opgedeeld. In het eerste deel is experimentontwerp gebruikt om de relatie te achterhalen tussen ingangsvARIABLEN (bewerkingsparameters en bewerkingspaden), en de procesrespons (gereedschapslijtage en oppervlaktekwaliteit). Met deze methode kunnen de significante variabelen geïdentificeerd worden door middel van ANOVA analyse, en de snijcondities kunnen navenant ingesteld worden om de procesoutput te optimaliseren. Bijvoorbeeld, voor de voorbereidingsstap is het van belang een lange levensduur van het gereedschap te hebben, voor de nabewerkingsstap is het belangrijk een goede oppervlaktekwaliteit te verkrijgen.

In het tweede deel van de procesplanning is een kennisgestuurd model gebruikt om de snijcondities te bepalen voor het bewerken van micrometerdetails met hoge aspect ratio's. De selectie van bewerkingsparameters is gedaan door middel van een krachtenmodel dat de relatie beschrijft tussen de bewerkingsparameters en de gemiddelde krachten. De bewerkingspaden zijn getest met een eindige elementen model. Experimenten zijn uitgevoerd met condities gekozen op basis van de theoretische analyse. De resultaten toonden de validiteit van de ontwikkelde methode aan. Micro-ribben met aspect ratio's hoger dan 50 zijn succesvol bewerkt.



# Contents

<b>Acknowledgement</b>	<b>iii</b>
<b>Summary</b>	<b>v</b>
<b>Samenvatting</b>	<b>vii</b>
<b>Contents</b>	<b>xi</b>
<b>Nomenclature</b>	<b>xv</b>
<b>Chapter 1 Introduction</b>	<b>1</b>
1.1 Increasing demand on miniaturized components	1
1.2 Micromilling and its components	2
1.3 Cutting mechanism	4
1.3.1 Cutting edge radius effect	5
1.3.2 Workpiece microstructure effect	7
1.3.3 Transformation of the knowledge into micromilling	8
1.4 Application of micromilling	9
1.4.1 Performance of micro endmills	9
1.4.2 Surface quality	11
1.4.3 Burr formation	13
1.4.4 Bending of micro endmills	14
1.5 Discussion	14
<b>Chapter 2 Research goal and approach</b>	<b>17</b>
2.1 Case study: micromilling of a micro part for a micro gripper	17
2.2 Goal of the research	18
2.3 Working approach	19
2.4 Structure of the thesis	21
<b>Chapter 3 Experimental and measurement equipment</b>	<b>23</b>
3.1 Micro endmills	23
3.2 Machine tools	27
3.3 Workpiece materials	29

3.4	Measurement equipment	31
<b>Chapter 4</b>	<b>Performance evaluation of micro endmills</b>	<b>33</b>
4.1	Motivation, objective, and approach	33
4.2	Tool wear types and mechanism	35
4.2.1	Wear of micro square endmills	35
4.2.2	Comparison with macro end milling	39
4.3	Workpiece quality	40
4.3.1	Form accuracy	41
4.3.2	Burr formation	42
4.3.3	Roughness	43
4.4	Analysis	45
4.4.1	Commercial tool geometry	45
4.4.2	Cutting conditions	47
4.4.3	Workpiece properties	48
4.4.4	Runout	49
4.4.5	Chatter effect	54
4.5	Discussion	56
<b>Chapter 5</b>	<b>Influence of cutting conditions on tool wear and surface quality</b>	<b>59</b>
5.1	Motivation and objectives	59
5.2	Approach	60
5.3	Study of tool paths and $a_e$	61
5.3.1	Design of experiments and experimental conditions	61
5.3.2	Results in terms of tool wear	64
5.3.3	Results in terms of surface finish	68
5.4	Study of $v_c$ , $a_{pr}$ , and $f_z$	71
5.4.1	Design of experiments and experimental conditions	72
5.4.2	Results in terms of tool wear	74
5.4.3	Results in terms of surface finish	78
5.5	Discussion	79
<b>Chapter 6</b>	<b>Design of micro endmills</b>	<b>81</b>
6.1	Motivation and approach	81
6.2	Design guidelines	84
6.3	Design of micro square endmills	85
6.3.1	Design of the neck part	85
6.3.2	Design of the cutting part	89
6.3.3	Other aspects	93
6.3.4	The complete new tool design	94
6.4	Manufacturing of the newly designed tools	96
6.5	Experimental validation	97
6.5.1	Tool stiffness	97

---

6.5.2	Tool wear and tool life	98
6.5.3	Workpiece quality	101
6.5.4	Force data	102
6.6	Summary	103
<b>Chapter 7</b>	<b>Machining of micro ribs with high aspect ratios</b>	<b>105</b>
7.1	Motivation, objective, and approach	105
7.2	Selection of the example geometry	106
7.3	Selection of machining parameters	107
7.3.1	Study of micromilling forces	108
7.3.2	Strategy for force modeling	113
7.3.3	The average force model	114
7.3.4	Analysis with the force model	117
7.4	Selection of tool paths	120
7.4.1	Conventional tool path and improved tool path	120
7.4.2	FEM model of the rib	121
7.4.3	Results and analysis	121
7.5	Behavior of the thin ribs	122
7.6	Machining of micro ribs	124
7.7	Results and analysis	125
7.7.1	General observations	126
7.7.2	Tool paths	129
7.7.3	Cutting conditions	130
7.8	Discussion	132
<b>Chapter 8</b>	<b>Conclusions and recommendations</b>	<b>135</b>
8.1	Background, project goal and approach	135
8.2	Conclusions	136
8.3	Recommendations	138
<b>Bibliography</b>		<b>141</b>
<b>Appendix A</b>	<b>Measurement of the dynamic cutting radius of a micro endmill</b>	<b>151</b>
<b>Appendix B</b>	<b>Method to set up the workpiece coordinate in Z direction</b>	<b>153</b>
<b>Appendix C</b>	<b>Selection of spindle speed to minimize the motion error</b>	<b>155</b>
<b>Appendix D</b>	<b>Checking of the tool wear data</b>	<b>157</b>
<b>Curriculum vitae</b>		<b>159</b>



# Nomenclature

$a_e$	Width of cut	mm
$a_p$	Depth of cut	mm
$d$	Diameter	mm
$dF$	Elemental force	N
$dz$	Elemental depth of cut	mm
$E$	Young's Modulus	GPa
$E(y)$	Expected response of the model	
$F$	Force	N
$\bar{F}$	Average force	N
$F_t$	Force in the tangential direction	N
$F_r$	Force in the radial direction	N
$F_c$	Cutting force	N
$F_e$	Edge force	N
$F_x, F_y, F_z$	Forces in the Cartesian coordinate system	N
$f_z$	Feed per tooth	mm
$h$	Instantaneous chip thickness	mm
$h(\theta)$	Chip thickness at immersion angle $\theta$	mm
$I$	Moment of inertia	mm <sup>4</sup>
$K_{tc}$	Cutting force coefficient in tangential direction	N/mm <sup>2</sup>
$K_{rc}$	Cutting force coefficient in radial direction	N/mm <sup>2</sup>
$K_{te}$	Edge force coefficient in tangential direction	N/mm
$K_{re}$	Edge force coefficient in radial direction	N/mm
$l$	Length	mm
$l_s$	Length of the shank part of the endmill	mm
$l_n$	Length of the neck part of the endmill	mm
$l_c$	Length of the cutting part of the endmill	mm
$M$	Bending moment	N·mm
$N$	Number of flutes	
$r$	Radius	mm
$r_c$	Cross section radius of the cutting part of the endmill	mm
$r_{eff}$	Effective tool cutting radius	mm

$r_n$	Cross section radius of the neck part of the endmill	mm
$r_s$	Cross section radius of the shank part of the endmill	mm
$\Delta r$	Difference between radii	
$Ra$	Arithmetic average roughness	$\mu\text{m}$
$Rz$	Mean roughness depth	$\mu\text{m}$
$Sa$	Surface amplitude parameter, arithmetic mean deviation	$\mu\text{m}$
$v_c$	Cutting speed	m/min
$v_f$	Feed rate	mm/min
$x_i$	Coded design variable	
$\hat{y}$	Estimated yield of the mathematical model	
$a$	Tool radial rake angle	$^\circ$
$\beta$	Tool helix angle	$^\circ$
$\beta_{ij}$	Coefficients of the mathematical models	
$\gamma$	Tool radial relief angle	$^\circ$
$\delta$	Runout magnitude	mm
$\delta$	Tool deflection magnitude	mm
$\theta$	Tool neck angle	$^\circ$
$\theta$	Tool immersion angle	$^\circ$
$\lambda$	Runout angle	$^\circ$
$\rho$	Density	$\text{g}/\text{mm}^3$
$\sigma$	Stress	GPa
$\sigma$	Standard deviation	

**Abbreviations**

3D	Three-dimensional
AISI	American Iron and Steel Institute
ANOVA	Analysis of Variance
AR	Aspect Ratio
BNC	Bayonet Neill-Concelman connector
BUE	Build Up Edge
CAD	Computer Aided Design
CAM	Computer Aided Manufacturing
CBN	Cubic Boron Nitride
CCD	Central Composite Design
DIN	Deutsches Institut für Normung
DOE	Design of Experiments
ECM	Electro Chemical Machining
EDM	Electro Discharge Machining
EDS	Energy Dispersive Spectroscopy
FEM	Finite Element Method
FFT	Fast Fourier Transform
FIB	Focused Ion Beam
HRC	Rockwell Hardness C-Scale
HSM	High Speed Milling
HSC	High Speed Cutting
MCT	Minimum Chip Thickness
MEMS	Microelectromechanical Systems
MR	Material Removal
MRR	Material Removal Rate
MST	Microsystems Technology
MQL	Minimum Quantity Lubrication
NC	Numerical Control
PMMA	Polymethyl Methacrylate
PSD	Power Spectral Density
SEM	Scanning Electron Microscope
TiAlN	Titanium Aluminum Nitride
TRS	Transverse Rupture Strength
VSI	Vertical Scanning Interferometry
WLI	White Light Interferometer



# Chapter 1 Introduction

In this chapter, a brief introduction to the micromilling technology and the state of the art development in research are given. In Section 1.1, the miniaturization trend of products and requirements on micromachining technologies are described. In Section 1.2, the micromilling technology and its main components are introduced. In Section 1.3 and Section 1.4, the state of the art research in micromilling are presented in the aspects of fundamental cutting mechanism and issues related to the application of this technology, respectively. This Chapter ends with a discussion in Section 1.5.

## 1.1 Increasing demand on miniaturized components

Miniaturized parts/features, in the dimension of a few millimeters to a few micrometers, are increasingly demanded in the fields such as medical, transportation, environmental, and communication industries. According to a market analysis released by NEXUS [1], the total market for Microelectromechanical Systems/Microsystems (MEMS/MST) products will grow to \$ 57 billion in 2009 in comparison with \$ 33 billion in 2004. Besides the amount of products, there are also new requirements on the quality of micro components, such as high accuracy, three-dimensional (3D) geometries, and a broader material pallet including metals.

The current prevalent micromachining technologies, such as wet etching, optical lithography, are primarily developed for MEMS products, targeting on silicon or silicon-like materials [2]. Besides, these processes are mainly applicable for simple planar geometries, and not cost effective for small and medium lot sizes. Therefore, there is a need to develop new micromachining technologies that can overcome these significant drawbacks; attempts have been made to scale down conventional mechanical machining processes, such as milling, turning, and grinding, to make use of their capability of machining 3D features on a broad range of materials [2-6].

In this project, the micromilling technology will be investigated in detail.

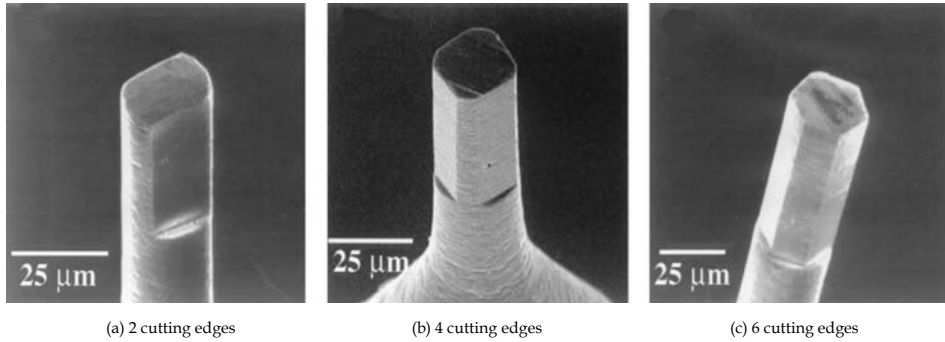


**Fig. 1.1:** Micro endmills made by FIB [7].

## 1.2 Micromilling and its components

Milling is a traditional chip removing operation, it is widely applied in industries, and has been investigated since the 19<sup>th</sup> century [8].

Micromilling is not a new type of machining technology; it is simply the scaling down of the macro milling process, which means the machining is done by endmills with relatively small cutting diameters. In this research, micromilling is defined as the milling operation conducted with endmills smaller than 1 mm in cutting diameter.

Therefore, the basic kinematic movements in micromilling are the same as those in macro milling. In milling, material removal is achieved by the interaction between a cutting tool and a workpiece. There exist two main movements: the rotation of a cutter and the translative feed motion of the cutter through the workpiece [9].

Three main hardware components of micromilling are cutting tools (micro endmills), machine tools, and workpiece materials.

- Micro endmills: Commercial micro endmills have similar cutting geometries to macro endmills; both square and ball nose endmills are seen in the market. Tool substrate material for commercial tools is mainly ultra-fine grain (grain size  $< 0.5 \mu\text{m}$ ) tungsten carbide with cobalt as binder. The commonly used coating is TiAlN. CBN tools and carbide tools with diamond coating are also available recently [10, 11]; however, since they are not widely used, they will not be investigated in this research.

Micro endmills are mainly manufactured by the grinding process. Therefore, the quality of micro cutting tools depends on the properties of the grinding

wheel, such as the wheel size, cutting edge radius, and wear. With the continuous development of the tool manufacturing process  $\varnothing$  0.025 mm endmills can be ground and are commercially available now [12]. However, application of commercial cutting tools in such a scale is rarely seen in literature, and not commonly applied in industrial applications yet. Most micromilling research was done by endmills in the range of 0.3 mm ~ 1 mm (e.g. [13-15]).

In research, Focused Ion Beam (FIB) was used to produce tools smaller than  $\varnothing$  0.025 mm with unconventional geometries. An example of tools made by the FIB is shown in Fig. 1.1. These tools were mainly used in research, and are not commercially available.

- Machine tools: At the early stage of the micromilling research, micromilling experiments were mainly done on conventional (high speed) milling machines (e.g. [7, 11, 16-20]). With the increasing understanding of the process, researchers realized that micromilling has special requirements on machine tools, such as stiffness, damping, thermal deformation, spindle speed, and acceleration [21, 22]. Therefore, commercial machines specially designed for micromilling applications (e.g. [23, 24]) and self-developed micromilling experimental setups (e.g. [13, 25-31]) are more and more seen in literature.
- Workpiece materials: Very broad range of materials can be machined by the micromilling process, such as aluminum and its alloys (e.g. [7, 16, 17, 32-34]), copper and its alloys (e.g. [7, 18, 19, 30, 33, 35]), steels (e.g. [7, 23, 36-40]), polymers (e.g. [41]), ceramics (e.g. [7, 17, 41]), and graphite (e.g. [16, 17, 20]).

In recent years, research on micromilling of hardened tool steels is getting more and more attention; this is because micromilling has the potential to replace Electro Discharge Machining (EDM) process in dies and moulds manufacturing to save through-put time and production cost.

As described in Section 1.1, as there is an increasing demand on the micro components, in order to make the parts cost-effectively, mass replication methods have to be applied. Micro injection molding is one of methods that can be used [42].

Currently, EDM is mainly used to manufacture the needed moulds for micro injection molding [43]. In order to achieve the final shape, several electrodes have to be made by milling with different levels of geometrical accuracy. The material removal rate (MRR) of EDM is rather low (about 0.6~6 mm<sup>3</sup>/h for  $\varnothing$  0.1 mm electrodes [44]). These result in a long throughput-time and high manufacturing cost. Therefore, industries are looking for alternative technologies to overcome these drawbacks, and micromilling is one of the promising technologies.

**Table 1.1:** Comparison between micromilling and micro EDM [44, 45].

	Micromilling (carbide tools)	Micro sink-EDM
Workpiece materials	Metals, ceramics, graphite	Metals, ceramics
Lateral structure ( $\mu\text{m}$ )	10 - 1000	20 - 40
Aspect ratio	2 - 15	10 - 25
Geometrical freedom	++	+
Surface quality $Ra$ ( $\mu\text{m}$ )	0.3	0.2 - 0.4
MRR ( $\text{mm}^3/\text{h}$ )	30	6

By applying micromilling in mould manufacturing, steels already heat-treated can be machined directly by micro endmills to achieve 3D geometries with high material removal rate and dimensional accuracy. The MRR of micromilling is about  $30 \text{ mm}^3/\text{h}$  when using a  $\varnothing 0.1 \text{ mm}$  tool, which is much higher than that of micro sink EDM. In Table 1.1 a comparison between micromilling and micro EDM is given.

Although micromilling is in principle the scaling down of the macro scale milling process, the application of knowledge in conventional milling in micromilling is not straight forward. It has been found in research that micromilling is fundamentally different from macro scale milling in some aspects, which influences the cutting process significantly. In the following sections, the state of the art of research in micromilling is summarized.

### 1.3 Cutting mechanism

Before introducing results published in literature, it has to be pointed out that due to the complexity of the endmill geometry the fundamental understanding of the cutting mechanism in micromilling was mainly derived from orthogonal cutting operations, including micro turning (e.g. [46-51]), and (macro) ultraprecision machining (e.g. diamond turning [52-56]). The knowledge of the latter could be used because normally small chips are cut in order to achieve good surface finish [57], which is similar to the case of micro cutting.

Micro cutting is significantly influenced by the size effect. With the scaling down of cutting geometry, the applicable machining parameters in micro cutting (e.g. feed per tooth,  $f_z$ ) are comparable in magnitude to the cutting edge radius of micro cutting tools and the grain size of workpiece materials, which in turn affects chip formation, tool performance, surface formation, etc.

The size effect is illustrated in Fig. 1.2, which shows the interaction between the cutting tool and the workpiece in orthogonal cutting, both in micro scale and macro scale.

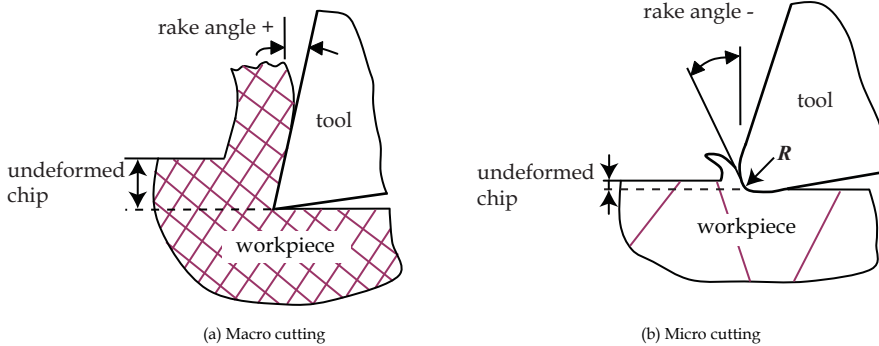


**Fig. 1.2:** Illustration of tool-workpiece interaction in macro scale and micro scale cutting.

### 1.3.1 Cutting edge radius effect

In macro scale milling, see Fig. 1.2a, since the ratio between the undeformed chip thickness (e.g. 0.2 mm for a  $\varnothing$  10 mm endmill) and the cutting edge radius (e.g. 0.002 mm) is relatively big, the cutting edge radius can be omitted and the tool is assumed to be sharp. Normally the rake angle of the cutting tool is chosen to be positive, and as seen in this figure, the effective rake angle is also positive. Chips are generated by shearing forces according to the conventional cutting theory [9].

While in micro cutting, see Fig. 1.2b, the ratio between undeformed chip thickness (e.g. 0.001 mm for a  $\varnothing$  0.1 mm endmill) and cutting edge radius (e.g. 0.002 mm) is small, therefore, the cutting tool cannot be assumed to be sharp anymore, and the cutting edge radius starts to play a role in chip formation. As also seen in this figure, the effective rake angle becomes negative although the cutting tool has a nominal positive rake angle. During machining, this unsharp tool 'ploughs' through the workpiece surface; as a result, only a portion of the total cutting force contributes to chip formation, the rest is due to friction between the tool and the workpiece and ploughing force at the edge [58]. This is the reason why it was observed in research that the specific cutting energy (cutting power divided by volume of material removed per unit time) increases when the undeformed chip thickness is smaller than a certain value [49, 50, 52, 59, 60].

Besides the effective negative rake angle and the ploughing effect, another important phenomenon in micro cutting is Minimum Chip Thickness (MCT). It was observed in research that when the ratio between the undeformed chip thickness and the cutting edge radius is smaller than a critical value, the

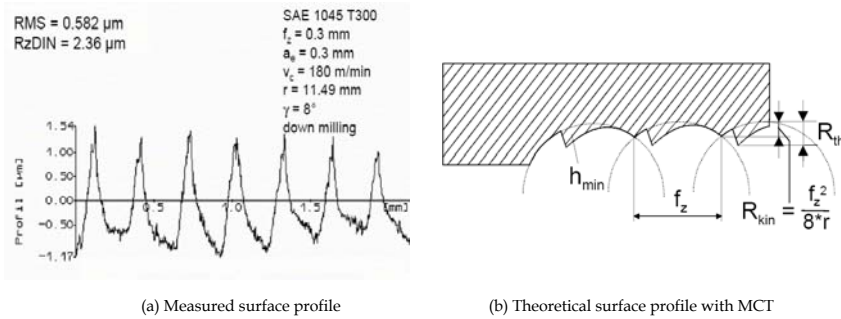


**Fig. 1.3:** Surface formation by taking into account of MCT [36]. In (b)  $h_{min}$  stands for the critical value for the MCT.

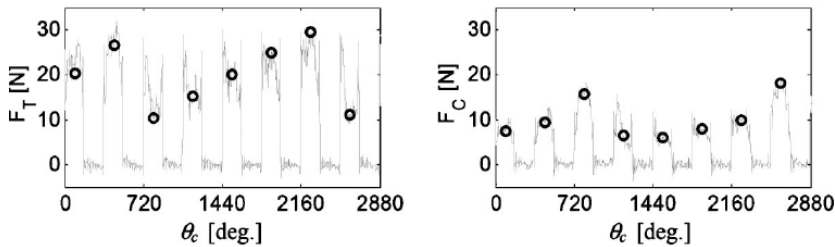


**Fig. 1.4:** Variation of measured thrust force ( $F_t$ ) and cutting force ( $F_c$ ) due to MCT [67]. Feed per tooth was  $3 \mu\text{m}$ .

workpiece material will only be elastically-plastically deformed, and no chip will be generated [36, 53-55, 61, 62]. This critical chip thickness value is referred as MCT. Its value depends on the tool edge radius and the properties of workpiece materials [63]. Effort has been spent to predict it both theoretically [51, 63-65] and experimentally [36, 66]. For example, it was reported to be 20-30% of the cutting edge radius for pearlite and ferrite materials [65], and 20-40% for aluminum [63].

The MCT effect has an influence on the surface formation. A saw-tooth like profile was observed in [36] in machining of AISI 1045 steel by a cutting tool with an edge radius of  $5 \mu\text{m}$ . It was explained by the authors by the MCT theory, as illustrated in Fig. 1.3.

The MCT effect will also cause fluctuation of the cutting forces. Vogler et al. [68] observed a subharmonic of the tooth passing frequency in the frequency spectrum of the micromilling force at a feed rate less than the critical chip value. Kim et al. [67] noticed a periodic increase of force magnitude in several consecutive tool rotation revolutions (refer to Fig. 1.4). These observations were

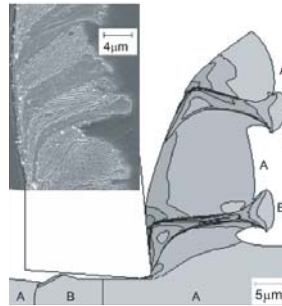


**Fig. 1.5:** Simulated chip in machining of AISI 1045 and the experimentally observed chip (left up corner). Letter A represents pearlite, letter B represents ferrite [48].

attributed to the MCT effect by the authors.

### 1.3.2 Workpiece microstructure effect

The workpiece microstructure effect is also illustrated in Fig. 1.2. In macro scale cutting, the cutting tool removes a bulk piece of workpiece material off in the form of chips, as shown in Fig. 1.2a. While in micro cutting, chip formation takes place inside the individual grains due to the size effect. As a result, the grain boundaries, type of grains, and crystallographic orientation influence the chip formation [46-48, 69-71], surface formation [46, 48, 69, 72], burr size [73], and cutting forces [69, 74].

Ueda et al. [69] investigated the effect of crystallographic orientation on chip types, shear angle value, cutting forces, and surface integrity in diamond turning of  $\beta$ -brass. It was observed that continuous chips are mainly due to a lamellar slip structure formation in the shear zone; discontinuous chips are caused by micro-cracking for the particular orientation. Depending on the crystallographic orientation the shear angle can vary between 15 to 60 degrees. The measured cutting force and machined surface integrity are also found to be affected by the crystallographic orientation.

Simoneau et al. [46-48] studied chip formation and surface generation in micromachining of pearlitic-ferritic type of material (AISI 1045 steel) by a Finite Element Method (FEM). It was found that the mechanical property of different grains plays an important role in chip formation: the extrusion of softer grains (ferrite) is seen in between two harder grains (pearlite) in chips, as shown in Fig. 1.5. The formation of surface defect, dimples, was explained by the plastic dissipation energy theory: a large amount of energy is absorbed by the softer grain (ferrite) instead of the harder grain (pearlite), which results in significant

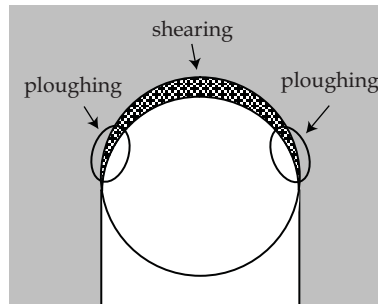


Fig. 1.6: Illustration of MCT effect on chip formation in micromilling.

plastic strain at the boundary between two types of grains [46]. Similar results were observed in [70, 71], which conducted FEM simulation on similar materials but in macro scale.

The relation between crystallographic orientation and burr height was studied in [73] by Min et al. A strong correlation between the crystal orientation of single crystal oxygen-free copper and burr height was observed in the (110) and (111) workpieces while not in (100) workpiece. This was explained by the dependency of the side flow of materials on the plastic anisotropy of the crystal. The (100) orientation is more symmetric compared with the other two orientations. Besides, the correlation was more significant in up milling than down milling. The authors assumed that this phenomenon was related to the Poisson deformation and tool edge conditions.

To et al. [72] studied the crystallographic anisotropy on chip formation, cutting force variation, and surface formation in diamond turning of aluminum single crystals. It was observed that independent of crystal orientations continuous chips were always formed. However, the oriented crystals had an influence on the magnitude of cutting forces and surface quality. Best surface finish was achieved in the (100) direction.

### 1.3.3 Transformation of the knowledge into micromilling

Due to the nature of milling operation, the instantaneous undeformed chip thickness is not constant; rather it varies with the rotation of the cutting tool. As a result the chip formation in one tooth passing period is separated into two different areas according to the dominant cutting mechanism: ploughing dominant area and shearing dominant area, as illustrated in Fig. 1.6. When the tooth is at the entrance and exit of the immersion, the undeformed chip thickness is small and the process is ploughing dominant. When the tooth is in

the middle of the immersion, the undeformed chip thickness is bigger than the critical MCT value, and the process is mainly due to shearing. However, ploughing still plays a role due to the finite radius of the cutting edge. The bigger the size of the cutting tool, the less influence the ploughing effect has on the process.

The difference in the cutting mechanism between macro scale milling and micromilling has been considered in the modeling of micromilling forces, especially when the dynamic forces are of interest [67, 75-82]. These models are called mechanistic models; they are in nature empirical models: forces and machining parameters are related by coefficients which will be found through curve fitting by using data collected in calibration experiments. The basic principle of these models is to divide the whole micromilling process into a shearing period and a ploughing period as described above, calculate the forces in these two periods separately, and then combine them to generate the total cutting force.

In [68] slip-line plasticity model was used for the period with chip formation and volumetric interference model for the period without chip formation. In [83, 84], slip-line theory was used for both the shearing dominant and the ploughing dominant periods.

Other factors considered in micromilling force models include the trochoidal tool movement [17], runout [83, 85], tool wear [86], build up edge [87], microstructure of the workpiece material [88-90].

## 1.4 Application of micromilling

The majority of the above described observations were achieved under well controlled (orthogonal) experiments or simulations with ideal situations. In practice, the micromilling process is complicated by many factors, such as wear of cutting edges, runout, stiffness, and errors from machine tools.

Compared with relatively well understood cutting mechanism, very limited results could be found about issues related to the application of micromilling technology. Besides, among the available results, inconsistent observations were commonly seen among research, which makes it difficult to draw a general conclusion about the technology and apply the reported knowledge in practice.

### 1.4.1 Performance of micro endmills

The performance of commercial micro endmills is not satisfactory due to the

encountered problems such as tool (premature) breakage, severe tool wear, and as a result short tool life. Some researchers claimed that micro tools have become the bottleneck of micromilling technology [14, 91].

The observations can be summarized as follows:

- Different failure types of micro endmills were observed when machining soft materials and hard materials.

When machining soft materials (e.g. graphite, aluminum, copper), the failure of micro endmills is mainly due to corner and edge wear (e.g. flank wear, crater wear, edge rounding) [18, 19, 30, 34], the endmill seldom breaks [30], the wear rate is relatively slow [16].

When machining hard materials (e.g. hardened steels), micro endmills show abrasive wear, edge chipping, crack [37, 92], and (premature) breakage [16, 38, 93]. As a result, tool life ends quickly [86]. The causes of tool breakage include chip clogging, fatigue, excessive stress [16], and errors in setting up of parameters (e.g. depth of cut) [94].

It was also observed that the cutting edges of micro endmills showed different wear magnitude due to runout [38, 95].

- The dominant failure type in micromilling is different from that in macro scale milling, especially in hard milling.

In macro scale milling, flank wear is normally the main wear type and is used as tool life criterion [96-101]. Many methods to monitor tool conditions were developed by using the relation between process signals (e.g. cutting force, cutting power) and flank wear [102-107].

However, flank wear becomes less significant in micromilling and cannot be used to sufficiently describe tool conditions anymore. The effect of tool failure in micromilling is the increase of the cutting edge radius, and the decrease of the cutting diameter [30].

Due to this reason, Tansel et al. [16] proposed a new definition for tool wear in micromachining: any change in the geometry of micro endmills is referred to as wear, including the loss of tool material, deposition of workpiece particles on tool surfaces, etc.

- Very limited results have been reported about the influence of cutting conditions (machining parameters and tool paths) on performance of micro endmills. Besides, among the available results [18, 30, 77], the cutting conditions were tested by using one-factor-at-a-time method, and the interaction among cutting conditions has not yet been investigated.

Rahman et al. [18] machined pure copper by  $\varnothing$  1 mm carbide square

endmills. It was observed that higher depth of cut and lower cutting speed gave minimum tool wear rate. This observation is consistent with the observation by Zaman et al. [77]. Filiz et al. [30] conducted micromilling experiments by  $\varnothing$  0.254 mm square endmills on copper 101 under different feeds per tooth (0.75–6  $\mu\text{m}$ ). The highest tool wear was seen at the lowest feed rate; this was explained by the fact that individual tungsten carbide particles are more easily dislodged from the tool at low feed rates.

- Currently there are no good guidelines or methods available for the planning of cutting conditions in micromilling.

Unlike in macro scale milling, there is no handbook available in micromilling for the selection of cutting conditions. Most micromilling experiments in literature were done by using cutting conditions recommended by tool suppliers [92, 108, 109]. However, these recommendations are mostly based on experiences in macro scale milling and trial-and-error practice in micromilling. Their validity is not fully evaluated due to the fact that limited results are published in this aspect.

It is known in macro scale milling that the tool performance (e.g. tool wear rate) depends on tool-workpiece combination because of the inconsistency in the quality of cutting tools (such as deviations of tool geometry) and properties of workpiece material [9]. The situation is further complicated in micromilling; tool performance is also heavily influenced by many other factors, such as machine tools [11, 42, 94]. Therefore, 'optimized' conditions for one tool-workpiece-machine combination in micromilling may not be appropriate when the conditions have changed. In this case, the method to plan cutting conditions is more valuable for the development of micromilling than the specific observations in experiments.

- Research about tool condition monitoring is at the initial stage.

Acoustic emission and neural networks were used in [86, 110-112] to predict remaining tool life and detect breakage. However, these approaches require extensive experimental data and are often inconsistent for different material and cutting conditions [5]. In [34] a sensor-fusion method was used to monitor tool condition in combination with the visual check by an optical microscope. The used sensors included accelerometer, force sensor, and acoustic emission sensor. Again training data are needed to establish the neuro-fuzzy model.

### 1.4.2 Surface quality

The roughness of the machined surfaces in micromilling depends on machining parameters (e.g. feed per tooth, cutting speed, depth of cut) [19, 25, 30, 38, 39,

113, 114] and their interaction [25], tool cutting edge radius (scaling effect) [38, 65], tool wear [14, 30, 35, 37-39], tool diameter [25], tool paths [108, 113], properties of workpiece material [39, 65, 115].

- **Cutting conditions and the scaling effect:** When feed per tooth is bigger than the MCT value, surface roughness increases with the increase of feed per tooth [25, 30, 37-39, 65, 113], which is consistent with the observation in macro scale milling. When feed per tooth is smaller than the MCT value, it was noticed in [37, 38, 65] that surface roughness increases with the decrease of feed per tooth; however, this trend was not observed in [25, 30].

It was reported in [36] and [19] that the higher the cutting speed, the better the surface finish is. However, contrary observation was seen in [25, 30], and no clear relation was found in [30] between cutting speed and roughness.

It was a consensus that depth of cut has no influence on workpiece surface roughness [25, 65, 113].

- **Tool wear:** Fang et al. [35] noted that the surface roughness got worse when the micro endmill wore out, this is the reason that Uhlmann et al. [14] used roughness value ( $R_z$ ) as tool life criterion in micromilling tests. However, this trend was not observed in [30, 39]. Filiz et al. [30] found the surface finish got better when the tool was worn, and it was explained by the increase of the cutting edge corner due to wear, which reduced the cusp height and lowered the roughness.

Aramcharoen et al. [37] experimentally studied the relation between types of wear and the surface roughness, and claimed that chipped and cracked cutting edges produced poorer surface finish than other types of tool wear. However, no discussion was given in this paper about the repeatability of this observation.

- **Tool path:** Dimov et al. [108] studied the effect of 8 types of tool paths on surface finish in micromilling, and concluded that machining strategy has significant effect on surface roughness. The best surface was achieved by using follow\_hardwall and constant\_load strategies.

Litwinski et al. [113] observed that up milling generally produces a better surface finish compared with down milling, and there is no difference between raster tool path and offset tool path. However, Takács et al. [38] reported that roughness in up milling is worse than that in down milling.

- **Workpiece properties:** In general the harder the workpiece material, the better the surface finish is [36, 38, 39], because soft materials are more ductile and the elastic recovery increases the surface roughness [19]. Besides, homogeneous microstructure [19] and fine grain size [115] improve the surface quality. Furthermore, Vogler et al. [65] found that multiphase

materials (pearlite ductile iron) show rougher surfaces than single phase material (pearlite) due to phase boundary effect: the cutting process is interrupted when the cutting tool moves across the phase boundary and a burr forms at this location.

- **Tool dimension:** Wang et al. discovered that roughness increases with the decrease of tool diameter [25] because micro tools bend more under cutting forces.

### 1.4.3 Burr formation

When the material is attached to the workpiece instead of being removed as chips, it will form burrs. In micromilling burrs become a serious problem because the burr volume can be comparable with the dimension of micro components.

Burr size is influenced by machining parameters [39, 113, 116-119], tool wear [30, 39, 116, 118], tool paths [39, 113, 119, 120], runout [119], and workpiece hardness [39, 116, 120]. Again inconsistent observations were reported.

- **Machining parameters:** It was noticed in [117-119] that burr size (height) increased with the increase of feed per tooth. However, it was reported in [38, 113] that burr height decreased with the increase of feed per tooth, and no relation was found between burr size and machining parameters in [116].

In [117, 119] authors reported that burr size increased with the increase of depth of cut. However, it was observed in [113] that a smaller burr was achieved at a bigger depth of cut.

For cutting speed, Schmidt et al. [39] found that with the increase of cutting speed the burr size increased at the up milling side, but decreased at the down milling side. Litwinski et al. [113] did not observe any significant effect of cutting speed on burr formation.

- **Tool wear:** It was a consensus that worn tools produced bigger burrs [30, 39, 116, 118].
- **Tool paths:** The burr size is clearly smaller at the up milling side than that at the down milling side; this was noted in [39, 119, 120]. However, this trend was not seen in [113], where up milling produced larger burrs than down milling under some combination of machining parameters.
- **Workpiece hardness:** Horsch et al. [120] and Schmidt et al. [39] observed that softer materials showed smaller burr size; this was explained by the high wear rate of cutting tools at higher workpiece hardness.

- **Runout:** Lee et al. [119] claimed that the bigger the runout the bigger the burr size will be.

Since burrs are detrimental for the quality of the micro components, burr formation has to be controlled by controlling the aforementioned factors or applying deburring techniques [116].

#### 1.4.4 Bending of micro endmills

Endmills are normally modeled by the cantilever beam theory [121-123], where the tool stiffness is proportional to 4<sup>th</sup> power of the tool cutting diameter. If tool diameter is decreased by a factor of 2, tool stiffness will decrease by a factor of 16. Therefore, the stiffness of micro cutting tools is rather low. For example, the stiffness of a commercial  $\varnothing$  0.1 mm endmill (underneck length 0.45 mm) is measured to be 0.008 N/ $\mu$ m [124]. Uriarte et al. [125] claimed that micro endmills account for up to 90% of the total compliance in the stiffness chain of the micromilling setup.

The low tool stiffness will result in bending of the cutting tool under micromilling forces during machining [126], and will result in dimensional errors of the machined parts. Dow et al. [15] tried to compensate the dimensional error caused by tool bending through an open-loop algorithm. The basic procedure is:

- Predict cutting forces under given cutting conditions;
- Calculate tool bending under the predicted forces;
- Predict dimensional errors of machined parts;
- Adjust tool paths to take into account tool bending.

### 1.5 Discussion

In this chapter, a brief introduction is given to micromachining technology and the state of the art research results of micromilling. It is clearly understood that the micromachining process is strongly influenced by the scaling effect. As a result, some phenomena that are not prevalent in macro scale cutting, such as ploughing, become dominant in micro scale cutting. This has an influence on the chip formation, surface formation, etc.

It is also pointed out in this chapter that most of the fundamental research was done on orthogonal cutting. For this reason, there is an issue how to transfer the knowledge into milling. For this purpose, three aspects have to be considered.

The first aspect is the kinematic movement of the milling process. As discussed in Section 1.3.3 already, this divides the tooth immersion period into the ploughing dominant period and the shearing dominant period. The second aspect is the smallest size of the cutting tool used. As described in Section 1.2,  $\varnothing$  0.3 mm endmills are the most commonly used micro endmills in research. The third aspect is the productivity. In applications, it is common practice to choose higher value in the process window. For example, it is reasonable to assume that a feed per tooth of 6  $\mu\text{m}$  is used for a  $\varnothing$  0.3 mm square endmill.

According to values given above, it is possible to calculate the percentage of ploughing and shearing periods in the total tooth immersion. Suppose the cutting edge radius of the tools is 2  $\mu\text{m}$  for a new tool and the critical MCT value is 40% of the cutting edge radius, the shearing dominant period would be 91.5% of the total tooth immersion, and the ploughing dominant period 8.5%. This calculation shows that the general performance of the micro endmill is still determined by the shearing dominant period at this scale. Of course, this ratio will change when the tool wears out and the cutting diameter of the tool changes.

In comparison with relatively well-understood cutting mechanism of micro machining, the application of micromilling is not well investigated yet. First of all, very limited results can be found in the aspects related to the application of micromilling, such as tool wear, workpiece quality, and their relation with cutting conditions. Secondly, among the available results, inconsistent observations were reported from research to research. One possible reason could be the inconsistency in the quality of cutting tool, workpiece material, and different performance of machine tools. This implies that it may not be appropriate to apply acquired knowledge from other research for a new application case in micromilling. Thirdly, the majority of experimental investigations were currently done by using the trial-and-error method; it is necessary to develop/select a systemic approach to study the micromilling process and plan cutting conditions to achieve optimum cutting conditions. Fourthly, according to the published results, it seems that the critical problem is the performance of micro endmills: micro endmills showed severe tool wear and short tool lives, especially in machining of high strength materials. Some researchers claimed the micro cutting tools have become the bottleneck for the development of the micromilling process.

In summary, in order to apply the micromilling technology in moulds industries to make full use of its potential advantages, more research needs to be done to understand the micromilling process.



## Chapter 2 Research goal and approach

In this chapter, the research goal and working approach are addressed. In Section 2.1, a preliminary micromilling test is introduced. The research goal and working approaches are addressed in Section 2.2 and Section 2.3, respectively. The structure of the thesis is described in Section 2.4.

### 2.1 Case study: micromilling of a micro part for a micro gripper

At the initial stage of this research a micro part was milled to get some practical experiences about the micromilling process.

The chosen part was a component of a micro gripper. The CAD drawing of this micro part is shown in Fig. 2.1a. Its dimension is  $\varnothing 1.8 \times 0.6$  mm. To make this part, its negative shape was first machined in a piece of stainless steel (grade 316), and then the part was produced by injection molding.

The used cutting tools were commercial  $\varnothing 0.15$  mm square endmills. The machining parameters were chosen according to the recommendations of the tool supplier. The tool paths were generated by a commercial CAM package. The machine tool was Mikron HSM700 located at TNO Science and Industry in Eindhoven.

Although only about  $4 \text{ mm}^3$  material had to be removed, the machining of this micro part was not successful at all. A replicated part is shown in Fig. 2.1b. In order to machine this micro cavity, altogether 12 micro endmills broke. The total machining time was about 3.5 hours. The surface roughness of the machined part was high, micro burrs showed up, and the dimensions were out of tolerance.

The unsuccessful machining of this part illustrated that the application of micromilling process was not straightforward. This example also demonstrated that the micromilling process was far from a qualified process for industries yet.

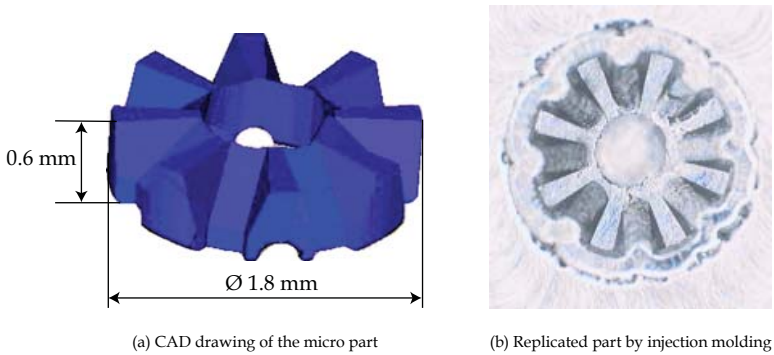


**Fig. 2.1:** CAD drawing and achieved micro part.

Although material removal was possible, the right cutting conditions were unknown, tool performance was unpredictable, and the workpiece quality was not achieving the requirements at all. Because of all these, the possible economic advantage of micromilling could not be achieved.

## 2.2 Goal of the research

In order to apply micromilling technology in industries, the aforementioned problems have to be overcome, the causes need to be found, and the reliability of the process has to be improved greatly.

In this research, it is desired to generate knowledge for the Dutch die and mould industry to provide it with an alternative technique for the manufacture of small- to medium-sized dies and moulds with a high degree of complexity and high accuracy. Therefore, hardened tool steels will be used as the workpiece material in this research.

Based on the above reasons, the general goal of this research is defined as: **to develop and describe a reliable micromilling process for precision machining of hardened tool steels.**

According to the literature survey and initial micromilling tests in this research, it was decided to realize the research goal in two steps. The first step is targeted to improve the performance of micro endmills, e.g. to minimize tool wear to achieve a reasonable tool life. This is the prerequisite before any other work can be done. The second step is to improve the performance of the process, e.g. improve surface finish or process capability.

The expected knowledge at the end of this project includes:

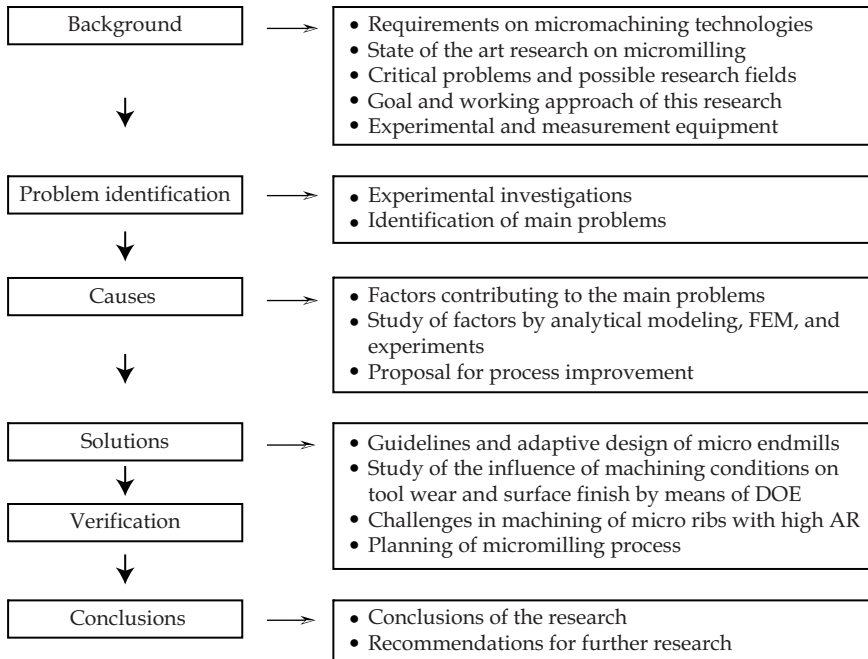


Fig. 2.2: Illustration of working approach and structure of this thesis.

- Fundamental understanding of the micromilling process, e.g. wear types of micro cutting tools and corresponding wear mechanism in machining of hardened tool steels.
- Knowledge about design of micro endmill geometry. Fundamental understanding of how the geometrical features of the micro endmill will influence its performance and how to choose values for these features to achieve desired performance.
- Fundamental understanding of how machining parameters and tool paths will influence the micromilling process.
- Development of knowledge based methods to plan cutting conditions for a given output criterion, such as less tool wear or better workpiece surface finish.

## 2.3 Working approach

The basic approach used in this research is illustrated in Fig. 2.2, and briefly

introduced as follows.

- **Problem identification:** First, experiments will be designed and conducted to identify the main problems in micromilling of hardened tool steels. Experimental study instead of theoretical analysis is chosen as the main approach in this step because both the literature survey and the initial test showed that the actual micromilling process is rather complicated to be accurately described by theoretical models.

Although the goal of the research is to develop the micromilling technology for dies and moulds applications, 3D parts will not be machined in this work. Instead, simple machining operations (such as slot milling and side milling) will be conducted because they are more suitable for fundamental research.

Hundreds of cutting tools, a few types of workpiece materials, and several machine tools are used in this research. It is difficult to guarantee the consistency of these components. Therefore, comparison and qualitative study, instead of quantitative study, will be conducted. For a comparison study, it is necessary to use tools from the same batch and conduct experiments on one setup in order to draw a valid conclusion.

- **Causes:** After identifying the main problems, analysis is conducted to find out the causes for these problems. In this step, both theoretical analysis and experimental study are used. Besides, it is necessary to distinguish the most significant causes under the given experimental conditions.

It was decided to solve the existing critical issues instead of potential problems. Some causes may be important according to the knowledge in macro scale machining or results from other research, e.g. chatter; if they do not show a significant effect on the micromilling process in this research, they will not become the focus of this work.

- **Solutions:** When the problems and their causes are understood, appropriate solutions can be proposed to improve the micromilling process. Since it is not possible to solve the problems from all aspects, it is important to identify and work on the most critical problems. Besides, in order to guarantee the the realization of the project goal, proposed solutions should also take into account available knowledge and resources in the research environment (such as the availability of machine tools).

Compare with specific observations (e.g. exact tool life when machining a type of material), it is more preferable to develop methods or knowledge about how to improve the micromilling process in general (e.g. how to adjust tool geometry for a certain purpose). This is because the specific observation can vary when some factor in the tool-workpiece-machine combination change; while the method or knowledge will be widely

applicable.

- **Verification:** The proposed solutions will be verified in experiments to prove their validity. The experimental results will be compared with the theoretical analysis.

## 2.4 Structure of the thesis

In Chapter 3, the experimental and measurement equipment used in this research are introduced, including micro cutting tools, machine tools, workpiece materials, force sensor, microscopes, etc.

In Chapter 4, the results of experimental investigations are given which were designed and conducted to determine the performance of commercial micro endmills in machining of hardened tool steels. The tool wear types and mechanism of micro square endmills are described, the relation between tool conditions and workpiece quality is discussed, and the factors that influence the tool performance are analyzed.

The influence of machining parameters and tool paths on the performance of micro endmills and surface quality of machined workpiece is investigated in Chapter 5. These studies are done by means of experimental design and statistical analysis.

In Chapter 6, the effort to improve the geometry of micro endmills is presented. Design guidelines for micro cutting tools are presented. This part of work is done first by using theoretical modeling, and then verified through experiments.

In Chapter 7, machining of micro ribs with high aspect ratios (AR) by means of a knowledge-based method is introduced. The selection of machining parameters and tool paths is done by means of a force model and a FEM model, respectively. The theoretical analysis is validated through experiments.

Finally, conclusions and recommendations for further research are presented in Chapter 8.



# Chapter 3 Experimental and measurement equipment

In this chapter, the used experimental and measurement equipment, such as the cutting tools, machine tools, workpiece materials, and microscopes, are introduced.

## 3.1 Micro endmills

The main type of cutting tools used is a  $\varnothing$  0.5 mm square endmill. It is chosen based on the following arguments: firstly, it was observed in the preliminary tests that  $\varnothing$  0.1 mm and  $\varnothing$  0.3 mm endmills exhibited more premature breakage which reduced the reproducibility of the process; while  $\varnothing$  0,5 mm endmills showed more consistent behavior. Secondly, the complexity of the geometry of ball nose endmills makes them less preferable for fundamental research compared with square endmills. Besides, the knowledge gained from results by square endmills can be transferred to ball nose endmills in the future by taking into account the difference in geometry.

All the experiments presented in this work were done with commercial endmills from one company; an example of the tested commercial  $\varnothing$  0.5 mm 2-flute square endmill is shown in Fig. 3.1. During this research limited experiments were also conducted by using micro tools from three other companies for comparison. However, since those endmills did not show any advantage over the chosen commercial tools, the results with those tools are not included in this thesis.

The tool substrate material is ultra-fine grain (grain size  $< 0.6 \mu\text{m}$ ) tungsten carbide with cobalt as the binder, which is commonly used in commercial tools. The detailed property of the tungsten carbide is not disclosed by the tool manufacturer; the following data are found from a carbide supplier [127] according to the grade of tungsten carbide and used in the future analysis: Young's Modulus ( $E$ ) 560 GPa, Poissons Ratio ( $\nu$ ) 0.22, density ( $\rho$ )  $0.0136 \text{ g/mm}^3$ ,

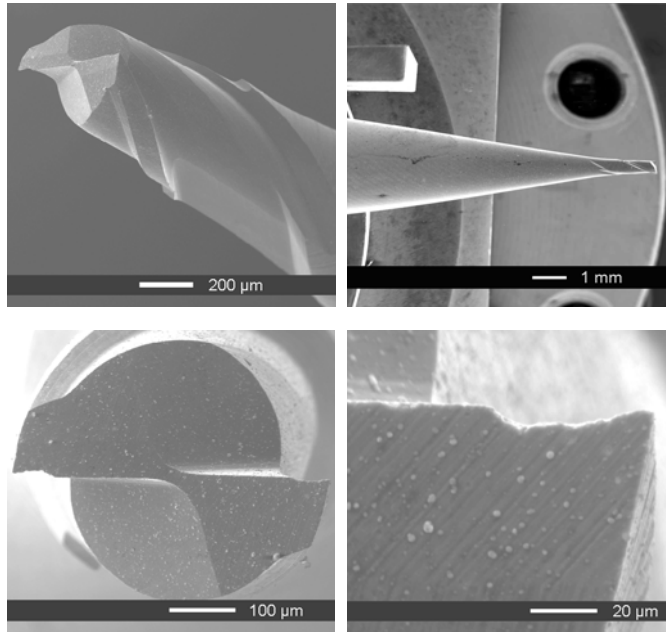


**Fig. 3.1:** SEM photos of the tested commercial  $\varnothing$  0.5 mm square endmill.

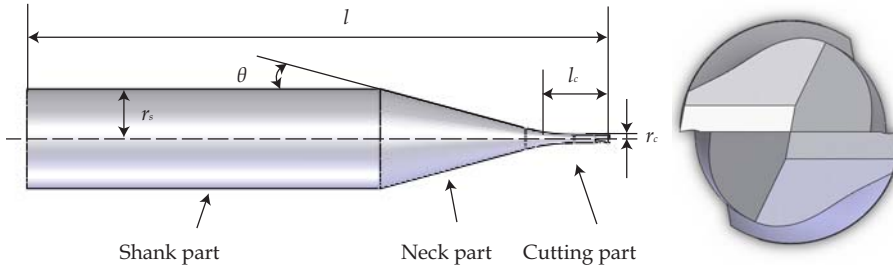


**Fig. 3.2:** Schematic view of the global geometry of a micro endmill.

and Transverse Rupture Strength (TRS) 4.2 GPa. Since mainly comparison analysis will be conducted in this research, the possible error due to this assumption is not critical.

All the tested commercial micro endmills are TiAlN coated, which is a frequently applied coating type in commercial macro and micro endmills in the market. The function of the coating is to increase the surface hardness and reduce the friction between chips and the tool surface. The preliminary tests showed that non-coated micro endmills have much shorter tool lives compared with coated endmills in machining hardened tool steels (e.g. AISI H11 of 44 HRC). Therefore, only coated endmills are used in this research.

**Table 3.1:** Nominal specifications of the commercial micro endmill.

Components	Symbols	Values
Total length	$l$	64 mm
Shank radius	$r_s$	3 mm
Cutting length	$l_c$	0.8 mm
Cutting radius	$r_c$	0.25 mm
Neck angle	$\theta$	12°
Helix angle	$\beta$	30°

Note: the shank length ( $l_s$ ) and neck length ( $l_n$ ) can be calculated from given parameters.

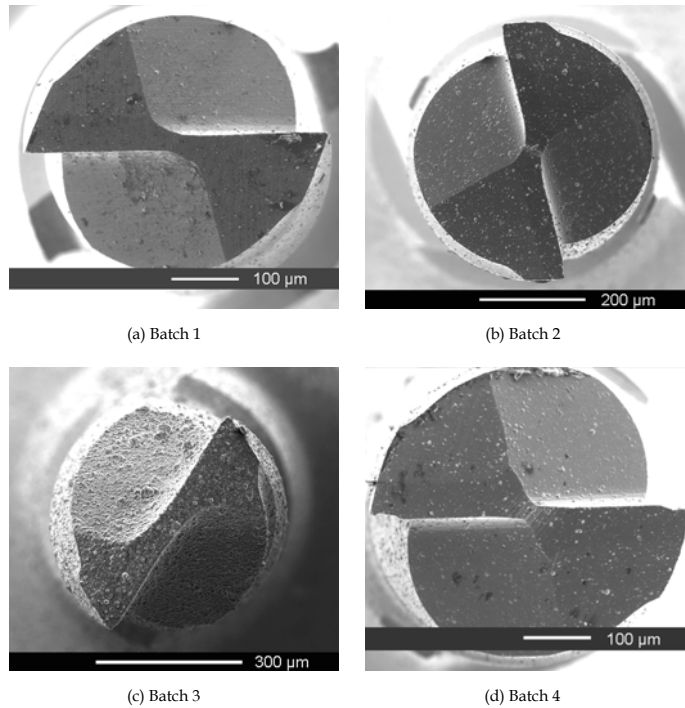


**Fig. 3.3:** Top views of  $\varnothing 0.5$  mm endmills with the same nominal specifications, but produced from four different batches. The endmill from the batch 1 (Fig. 3.3a) has a very big radial relief angle; while the endmill from the batch 4 (Fig. 3.3d) has an obvious positive radial rake angle.

The typical global geometry of the commercial micro square endmill is shown in Fig. 3.2. It includes three main parts, namely the shank part, the neck part, and the cutting part, represented by subscript  $s$ ,  $n$ , and  $c$ , respectively. The letter  $l$  represents length,  $r$  radius, and  $\theta$  neck angle. The function of the shank part is to connect the tool to the tool holder. The cutting part is where the cutting edges are. The neck part connects the cutting part with the shank part. The detailed

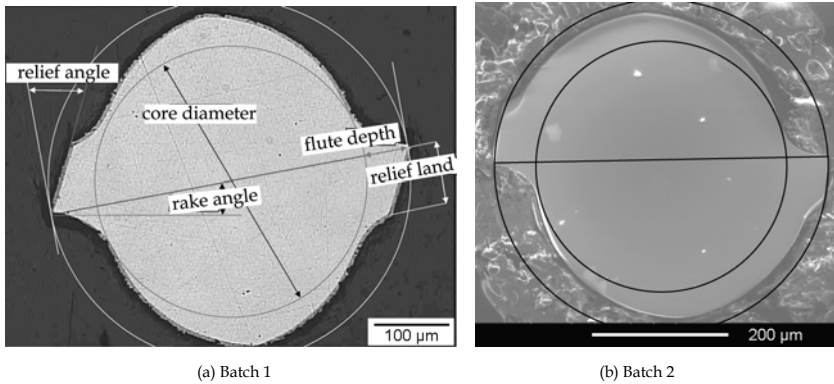


**Fig. 3.4:** Cross sections of  $\varnothing 0.5$  mm square endmills from two batches.

**Table 3.2:** Results of tool geometrical check corresponding to Fig. 3.4.

Geometry	Designed value	Batch 1	Batch 2
Cutting diameter (mm)	0.488-0.498	0.490	0.490
Core diameter (mm)	0.36	0.370	0.369
Rake angle ( $^{\circ}$ )	8	-11	-9
Relief angle ( $^{\circ}$ )	10	25	6
Relief land (mm)	0.075	0.095	0.063

values for these parameters are listed in Table 3.1. All the tested commercial  $\varnothing 0.5$  mm square endmills have 2 cutting edges.

Before using the commercial tools, the tool geometry was examined in detail, and the following aspects are observed:

- The geometry of the commercial micro endmill is derived from that of macro endmills. This means that macro ( $\varnothing > 1$  mm) and micro endmills from the same series share the same values for geometrical features: e.g. rake angle ( $\alpha$ ), relief angle ( $\gamma$ ), and ratio between the flute depth and tool cutting diameter.
- However, due to the limitation of the manufacturing process (grinding), the designed values cannot be fully achieved on micro endmills. Relatively large geometrical deviations are seen among micro tools from the same batch due to the wear of grinding wheels, and among micro tools from different batches due to inconsistency in the manufacturing system, as shown in Fig. 3.3.

The results from the visual check were confirmed by quantitative measurements. The cross-section of the cutting part of two micro endmills from two different batches are shown in Fig. 3.4, measured values of some geometrical features are shown in Table 3.2. It is seen that although these

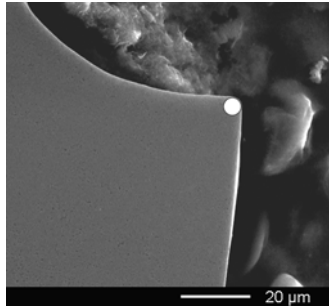


Fig. 3.5: Illustration of cutting edge radius measurement.

two endmills have the same nominal specifications, the real geometries are significantly different.

- The cutting edge radius is also measured on the cross section picture by fitting a circle, as illustrated in Fig. 3.5; the value is about  $2\ \mu\text{m}$  on average. According to [2], the critical MCT value can be estimated to be 20-40% of the cutting edge radius; therefore, the critical MCT value in this work is assumed to be  $0.8\ \mu\text{m}$ . This value will be taken into account when planning the machining parameters.
- Other problems related to the commercial micro endmills include damage of cutting edges during handling, coating droplets, uneven coating, etc. Since these problems are not dominant, they will not be introduced here.

The geometrical examination shows that it is very important to check the quality of each micro endmill carefully before conducting experiments with it. Besides, it is critical to use endmills produced from the same batch in one series of experiments to minimize the influence of variation of tool quality on end results. This is one of the reasons in this work that comparison experiments were mainly conducted. In following chapters, if not otherwise mentioned, the results presented under the same topic were achieved by endmills from the same batch.

## 3.2 Machine tools

Altogether four machine tools were used: the Fehlmann Picomax 60 HSC [128] and the Mikron HSM700 [129] located at TNO Science and Industry Eindhoven, the KERN EVO [130] at the Mondragon University in Spain, and the KERN EVO at the Cranfield University in UK, see Fig. 3.6. The main specifications of these machine tools are summarized in Table 3.3.



**Fig. 3.6:** Machine tools used in experiments.

The practical problems encountered in experiments are to measure the dynamic cutting diameter of micro endmills and to set up the workpiece coordinate accurately. Although these machines are equipped with state of the art measurement tools, such as the BLUM laser tool setting system, the infrared touch probe, and the possibility to compensate the thermal elongation automatically, accurate setting of the micromilling experiments is still very challenging.

The dynamic cutting diameter of micro endmills is influenced by many factors, such as runout of the tool, the thermal state of the spindle, mass imbalance, spindle motion errors at different rotational speeds, and errors in tool clamping. Failure to measure the dynamic cutting diameter accurately can lead to tool damage, shorten tool life, and produce out-of-tolerance parts. It was found in this research that neither the Micro type BLUM nor the Nano type BLUM was able to measure the tool dynamic cutting diameter accurately. This issue is further discussed in Appendix A.

During machining, the generated heat from the components of the machine tool

**Table 3.3:** Summary of the main specifications of the machine tools.

	Fehlmann Picomax 60HSC	Mikron HSM700	KERN EVO
Machine type	Conventional high speed milling machine	Conventional high speed milling machine	Micromilling machine
Axes	X, Y, Z, B, C	X, Y, Z	X, Y, Z, B, C
Spindle type	Fischer Hybrid bearing	Step-Tec Hybrid bearing	Precise Hybrid bearing
Max spindle speed (rpm)	36000	42000	50000*
Tool clamping interface	HSK-E50	HSK-E40	HSK-E25
Tool holder	Shrink fit	Shrink fit	Collet
Tool setting	BLUM Micro	Manually	BLUM Nano
Workpiece setting	Touch probe	Touch probe	Touch probe
Resolution ( $\mu\text{m}$ )	1	0.1	0.1
Position tolerance ( $\mu\text{m}$ )	$\pm 5$	$\pm 7$	$\pm 1$
Feed rate in X/Y/Z (m/min)	20	20	16
Automatic thermal compensation	Yes	Yes	Yes
MQL	Yes	Yes	Yes
Control unit (Heidenhain)	iTNC 530	iTNC 530	iTNC 530

\*This machine has two spindles; the second spindle has maximum speed of 160000 rpm, however, it was not available for tests in this research.

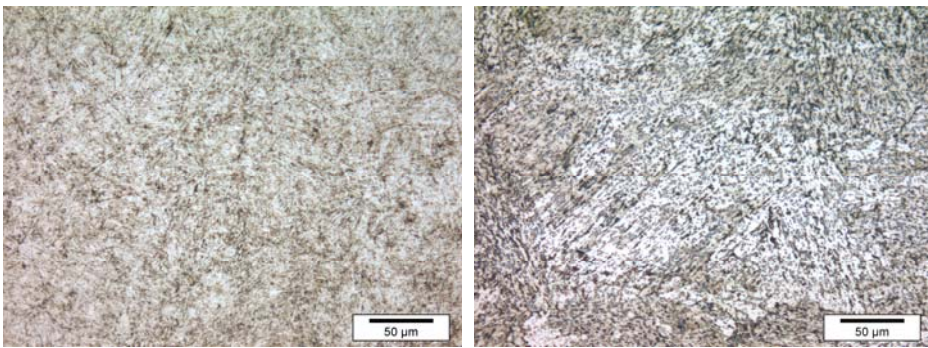
will lead to thermal errors, which influence the accuracy in the coordinate setting. The thermal elongation of the spindle results in the change of the coordinate of the workpiece, especially in the Z direction. For example, it was found that the Fehlmann machine showed on average a 0.01 mm difference between the commanded depth of cut and the achieved depth of cut on the workpiece even when the automatic thermal compensation function of the machine was on. This could lead to premature breakage of micro cutting tools, and wrong interpretation of the experimental results. Therefore, before using each machine tool, the accuracy of the coordinate setting was tested. Besides, a method was used to set up the Z coordinate manually. The used method is described in Appendix B.

### 3.3 Workpiece materials

The workpiece materials are pre-defined in this research: hardened tool steels

**Table 3.4:** Summary of the workpiece material properties.

Nr.	Material type	Chemical composition (weight %)	Hardness (HRC)
1	AISI H11	C 0.38, Mn 0.40, Si 1.10, Cr 5.00, Mo 1.30, V 0.40	44, 52, 54, 56
2	AISI H13	C 0.32-0.45, Mn 0.40, Si 1.10, S< 0.003, Cr 5.20, Mo 1.40, V 0.95	54
3	AISI D2	C 1.45-1.60, Mn 0.20-0.60, Si 0.10-0.60, S 0.03, P 0.03, Cr 11.0-13.00, Mo 0.70-1.00, V 0.70-1.00	50
4	BÖHLER M261	C 0.13, Mn 2.00, Si 0.30, Cr 0.35, Ni 3.50, Cu 1.20, Al 1.20	46



(a) AISI H11 of 54 HRC

(b) BÖHLER M261

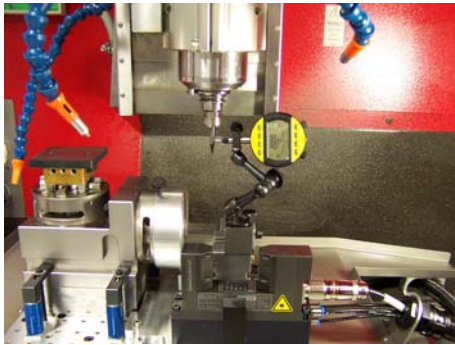
**Fig. 3.7:** Microstructure of AISI H11 AND BÖHLER M261.

for dies and moulds applications.

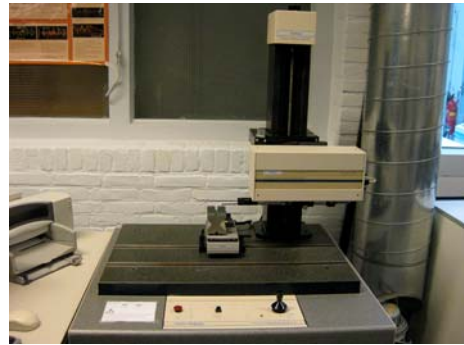
Altogether 4 types of materials are used, namely AISI H11 (DIN 1.2343), AISI H13 (DIN 1.2344), AISI D2 (DIN 1.2379), and a mould steel from the BÖHLER Company (BÖHLER M261). These steels are chosen because they are widely used in dies and moulds industries, and also in micromilling research in literature, which makes it possible to compare the observations in this research with results from other research groups.

These materials were hardened to different hardness, and cut into blocks of  $20 \times 20 \times 10 \text{ mm}^3$ . The surfaces of the blocks were ground to achieve flatness better than  $2 \text{ }\mu\text{m}$ . The properties of these types of workpiece materials are summarized in Table 3.4.

The majority of the experiments were done with AISI H11 and BÖHLER M261;



(a) Precision probe and magnetic stand



(b) Talysurf Series 120L



(c) Veeco Wyko NT3300



(d) JEOL JSM-6300

**Fig. 3.8:** Some measurement equipments.

limited tests were done with AISI H13 and D2 for the comparison purpose. The typical micrographs of the microstructure of AISI H11 and M261 are shown in Fig. 3.7.

### 3.4 Measurement equipment

The static runout at the end of the tool shank part was measured by a high precision probe (resolution 0.001 mm) together with a magnetic stand. The setup is shown in Fig. 3.8a. If the measured static runout is bigger than  $1\ \mu\text{m}$ , the tool holder will be taken out of the spindle, cleaned, and inserted into the spindle again. In the end, the static runout at the tool shank end was controlled to be smaller than  $1\ \mu\text{m}$  in experiments. This method cannot be applied to check the static runout at the tool tip due to the complex geometry of the cutting edge and the compliance of the cutting tool.

The cutting force is measured by the Kistler MiniDyn 9256C2 [131] shown in Fig. 3.6d, together with a Kistler 5070A Multi-channel charge amplifier [131]. The measuring range of the dynamometer is -250 N to 250 N, the threshold is 2 mN, and the natural frequency is above 4 kHz. The data acquisition board is NI 9215A with BNC, the maximum sampling rate is 100 kS/s per channel. The used sampling rate in experiments varied according to the spindle speed; at least 60 data points were collected per spindle revolution to capture the fluctuation of micromilling forces. Low pass filters were turned off during measurement, and the long time constant was used.

The quality of machined surface was checked by both the stylus method (a Rank Taylor Hobson type Form Talysurf Series 120L [132], shown in Fig. 3.8b, data resolution 0.25  $\mu\text{m}$ ) and the White Light Interferometer (WLI) (Veeco Wyko NT3300 [133], shown in Fig. 3.8c, vertical resolution 3 nm for the Vertical Scanning Interferometry (VSI) mode). When the stylus method is used, according to ISO4288, the sampling length is 0.8 mm, the evaluation length is 4 mm, the cut-off is 0.8 mm, and the bandwidth is 300:1.

Tool wear, burr formation, and workpiece form accuracy were checked by means of a Keyence VHX-100 microscope (lens 150 $\times$ -800 $\times$ ) [134], Scanning Electron Microscopes (SEM) (JEOL JSM-6300 [135] in Fig. 3.8d and FEI Quanta 600 scanning electron microscope [136]).

Besides, the cutting process was observed by a high speed camera Olympus i-speed 2 [137], This high speed camera has a speed range from 60 to 33000 frames/second; the CMOS sensor resolution is 800 $\times$ 600 pixels; the resolution under the maximum frame speed is 96 $\times$ 72 pixels; the maximum available magnification is 21. The hardness of the workpiece was checked by a Wilson Hardness Tester [138].

# **Chapter 4 Performance evaluation of micro endmills**

This chapter summarizes the results of the experiments which were designed to yield a fundamental understanding of the micromilling process. In Section 4.1, the motivation, objective, and approach are introduced. In Section 4.2, the problems in micromilling of hardened steels, including the tool wear types and mechanisms, are introduced. The quality of the workpiece and its relationship with conditions of cutting tools are discussed in Section 4.3. Analysis was conducted to find out the causes for the observed problems, this is presented in Section 4.4. In Section 4.5, discussions are given about how to improve the performance of micro cutting tools and the micromilling process.

## **4.1 Motivation, objective, and approach**

The machining of the micro gripper, introduced in Chapter 2, indicated that the micromilling process was not well understood; the direct application of macro scale milling knowledge could not achieve satisfactory results. In order to improve the reliability of the process, a fundamental understanding of the problems and the causes has to be gained first. Obviously, this cannot be done by using this simple example.

The reasons for the unsuccessful machining of the micro gripper can be from many aspects, such as the cutting tool, cutting conditions, the machine tool, and the workpiece material, as shown in Fig. 4.1. By using a geometry as complex as the micro gripper, it is not possible to decompose the contributions of different error sources and find out the crucial factors. Besides, the gripper was machined under one set of machining parameters, which could not be used to draw any conclusion about the process window. Furthermore, the tool paths were generated by a CAM software which was developed for macro milling; its effectiveness on micromilling was unknown.

Therefore, it is desired to design experiments in such a way that each possible

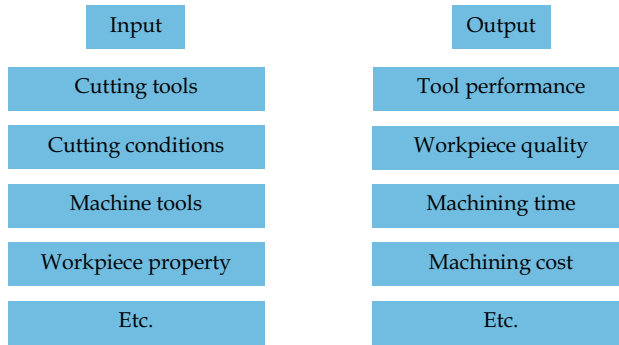


Fig. 4.1: Summary of input and output parameters.

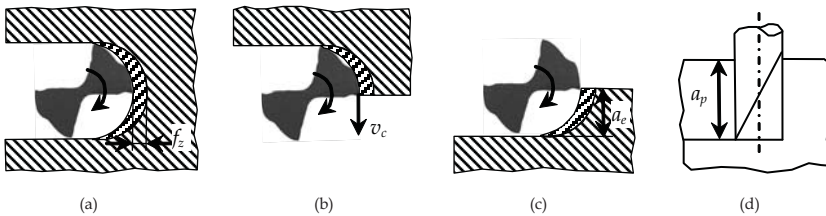


Fig. 4.2: Illustration of typical milling operations and machining parameters: top views, (a) slot milling; (b) up milling; (c) down milling; (d) side view.

error source can be tested separately to check its effect on the micromilling process. By doing so, the critical problem and its causes can be identified, and then solutions can be proposed accordingly to improve the process.

For this purpose, slot milling or side milling are chosen, as shown in Fig. 4.2. These operations are typical operations in milling. The process geometry is simple, the cutting conditions are constant during machining, and there is no abrupt change in cutting directions. Therefore, they are suitable for the purpose of this research.

There are normally four machining parameters to be varied, namely feed per tooth ( $f_z$ ), cutting speed ( $v_c$ ), width of cut ( $a_e$ ), and depth of cut ( $a_p$ ). The meaning of these parameters is demonstrated in Fig. 4.2. To test the effect of these machining parameters experiments will be conducted at several levels of each parameter, and their effect on the micromilling process will be evaluated by analyzing the results using a certain criterion.

The commonly used criteria to evaluate the milling process can be classified into two groups, quality-related criteria (e.g. tool wear and tool life, workpiece

surface quality, form accuracy, burr formation) and economical criteria (e.g. machining time and production cost), as shown in Fig. 4.1. Of course the economical criteria are only valid when the quality related criteria are satisfied. Since the objective of this research is to gain a fundamental understanding of the process, and no real product will be machined, the quality-related criteria, instead of economical criteria will be used to evaluate the results.

## 4.2 Tool wear types and mechanism

The observed tool wear types and mechanism of the used commercial  $\varnothing$  0.5 mm square endmills are summarized in this section.

### 4.2.1 Wear of micro square endmills

The definition of tool wear in micromachining by Tansel [16] is used in this study: any difference between a new and used tool is referred as wear.

**Experimental setup:** Experiments were done with commercial  $\varnothing$  0.5 mm square endmills. The workpiece material was tool steel AISI H11 with four levels of hardness, namely 44, 52, 54, and 56 HRC. The machine tool was the Fehlmann Picomax 60HSC and the KERN EVO. Minimum Quantity Lubrication (MQL) was used for all tests.

Slot milling and side milling were conducted. The cutting conditions were first chosen partly according to the tool supplier's recommendations, and then adjusted based on the experimental results. The spindle speed was varied between 10000 rpm and 36000 rpm,  $f_z$  0.002-0.009 mm, and  $a_p$  0.03-0.10 mm. The cutting process was interrupted at a certain interval to measure the wear of the cutting tool.

The cutting force was measured by the Kistler 9256C2. The tool wear, workpiece form accuracy and burr formation were checked by the FEI Quanta 600 scanning electron microscope and the Keyence microscope. The roughness of the milled surfaces was measured by the Talysurf Series 120L and the WYKO NT 3300 WLI.

**Observations:** In general, it is observed that micro square endmills suffered from severe tool wear in machining of hardened tool steels. The wear increases the cutting edge radius and decreases the effective cutting diameter. The observed wear types include chipping of the cutting edge corner, abrasive wear, flank wear, workpiece material adhered on the tool surface, etc. Premature breakage seldom happened for the tested  $\varnothing$  0.5 mm square endmills. The main wear mechanism is chipping at the early stage of machining, and then

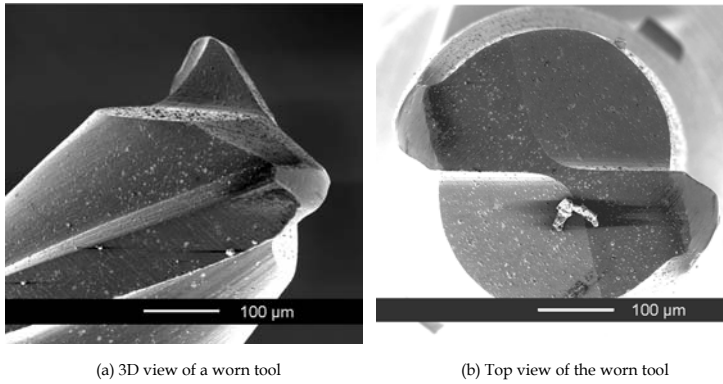


**Fig. 4.3:** A worn  $\varnothing$  0.5 mm square endmills.

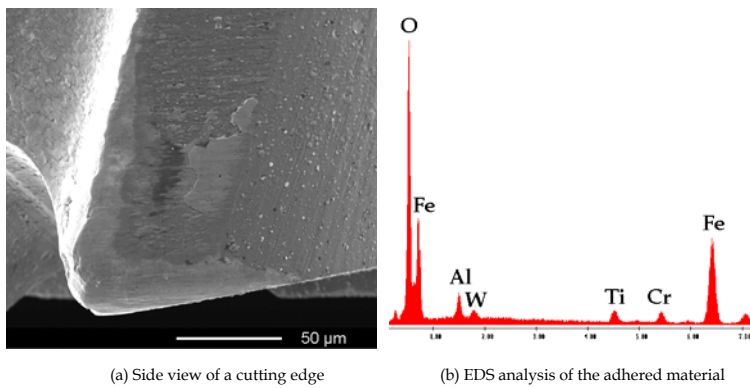


**Fig. 4.4:** Flank wear and workpiece material adhered on the tool surface.

plasticity-dominated wear. This is mainly because the experiments were done at a relatively low cutting speed range, and the micromilling process is interrupted cutting kinematically.

The observed main wear types are as follows:

- Chipping of the cutting edge corners: The milling process is an intermittent process; as a result, cyclic impact applies on the cutting edges of the micro endmills, which can initiate small cracks and then lead to chipping of cutting edge corners. An example of worn tools is shown in Fig. 4.3. Compared with the new tool, shown in Fig. 3.1, the worn tool lost its sharp edge corners. It was observed that the chipping normally happened at a very early stage of the machining. Besides, micro tools with a positive rake angle and/or a large relief angle were more prone to edge chipping than tools with a relatively big wedge angle (angle between the tool flank face and the rake face).

Furthermore, properties of the workpiece material and machining parameters also have significant effect on the chipping. Because of the small dimension of the micro endmill, the tool geometry changed greatly once chipping happened, and as a consequence the tool life was shortened.

This type of wear can be improved by a proper geometrical design to increase the strength of the cutting edges.

- Abrasive wear: After losing the initial cutting edge corners, tool substrate material (tungsten carbide) formed the new cutting edge. As a result, the tool cutting edge radius increased, and the cutting mechanism became more ploughing instead of shearing. Besides, without the protection of coating, cutting edges became less wear-resistant. Because of above reasons, there would be severe friction between the cutting tool and workpiece during machining. This can be seen from the smooth surfaces at the cutting edge corners of the worn tool in Fig. 4.3. The abrasive wear gradually decreased the effective cutting diameter of the tool; the produced part was out of tolerance.
- Flank wear: An example of flank wear on micro endmills is shown in Fig. 4.4a. In macro scale milling, flank wear is a common wear type and often used as the tool life criterion. However, it was observed in micromilling experiments that the flank wear was relatively small in magnitude and it could not be used to monitor the tool condition.

There are several reasons why flank wear became less significant in micromilling. Firstly, as discussed before, the chipping of the cutting edge corners happened at a very early stage of the machining, and it changed the shape of the cutting edges greatly. Secondly, the value of the applied  $a_p$  in the tests could be comparable with the magnitude of chipping (refer to Fig. 4.5). A part of, or even, the complete flank face that was involved in cutting chipped off. Thirdly, the magnitude of flank wear was small compared with the chipping effect, and it is difficult to evaluate it quantitatively.

- Material adhered on the tool surfaces: It can also be seen in Fig. 4.4a, that some materials adhered to the tool, both the flank face and the rake face. The Energy Dispersive Spectroscopy (EDS) analysis was conducted to study the chemical components of the adhered material. The result, shown in Fig. 4.4b, confirms that the material was from the workpiece.

The mechanism of this phenomenon is probably the high contact stress welded the ductile workpiece material on the tool surface at low cutting speed. If the size of the adhered material is too big, chip clogging could happen, which is one of the reasons for the premature breakage of micro endmills [16].

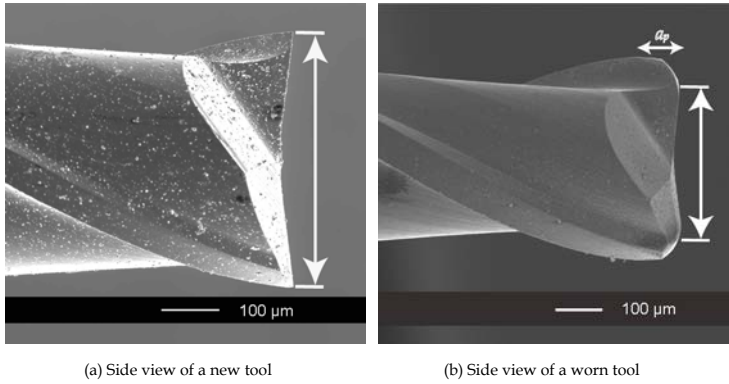


**Fig. 4.5:** Reduction of tool cutting diameter due to tool wear.

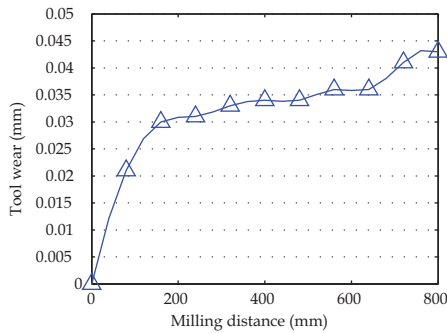


**Fig. 4.6:** Progress of wear of a  $\varnothing 0.5$  mm square endmill. Experimental conditions:  $v_c$  56.6 m/min,  $a_p$  0.08 mm,  $a_e$  0.5 mm,  $f_z$  0.006 mm, workpiece AISI H11 with 56 HRC, machine Fehlmann Picomax 60HSC.

- Tool premature breakage: For the tested commercial  $\varnothing 0.5$  mm square endmills, premature breakage seldom happened under the tested conditions. However, in preliminary tests with  $\varnothing 0.1$ - $0.2$  mm endmills premature breakage was commonly observed. When breakage happened, the tool always broke at the end of the cutting part, which has a change in the geometry.

Since  $\varnothing 0.5$  mm square endmills have been chosen as the main tool type in this research, and premature breakage seldom happened with this type of tool, the breakage issue will not be further discussed in the following chapters.

**Tool wear measurement method:** As a result of tool wear, the micro endmill showed a reduction of the cutting diameter, as seen in the comparison of side views of a new tool and a worn tool in Fig. 4.5. This observation is used in this

work as the method to evaluate the wear of micro square endmills quantitatively. Therefore, tool wear means the reduction of the cutting diameter in the following chapters, if not otherwise mentioned.

In Fig. 4.6, a typical wear curve of the  $\varnothing$  0.5 mm square endmill is shown. After slot milling 80 mm, there was a sudden increase of tool wear; this was due to the chipping of the cutting edge corners. Afterward, the wear increased gradually due to the abrasive wear.

If the tool life criterion is defined as 20  $\mu\text{m}$  reduction of the tool cutting diameter, this endmill could only remove about 3.2 mm<sup>3</sup> material, which is far too small for industrial applications. Therefore, before conducting any further research on micromilling, the life of micro endmills has to be improved greatly first.

**Others:** The cutting temperature could not be measured during experiments due to the lack of suitable instruments.

The FEM simulation in [139] predicted that the maximum cutting temperature is about 150°C when micromilling of AISI 4340 steel. It was concluded in this paper that thermal stress is not a dominant wear mechanism in micromilling. However, no experimental verification is done to prove this simulation.

More research needs to be done to study the thermal stress in micromilling in the future.

## 4.2.2 Comparison with macro end milling

All the wear types observed in this research are also known in macro scale milling; this means that no new wear type or wear mechanism shows up in micromilling. Therefore, the knowledge gained in macro scale hard milling (e.g. wear mechanism) can be used to explain the observations in micro hard milling.

The reason why tool wear is becoming critical in micromilling is simply because of the scaling effect: the relative size between wear magnitude and tool cutting diameter increases with the decrease of tool size. As a result, the cutting edges of micro endmills wear out, the tool geometry changes significantly. This effect is graphically illustrated in Fig. 4.7a (although quantitative investigations are needed).

In this figure, the relative effect of tool wear on different sizes of micro cutting tools is demonstrated. It is assumed that tool wear causes a 20  $\mu\text{m}$  reduction of the cutting diameter at the bottom surface of the tool. It is seen that when the tool cutting diameter is bigger than 1 mm, the tool wear does not have a big influence (less than 2% in this example) on the geometry of the cutting tool. However, for an endmill smaller than 1 mm in cutting diameter, the percentage

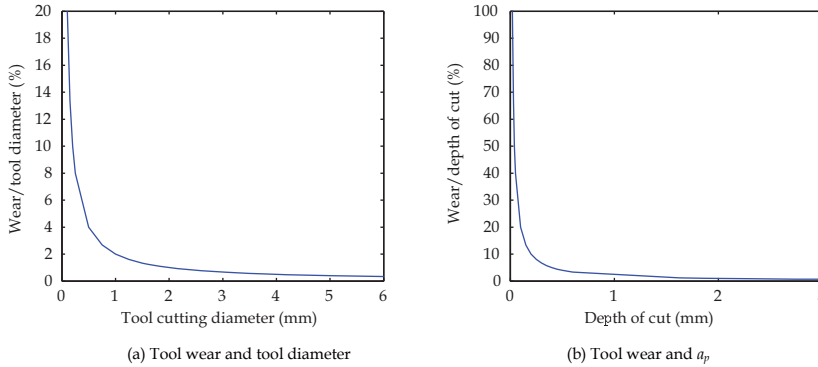


**Fig. 4.7:** Illustration of relative effect of tool wear on macro and micro endmills. Tool wear is assumed to be 20  $\mu\text{m}$ .

of chipping over tool cutting diameter increases rapidly. In this case, the tool will produce an out-of-tolerance part; therefore, its effect cannot be ignored anymore.

The scaling effect also changes the dominant wear type in micromilling of hardened tool steel. This is illustrated in Fig. 4.7b. When the cutting diameter decreases, the applicable  $a_p$  has to be decreased correspondingly to avoid premature breakage. This makes the cutting edge corners of the micro endmill the main cutting edges. The applicable  $a_p$  is directly related to the tool cutting diameter. For example, according to the recommendations of a tool supplier, when the cutting diameter ( $d$ ) of a square endmill is smaller than 3 mm,  $a_p$  can be  $0.05 \times d \sim 0.15 \times d$  for side milling. The plot in Fig. 4.7b shows that the smaller the  $a_p$  (tool diameter) is, the bigger the ratio between tool wear and  $a_p$  will be. Refer to Fig. 4.5b, when the tool wears out, the 'new' cutting edge within the  $a_p$  range is totally different from that of a new tool in Fig. 4.5a. This will influence the cutting mechanism. This also explains why flank wear cannot be used as the tool wear criterion in this work.

### 4.3 Workpiece quality

It is observed in experiments that the quality of the workpiece, in terms of form accuracy, burr formation, and surface quality, is closely related to the condition of micro endmills. The observations in these aspects are introduced in this section.

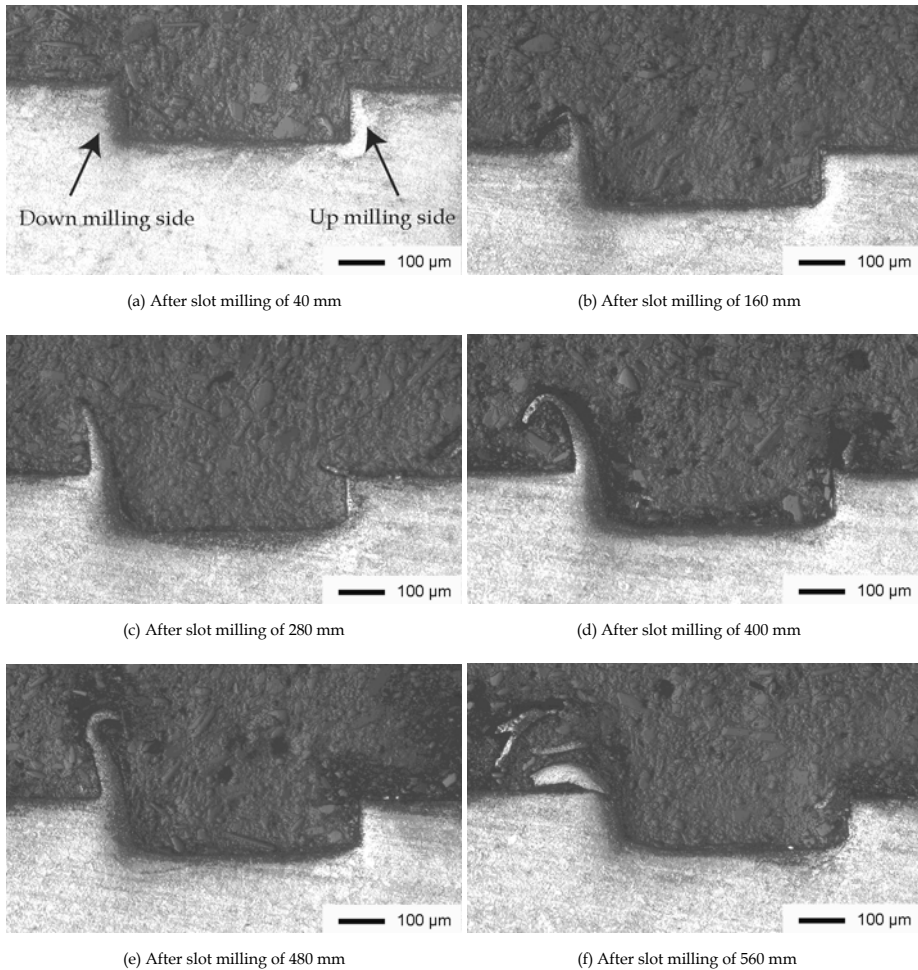


**Fig. 4.8:** Cross sections of the milled slots, form accuracy changed due to tool wear. Experimental conditions:  $v_c$  47.1 m/min,  $a_p$  0.07 mm,  $v_f$  420 mm/min, workpiece AISI H13 with 54 HRC, machine KERN EVO.

### 4.3.1 Form accuracy

In Fig. 4.8, the change of form accuracy with the progress of tool wear is illustrated. The slot shown in Fig. 4.8a was machined when the tool was new; two straight corners can be seen, which was a projection of the geometry of the new square endmill. The slot in Fig. 4.8f was machined when the tool was worn out, the rounding of the corners can be clearly seen, which corresponds to the shape of the worn tool.

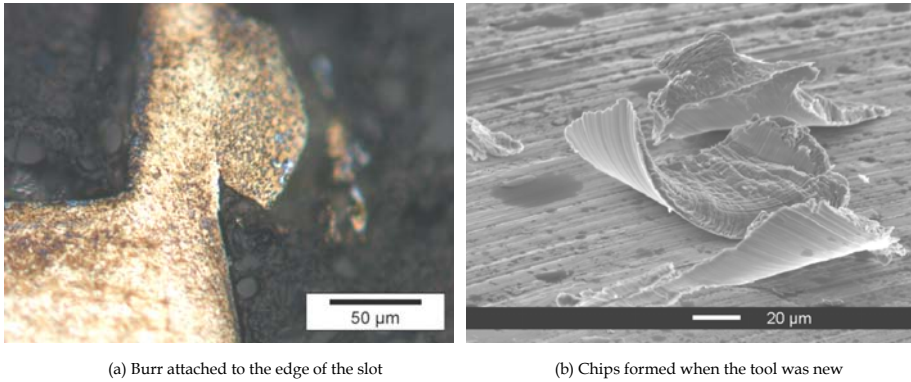


**Fig. 4.9:** Material removal at different tool conditions, (a) worn tool, (b) new tool.

For miniaturized applications, the relative accuracy (tolerance-to-feature size) is in the range of  $10^{-3}$  to  $10^{-5}$  [2]. For example the tolerance of a 0.5 mm long feature will be  $0.5 \mu\text{m}$ . This is very challenging for micromilling, and it is the reason why even an endmill which can still 'remove' materials needs to be changed, if the workpiece tolerance is violated, the cutting tool has to be changed, especially for the finishing operation. This example again demonstrates the importance of improving tool wear performance. It also shows that the tool wear evaluation method used in this research, the reduction of the cutting diameter, has its practical meaning.

### 4.3.2 Burr formation

Besides the change of form shapes, it is also observed that burr formation is closely related to the condition of micro cutting tools. Due to the curly shape of the burr, it is difficult to measure it accurately in a quantitative way; it will be described here qualitatively instead.

It can be seen from the photos in Fig. 4.8 that with the progress of tool wear, the burr volume at both sides of the machined slots increased. However, the burr volume at the down milling side was normally much bigger than that at the up milling side. This observation is consistent with the results reported in some literature [118].

The formation of burr can be examined in Fig. 4.9a, which is the zoom-in of the down milling side of a milled slot.

From this figure, the plastic deformation of the workpiece material in the burr can be clearly seen. This is because the cutting tool became blunt when worn

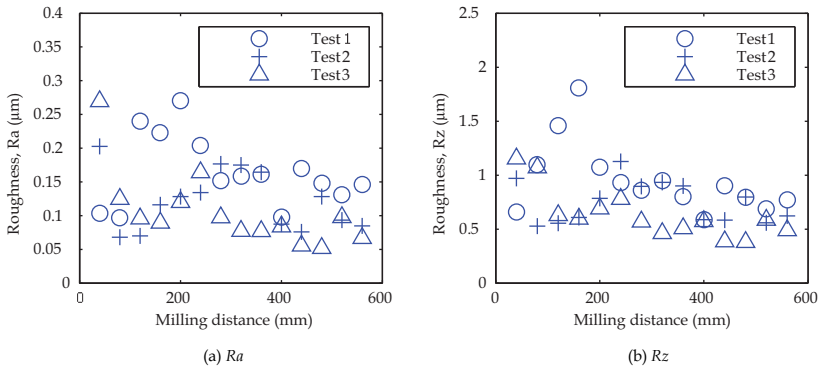


**Fig. 4.10:** Example of variation of surface roughness along milling distance, measured by Talysurf. Experimental conditions:  $v_c$  47.1 m/min,  $a_p$  0.07 mm,  $a_e$  0.5 mm,  $f_z$  0.002 and 0.007 mm, workpiece AISI H11 with 54 HRC, machine KERN EVO.

out, and the cutting mechanism was more ploughing and rubbing instead of shearing. As a result, a part of the plastically deformed workpiece material, which could not be removed in the form of a chip (see Fig. 4.9b), attached to the edge of the slot, forming burrs.

### 4.3.3 Roughness

In macro scale milling, the surface quality will deteriorate (roughness will increase) when the tool is worn out; therefore, it can be used as a criterion to evaluate the conditions of macro tools. In this work, the surface roughness milled by micro endmills was checked to see if this observation is still valid.

The roughness was measured on the bottom surface of milled slots. The measurement was taken in the middle of the slot along the feed direction. Both the stylus method (by Talysurf) and WLI (by WYKO) method were used.

In Fig. 4.10, the variation of surface roughness ( $Ra$  and  $Rz$ ) with the progress of tool wear is plotted for three tests as an example.

In general, it was observed that the surface roughness ( $Ra$ ) was better than  $0.3 \mu\text{m}$ , no matter it was formed by a new tool or a worn tool. And the surface quality is within the requirements of most mould products, which is in the range of  $0.1\sim 2.5 \mu\text{m}$  ( $Ra$ ).

Besides, unlike in macro scale milling, there is no sign of increasing roughness, neither  $Ra$  nor  $Rz$ , that can be observed in Fig. 4.10. On the contrary, it seems that the surface roughness was better when the tool wore out. This was

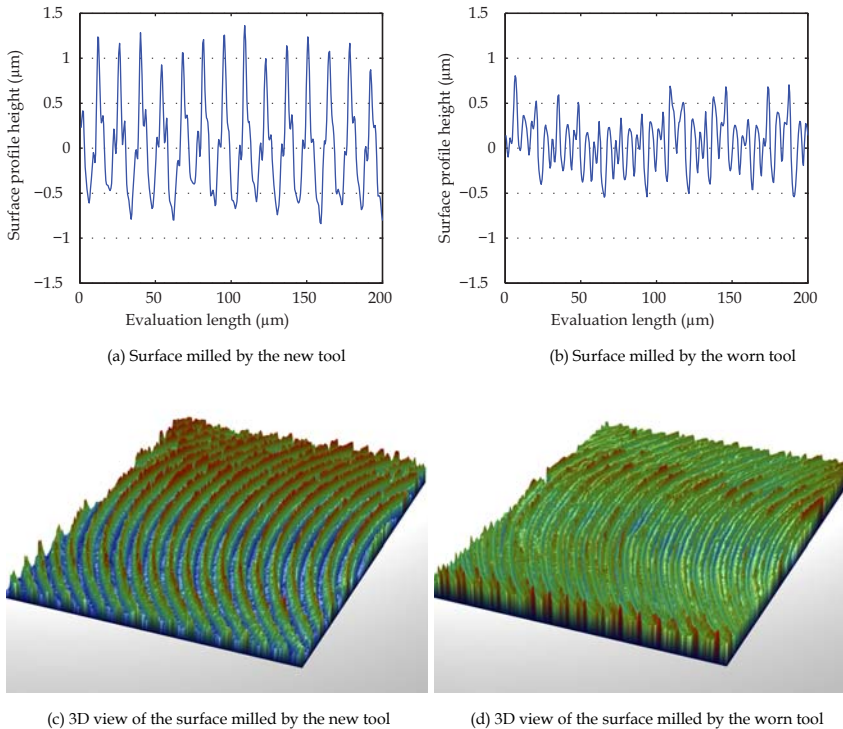


**Fig. 4.11:** Comparison of surface profiles, milled by the new tool and the worn tool. Data were extracted from the WYKO measurement.

commonly observed during the experiments in this work.

In order to find out the reason for this different observation, the surface profiles both for the new tool and the worn tool were examined. The test Nr. 2 in Fig. 4.10 is used here as an example.

It is seen from Fig. 4.11a that the surface milled by the new tool has a regular pattern. The distance between two adjacent local peaks or valleys in the horizontal direction is about  $14\ \mu\text{m}$ , which corresponds to the applied  $f_z$  ( $0.007\ \text{mm}$ ). The  $R_z$  value is the average distance between peaks and valleys in the vertical direction; it is about  $1.7\ \mu\text{m}$  for the new tool. The 3D interaction plot of this surface is shown in Fig. 4.11c; again, regular tool marks can be clearly seen.

When the tool was worn out, no clear pattern can be observed on the machined surface anymore on the machined surface, as shown in Fig. 4.11b and Fig. 4.11d. The  $R_z$  value is  $1.0\ \mu\text{m}$ , which is much smaller than that of the surface milled by the new tool. This is probably because the tool lost its sharpness when worn out;

the cutting edge radius increased, and the rounded cutting edges rubbed through the surface during machining which reduced the distance between peaks and valleys.

Above analysis shows that the surface roughness cannot be used as a criterion for tool wear in micro endmilling as is the case in macro scale milling.

Another observation from this example is that the distance between 2 adjacent local peaks/valleys equals twice the feed per tooth. This could be due to runout at the tool tip or bending of the micro endmill during machining.

Further research needs to be done in this area in order to have a better control of the surface quality.

## 4.4 Analysis

It has been shown in former section that the wear of micro endmills is the critical problem in machining of hardened tool steels. Due to tool wear, the life of micro endmills is the limiting factor for the application of the micromilling process. And the performance of the micro endmill is the direct reason for the unsatisfactory workpiece quality.

In this section, possible causes influencing the tool performance are discussed. Some tests were designed and conducted to identify the possible influencing factors. However, it is not possible or intended in this section to investigate each influencing factor exclusively; the experiments only served to identify the main contributors and to give clues about which aspects the tool performance can be improved.

### 4.4.1 Commercial tool geometry

Three properties of the micro endmill influence its performance: the substrate material, the coating, and the geometry.

For the chosen commercial micro endmills, as introduced in Chapter 1, both the substrate material (ultra-fine grain tungsten carbide) and the coating (TiAlN) are commonly used on commercial micro endmills in the market; there are no better alternatives at this moment. In this research, since all the cutting tools used in main experiments were brought from the same company, and tools used in a comparison test was produced from the same batch, the effect of the tool substrate material and the coating can be temporarily excluded. Therefore, it was decided not to investigate their effect in this research.

The geometry of the commercial tool was checked by means of FEM analysis to

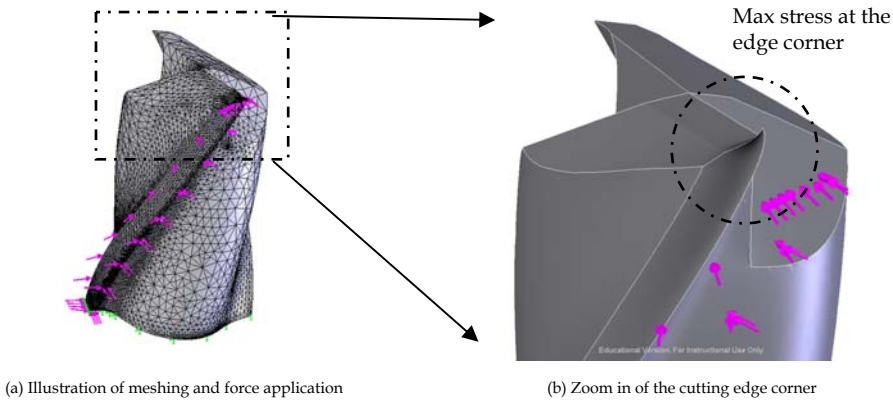


**Fig. 4.12:** CAD model of the cutting part of the micro square endmill and FEM analysis result.

study the stress distribution along the cutting edge.

Since the wear of the micro square endmill is of interest, only the cutting part of the tool was drawn in SolidWorks [140] for this analysis, as shown in Fig. 4.12a. The nominal specifications of the commercial  $\varnothing$  0.5 mm square endmill are used for the simulation; the possible geometrical deviations from the tool manufacturing process are unpredictable beforehand, and therefore not considered here.

The FEM analysis was done in COSMOSWorks [140]. Parabolic tetrahedral solid elements were used to improve the quality of meshing. Adaptive meshing was used to refine the mesh in critical regions, such as the cutting edge corners. Since cemented carbides are brittle materials, maximum stress criterion was used as the failure criterion.

During milling, the loads on the cutting tool are rather complex. Due to the existence of the helix angle and the special cutting mechanism of milling, the force (both magnitude and direction) along the cutting edge in the axial direction is not constant. Due to chip formation and friction, both normal and tangential stresses are applied on the rake face and on the flank face [9]. When the tool cutting edge radius cannot be ignored, as in the case of micromachining, a ploughing force will also be applied on the cutting edge corner [58]. The mechanism of chipping in orthogonal cutting (stress distribution in the cross section of the tool) has been studied and well understood in [9]; therefore, it is not repeated here.

In this research, the purpose is to study the influence of the tool geometry on the global stress distribution along the cutting edges. For this purpose some assumptions were made in simulation about the force on the tool. Firstly, constant forces are applied evenly along the cutting edge which simulates the

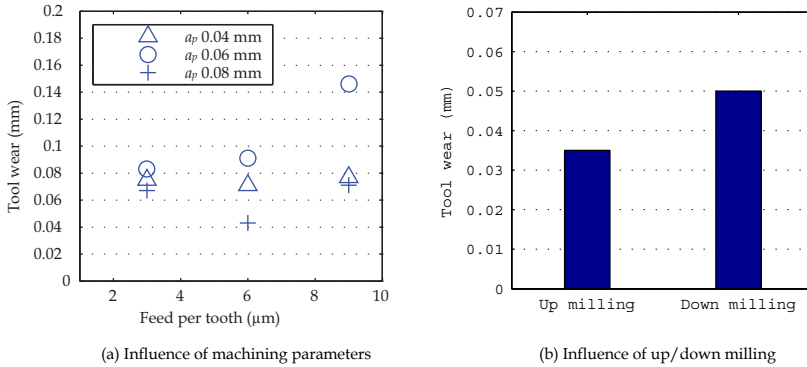


**Fig. 4.13:** Influence of cutting conditions on tool wear. Experimental conditions: (a) workpiece AISI H11 with 56 HRC,  $v_c$  56.6 m/min,  $a_e$  0.5 mm, after slot milling of 800 mm, machine Fehlmann Picomax 60 HSC; (b) workpiece AISI H11 with 54 HRC,  $v_c$  47.1 m/min,  $a_p$  0.1 mm,  $a_e$  0.12 mm,  $f_z$  0.007 mm, material removal of 20 mm<sup>3</sup>, machine KERN EVO.

worse loading situation (maximum force on the whole engaged part of the cutting edge). Secondly, the directions of the forces are assumed to be perpendicular to the rake face and the flank face of one cutting edge, as shown in Fig. 4.12a, which give a resultant force in the direction similar to that in orthogonal cutting.

The FEM analysis result, as shown in Fig. 4.12b, discloses that under the given tool geometry which is derived from macro endmills, the maximum normal stress (compressive stress) locates at the edge corner. This makes the cutting edge corners the weakest point on the cutting edges. When the localized stress due to cutting is higher than TRS of tungsten carbide, a part of the cutting edge corner will chip off.

In summary, the FEM analysis confirms the experimental observation. The current geometry of used micro endmills is one of the direct reasons for the observed tool wear and poor tool performance.

#### 4.4.2 Cutting conditions

The machining parameters and tool paths were varied to test their effect on the tool wear.

- **Machining parameters:** Slot milling tests were conducted with different combination of machining parameters; tool wear was measured and compared after removing the same amount of material. An example of the tests is shown in Fig. 4.13a. The results show that the tool wear magnitude

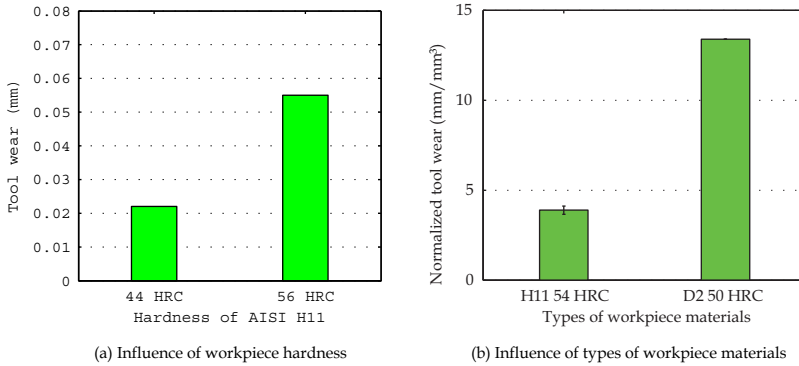


**Fig. 4.14:** Influence of workpiece properties. Experimental conditions: (a)  $v_c$  56.6 m/min,  $a_p$  0.08 mm,  $f_z$  0.009 mm, wear was measured after slot milling of 800 mm, machine Fehlmann Picomax 60HSC; (b)  $v_c$  47.1 m/min,  $a_p$  0.07 mm,  $a_e$  0.5 mm,  $f_z$  0.007 mm, wear was normalized by the material removal, machine KERN EVO.

varied when  $f_z$  or  $a_p$  changed. For example, when  $a_p$  was fixed at 0.06 mm, the tool wear increased from 83  $\mu\text{m}$  to 146  $\mu\text{m}$  when  $f_z$  changed from 3  $\mu\text{m}$  to 9  $\mu\text{m}$ .

Besides, it appears that the relationship between  $f_z$  and tool wear is a high order polynomial rather than a linear equation. This implies that there is possibility to optimize the machining parameters to achieve a minimum tool wear. In order to do so, experiments with more levels of each cutting parameter have to be conducted.

- **Tool paths:** At this stage, only up milling and down milling were compared. Side milling tests were conducted; the results are shown in Fig. 4.13b. It can be seen that there is a clear difference between the wear achieved in up milling and down milling after machining the same amount of material.

This test indicates that the tool paths have to be selected carefully in order to reduce tool wear and improve tool life. Further experimental investigation is required.

The influence of cutting conditions on tool performance will be further discussed in Chapter 5.

#### 4.4.3 Workpiece properties

From the knowledge in macro scale hard milling, it is known that the properties of the workpiece material influence the machining process. The term

machinability is often used to describe how material is more easily to be machined compared with another material. The criteria to evaluate the machinability include tool wear, surface finish, required cutting power, etc [58]. In order to test the machinability of one type of material, a series of experiments have to be conducted with carefully selected workpiece material and cutting tools because the results are highly dependent on the consistency of the quality of the workpiece material and cutting tool.

In this work, the workpiece materials are clearly defined, as described in Chapter 3. The machinability of hardened tool steels has been studied extensively in macro scale milling [101]. Therefore, it is not desired in this research to conduct a full set of experiments to repeat the reported work. Rather, limited experiments are conducted to examine if the knowledge in macro scale milling can be applied in micromilling; if not, further analysis will be required.

For example, it is known in macro scale milling that in general higher hardness will give poor machinability [58] due to the increase of yield stress, and a higher percentage (>0.22%) of carbon worsens the material machinability [141].

Simple comparison tests were conducted to examine wear of micro square endmills in machining of AISI H11 (44, 54, and 56 HRC) and AISI D2 (50 HRC). The results are shown in Fig. 4.14.

Fig. 4.14a plots the tool wear achieved when machining the same type of workpiece material but with different levels of hardness. It is seen that the wear in machining 56 HRC workpiece is about 55  $\mu\text{m}$ , which is about 2.5 times higher than that in machining 44 HRC workpiece, when all the test conditions were kept the same.

As expected, the wear in machining of AISI D2 with 50 HRC is much higher than that of H11 with 54 HRC, as shown in Fig. 4.14b. This is because of the high percentage of C and Cr in AISI D2 compared with H11.

The above experiments show that: firstly, the micromilling process is influenced by workpiece properties, and it is possible to achieve better tool performance by using appropriate workpiece materials (e.g. adjust heat treatment to vary the properties of the material); secondly, the experimental results were as expected according to the knowledge in macro scale milling, this means that the general performance of micro endmills is still influenced by macro properties of the workpiece material.

#### 4.4.4 Runout

It is commonly observed in experiments that the two cutting edges of the tested  $\varnothing 0.5$  mm endmills showed different wear magnitude. Besides, this observation

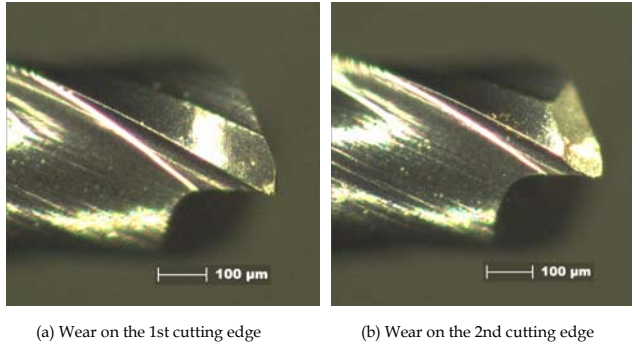


**Fig. 4.15:** Uneven wear observed on the tool cutting edges of one  $\varnothing$  0.5 mm square endmill.

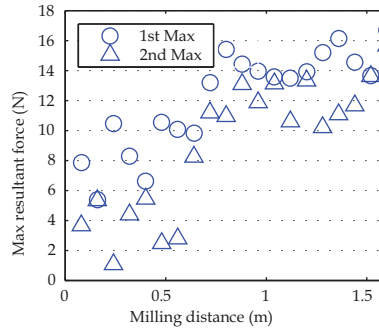


**Fig. 4.16:** Variation of maximum resultant forces on the two cutting edge of a  $\varnothing$  0.5 mm endmill. Experimental conditions: AISI H11 with 56 HRC,  $v_c$  56.6 m/min,  $a_p$  0.08 mm,  $f_z$  0.009 mm,  $a_e$  0.5 mm, machine Fehlmann Picomax 60 HSC.

is independent of cutting conditions. An example of the uneven wear is shown in Fig. 4.15. The two cutting edges belong to one cutting tool. It is clearly seen that one cutting edge (Fig. 4.15b) has much more severe wear than another cutting edge (Fig. 4.15a).

The uneven wear on different cutting edges implies that the two cutting edges had different chip loads during machining. This is confirmed by the study of the micromilling forces. In Fig. 4.16, the variation of the maximum resultant forces on the two edges of a  $\varnothing$  0.5 mm square endmill at different cutting intervals is plotted. At every measurement point, the tool was unloaded from the spindle and put back again, which would change the runout at the tool tip. It is seen in this figure that the maximum forces on the two cutting edges vary and seldom equal. At the beginning of the cut, the maximum force on one cutting edge is about 3.7 N, while it is about 7.9 N on another edge. This difference is believed to be mainly due to runout since the tool was new. With

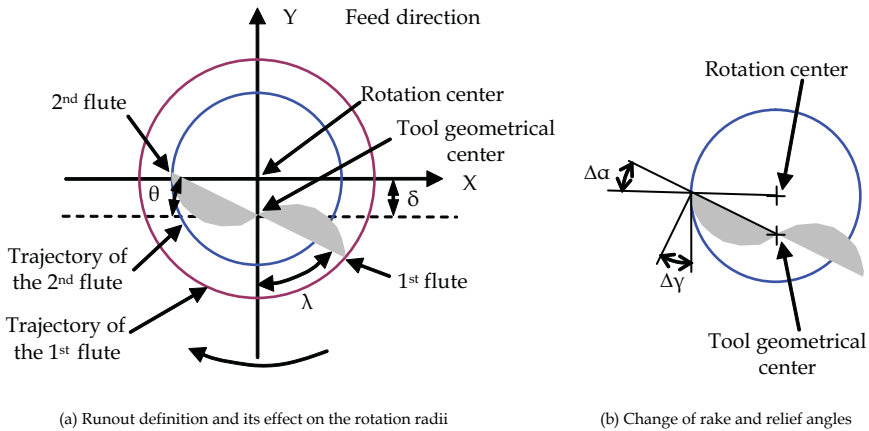


Fig. 4.17: Illustration of runout effect on micro endmills.

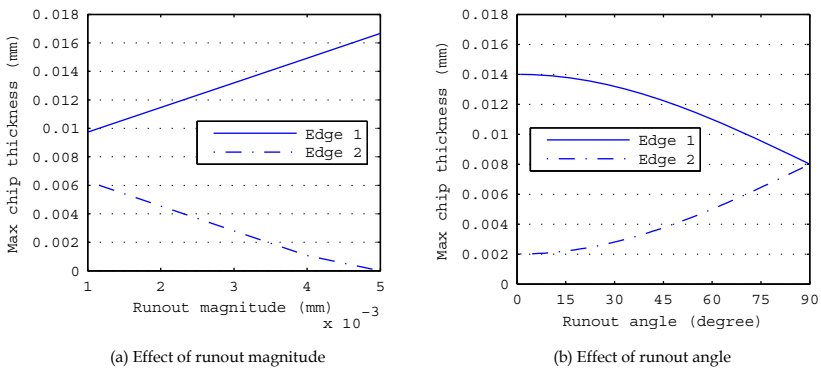
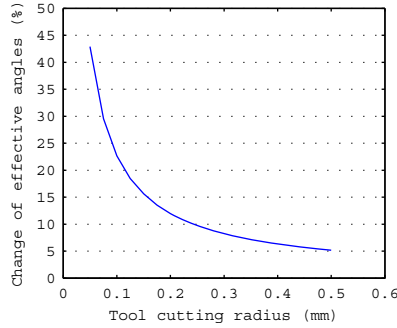


Fig. 4.18: Simulated runout effect on the maximum chip thickness on two cutting edges. Simulation conditions: (a)  $r_c$  0.25 mm,  $f_z$  0.008 mm,  $\lambda$  30°; (b)  $r_c$  0.25 mm,  $f_z$  0.008 mm,  $\delta$  3  $\mu$ m.

the usage of the tool, tool wear also contributes to the force difference.

The chip formation process was observed by means of a high speed camera, Olympus i-speed 2. It was observed through the recorded videos that chips were not formed by each cutting edge and not in every spindle revolution. It means that if the runout is larger than a certain value, one cutting edge of the cutting tool will not contact the workpiece. The study by the high speed camera gave a good indication of the runout effect on the micromilling process. However, due to the limitation of the instrument, it is difficult to conduct quantitative studies with it.

The sources of runout include: asymmetric tool geometry, imperfect tool alignment in tool holder, mismatch between tool holder and machine tool, mass



**Fig. 4.19:** Effect of runout on the tool effective rake angle. Simulation conditions:  $\lambda$  45°,  $\delta$  4  $\mu\text{m}$ , tool nominal rake angle is assumed to be 8°.

imbalance, spindle bearings, vibration of tools during machining, etc [118]. The final runout at the tool tip is an integration of all the error sources. Because of this, runout cannot be predicted beforehand. And because of the tiny dimension and complex geometry of the cutting part of micro endmills, there is no good solution to measure the dynamic runout at the tool tip online at this moment.

In macro scale milling, normally the ratio between runout and feed per tooth is small (e.g. 0.1), the runout has negligible effect on tool performance and the dimensional accuracy of the machined feature. While in micromilling, the ratio between runout and tool diameter becomes so high (e.g. 1) that it is not ignorable any more.

In this research, the influence of runout on micromilling is theoretically studied by means of a mathematical model. In this model, runout is modeled as a parallel eccentricity to the rotational axis. For simplicity, tool helix angle is not considered, and the cutting tool is assumed to have 2 cutting edges. The definition of runout magnitude  $\delta$  and runout angle  $\lambda$  is illustrated in Fig. 4.18.

The practical effect of runout is that the effective rotational radius of the two cutting edges changed. This can be calculated by

$$r_{\text{eff},i} = \sqrt{r_c^2 + \delta^2 - 2r_c\delta \cos\left(\frac{2\pi}{N}(i-1) - \lambda\right)} \quad (4-1)$$

where  $r_c$  is nominal tool cutting radius,  $N$  number of flutes,  $r_{\text{eff},i}$  is the effective tool cutting radius of tooth  $i$  ( $i=1, 2, \dots, N$ ). For a 2-flute endmill, the chip thickness at tool rotation angle  $\theta$  is calculated by

$$h(\theta) = f_z \sin(\theta) + \Delta r_{\text{eff},1,2} \quad (4-2)$$

where  $\Delta r_{\text{eff},1,2}$  is the difference between the two effective radii. Obviously, this

formula is only valid when  $h(\theta) > 0$  because chip thickness cannot be negative.

Analysis was done by using this runout model to study the effect of runout (magnitude and angle) on the micromilling process.

Firstly, the change of maximum chip thickness on the two cutting edges is studied. The results are shown in Fig. 4.18a and Fig. 4.18b. It is seen that due to runout the maximum chip loads on the two cutting edges of the micro endmill are different. When the runout angle is fixed, the difference between the maximum chip loads increases with the increase of runout magnitude, see Fig. 4.18a. For a  $\varnothing$  0.5 mm endmill with  $f_z$  of 0.008 mm, when the runout is bigger than 5  $\mu\text{m}$  in magnitude, the cutting edge 2 will have no load any more; all the cutting will be done by the edge 1. The analysis in Fig. 4.18b shows that for the given simulation conditions the difference between the maximum chip loads on the two cutting edges decreases when the runout angle increases. The difference in chip loads will be reflected on the cutting forces, which will in turn influence the tool wear.

Secondly, the change in the effective rake ( $\alpha$ ) and relief ( $\gamma$ ) angles of micro endmills due to runout, see Fig. 4.18b, is studied. The results are shown in Fig. 4.19. For one cutting edge, once the effective rake angle increases, the effective relief angle will decrease with the same magnitude. This effect is simulated versus the tool cutting radius. It is seen that the smaller the tool cutting radius is, the higher the influence of runout on the effective rake and relief angle. For example, for  $\varnothing$  0.1 mm endmill, the effective rake angle will change about 42.9%.

Besides, during machining, the cutting forces will apply a torque on the tool, which in turn will change the effective rake angle and relief angle [106].

It is known that the cutting force coefficients in the force model are dependent on the tool angles [121]. Therefore, when modeling the dynamic force in micromilling, the runout effect should be taken into account.

The runout effect is known theoretically; however, it is difficult to measure and control it in practice due to lack of suitable instruments. In this work, the static runout at the tool shank part is checked by a precision probe in each experiment. The dynamic runout at the tool tip was monitored by drilling a hole on a piece of resin, and comparing the measured hole diameter with the tool geometrical diameter (measured by an optical microscope) and the readout from the BLUM laser tool setting system. The detailed information about this method is included in Appendix A.

Runout will also be discussed in Chapter 6 and Chapter 7.

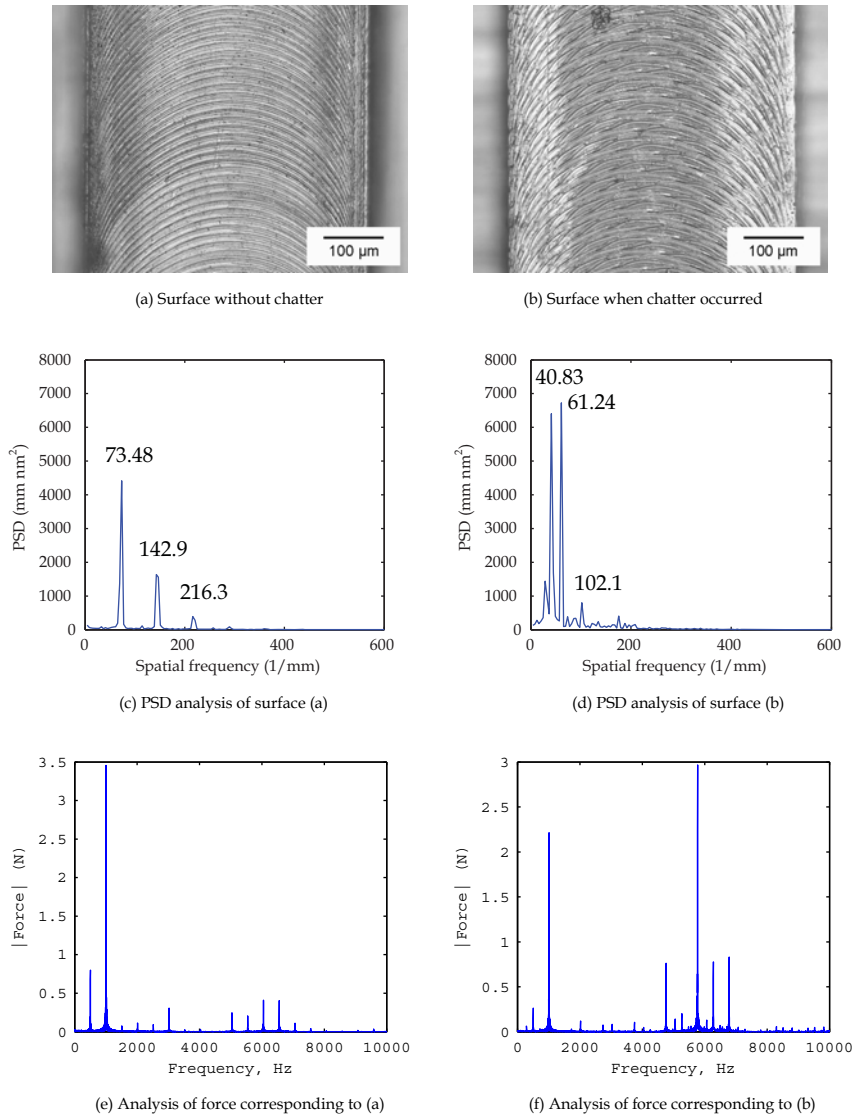


**Fig. 4.20:** Information about machined surface when (a) (c) (e) chatter did not occur and (b)(d)(f) chatter occurred. Experimental conditions: AISI H13 with 54 HRC,  $v_c$  47.1m/min,  $a_p$  0.07mm,  $a_e$  0.5mm,  $f_z$  0.007 mm, machine KERN EVO.

#### 4.4.5 Chatter effect

Chatter is an undesired phenomenon, which can damage the cutting tool,

machine tool, and produce a bad surface quality. It has been extensively studied in macro scale milling [142]. In this research, the objective is to check if chatter happens in the micromilling experiments, and if it is a reason for the wear of micro endmills.

The method used in this work to check the chatter phenomenon is by using the frequency analysis of the machined surfaces in combination with frequency analysis of the cutting force signals. By definition chatter is a transient vibration existing between the tool and workpiece during machining, and results in an irregular pattern on the machined surface [58]. Therefore, it is in theory possible to monitor the chatter effect by examining the surface formation in micromilling.

In detail, for each test, the machined surfaces were first checked by an optical microscope, and then by the WLI. By using the WLI data the spatial frequency components of the analyzed surface can be extracted. Based on this analysis, it is possible to check if any spatial frequency other than expected show up.

Afterwards, Fast Fourier Transform (FFT) analysis of the cutting forces was conducted to identify chatter frequencies, if applicable. The results of surface study and force analysis were combined in the end to draw a conclusion if chatter has occurred or not.

The effectiveness of this method is demonstrated in Fig. 4.20 by taking two tests as an example. These two tests were done under the same nominal conditions. The reasons why chatter occurred in one case while not in another are unclear. In Fig. 4.20a and Fig. 4.20b, the microscopic photos of the machined surfaces when chatter did not occur and occurred are shown, respectively. It is seen that when chatter did not occur, the machined surface showed regular patterns; the circular tool marks can be seen clearly. However, when chatter occurred, the circular tool marks are replaced by wave-like patterns.

The spatial frequencies of these two surfaces are shown in Fig. 4.20c and Fig. 4.20d, respectively. When chatter did not occur, the dominant spatial frequency corresponds to the applied  $f_z$ ; while when chatter occurred, the frequency does not relate to  $f_z$  any more. This difference can also be seen in the frequency analysis of the cutting force signals, as shown in Fig. 4.20e and Fig. 4.20f. When chatter occurred, a significant amount of energy was found at the frequency of 5800 Hz, which is near the resonance frequency of the force sensor and the workpiece. While when chatter did not occur, the dominant frequencies are the tool passing frequency, spindle frequency, and their harmonics.

The above example shows that the defined method can detect the occurrence of chatter effectively. Therefore, it is applied in each experiment to check if chatter has occurred. In the end it can be concluded that chatter seldom occurred in experiments; therefore, it is a direct reason for the wear of micro square endmills in this research. This is probably because the chosen cutting conditions

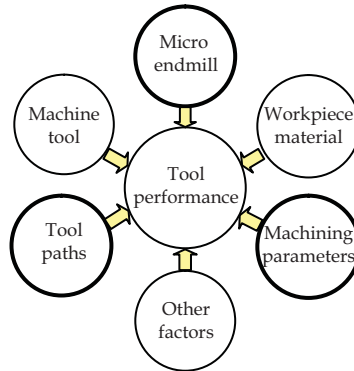


**Fig. 4.21:** Factors that influence the performance of micro cutting tools.

are within the chatter free area in the stability lobes diagram. Since the tool life is already very short under the chosen machining parameters, there is no practical meaning to test more aggressive machining parameters to check if chatter occurs or not.

However, chatter is an important issue for micromilling especially when automation of the process is of concern. Some researches have been reported in literature trying to model the chatter phenomenon in micromilling [83, 84, 143, 144]. However, these studies were only at the theoretical level; no experimental results were presented to verify the validity of the theoretically calculated stability lobes diagram for micromilling. More research needs to be done on this aspect.

## 4.5 Discussion

In this chapter, the experimental results about evaluation of the performance of micro endmills are introduced. The main wear types and mechanism of the chosen commercial square endmills under the given experimental conditions were understood. The relationship between the quality of workpiece and conditions of micro cutting tools is discussed. And the factors that caused the poor tool performance are analyzed.

In general, it is seen that micro endmills suffer from severe tool wear due to the scaling effect (relative relationship among wear, tool size, and cutting geometry); as a result, the tool life is too short to conduct a reliable cutting task.

Therefore, in order to achieve the research goal, to develop a reliable micromilling process, it is necessary to take measures to improve the tool

performance first. Only after this prerequisite is satisfied, the performance of the micromilling process can be improved.

The factors that influence the performance of micro endmills are summarized in Fig. 4.21. Of course, they can also be the directions from where the process can be improved. Due to the limitation of time and resources, decisions have to be made about which directions can be chosen as the working points in this research. The reasons are given as follows.

- **Geometry of micro endmills:** It has been discussed in Chapter 3 and this chapter that the current geometry of the tested micro square endmills is derived from macro endmills. By using such geometry, the cutting edge corners are the weakest positions along the tool cutting edges; it is one of the direct reasons for the observed tool failure. Besides, it also shows that the knowledge is not known by the commercial tool suppliers about how to design micro endmills adaptively for different applications.

Based on above reasons, the design of micro endmill is chosen as one of the working points in this research.

- **Machine tools:** It is realized that machine tools have significant influence on the micromilling process. However, since another project is running in parallel in the same department, targeting to build a micromilling machine, it was decided that the influence of machine tools is not covered in this work. The general requirements on the machine tool for micromachining can be found in [21]; some practical issues about machine tool setting can be found in Appendices A, B, and C.

Similarly, the monitoring of tool conditions is covered by another running project in the same department; therefore, it is not chosen as the working point in this research.

- **Workpiece materials:** As introduced before, the workpiece materials were pre-defined in this research; the types of materials (including the hardness) were given directly. Information about the machinability of these materials is available in macro scale machining, and has been proved to be still valid in micromilling when the general behavior of the cutting tool, rather the fluctuation, is of concern. Furthermore, it is realized in experiments that the critical problem in this research is not the high strength of these materials; rather it is how to use cutting tools with significantly reduced strength to machine these materials. Therefore, workpiece material is not chosen to be the focus for further research.
- **Machining parameters and tool paths:** These two aspects are chosen not only because they have shown significant effect on tool performance in experiments, but also because currently there is no good method or

**Table 4.1:** Recommended conditions by for  $\varnothing$  0.3mm endmills.

Tool supplier	$v_c$ (m/min)	$a_p$ (mm)	$f_z$ (mm)
A	200	<0.045	0.003-0.006
B	80	0.03	0.005
C	28	0.012	0.010
D	160	0.06	0.004

guidelines available about how to choose cutting conditions in micromilling.

As described before, at this moment the selection of machining parameters is mainly based on the recommendations of tool suppliers. To demonstrate the validity of this method, an example of the recommended cutting conditions for  $\varnothing$  0.3 mm endmills by four different tool suppliers is given in Table 4.1.

These conditions are given for tools of 2-flute TiAlN coated ultra fine grain tungsten carbide square endmills with similar cutting geometries in slot milling of hardened tool steels (52-56 HRC). It is seen in this table that there is a big difference among the recommendations from different companies; the highest  $a_p$  is about 5 times the lowest value. Furthermore, some recommended values are not achievable in practice. For example, in order to achieve 200 m/min cutting speed for a  $\varnothing$  0.3 mm endmill, a spindle speed of 210000 rpm is required, which is not commercially available in the market and certainly not commonly used in industries.

This example shows that there is a lack of knowledge about how to plan cutting conditions in micromilling. In order to achieve an optimum cutting tool life and good product quality, it is necessary to establish a knowledge based method to plan the cutting conditions for micromilling.

In summary, it was observed that the life of commercial micro endmills were too limited in machining hardened tool steels. Before any further research can be conducted on the micromilling process, it is necessary to improve the tool performance first. This can be done by redesigning the tool geometry and choosing suitable cutting conditions. Afterward, the performance of the micromilling process will be improved by knowledge-based methods to plan cutting conditions.

# Chapter 5 Influence of cutting conditions on tool wear and surface quality

In this chapter, the influence of machining parameters and tool paths on the performance of micro endmills and quality of machined surfaces is studied by means of Design of Experiments (DOE).

In Section 5.1 the motivation and objectives are introduced. The approach is described in Section 5.2. The experiments are divided into two groups for the convenience of analysis. The first group of variables includes  $a_e$  and different tool paths (raster up milling, raster down milling, and offset milling); the detailed experimental design and achieved results are presented in Section 5.3. The second group of experiments is designed to test  $v_c$ ,  $a_p$ , and  $f_z$ ; the used experimental design and results are presented in Section 5.4. This chapter ends with a discussion in Section 5.5.

The DOE method can also be used as a method to select suitable cutting conditions for micromilling when tool wear and surface finish are of concern.

## 5.1 Motivation and objectives

From the experimental results presented in the Chapter 4, the following conclusions can be drawn about the cutting conditions:

- The cutting conditions have significant effect on the micromilling process, and it is possible to improve the tool performance by optimizing the cutting conditions. In literature, this aspect has not been studied systemically yet.
- There is no good method available at this moment to select suitable cutting conditions for micromilling. Neither the recommendations of tool suppliers nor the trial-and-error method can guarantee a successful micromilling process.

Therefore, it is desired to achieve the following objectives in this chapter. Firstly, to test the influence of input variables ( $v_c$ ,  $a_p$ ,  $a_e$ ,  $f_z$ , and different tool paths) on the process response (tool wear and workpiece surface quality). Secondly, to identify the significant input variables. It is possible that many input variables will have an effect on the micromilling process; however, some variables will have more significant effect than others. By focusing on the most significant variables, the working efficiency will be improved. At last, to develop a method to plan cutting conditions in micromilling in order to achieve certain output performance, e.g. less tool wear or better surface finish.

## 5.2 Approach

There are also some requirements on the approach of the experimental study. Since it is costly and time consuming to conduct micromilling experiments, it is desired to conduct a minimal number of the experiments. Besides, because all the experiments have to be done at another location in a short period of time due to the availability of machine tools, the experiments have to be done efficiently. Furthermore, the experimental method should be reliable and widely applicable. Since it is learned from practice that the observations in milling depend on the experimental conditions, compared with specific observations, a method to select suitable cutting conditions is more preferable in this study.

Based on the objectives and requirements on the experiments, statistical Design of Experiments (DOE) is chosen as the method to plan and conduct experiments and analyze resulting data.

DOE is an efficient method to plan experiments; the data collected in experiments designed by DOE can be analyzed by means of statistical methods, based on which valid and objective conclusions can be drawn [145]. The basic approach of DOE is that multiple input variables of a tested process or system are changed deliberately by experimenters so that it is possible to observe and identify the causes for changes in the output response [146]. By choosing suitable experimental methods the amount of information that can be obtained from the experiments can be maximized. Moreover, significant input variables can be identified through a proper design; therefore, the process can be optimized by adjusting the input variables in terms of the response.

The normal procedures to conduct DOE are [146]: define the goal of the experiments and clarify the problems to be solved; decide the input variables to be varied and their levels, and the response variables to be evaluated; select the detailed experimental design (e.g. simple comparison experiments or response surface methods); conduct experiments; collect and analyze the results; and at

last conclude the experiments.

In order to improve the accuracy and minimize experimental errors, some techniques, such as replication, randomization, and blocking, can be adopted [147].

DOE can be used for many different purposes, such as to make a decision among alternatives, choose the important factors influencing a target, achieve a response criterion, maximize or minimize a target, and regression modeling. DOE also plays an important role in engineering, such as to improve the manufacturing process [146]. For example, it was used to study workpiece surface roughness in macro scale [148] and micro scale [25] milling, respectively.

### 5.3 Study of tool paths and $a_e$

The effect of tool paths on the performance of micro endmills is not seen in literature. Therefore, the first group of experiments is designed to test the influence of different tool paths on tool wear. For this purpose, side milling operation has to be adopted; therefore,  $a_e$  is also tested in this part.

Beside tool wear, another output variable is surface finish.

#### 5.3.1 Design of experiments and experimental conditions

The **goal** is to find out how the **input variables** (tool paths and  $a_e$ ) will influence the **output variables** (tool wear and workpiece surface quality), and which variable has a significant effect.

In general, tool paths in milling can be classified into three main types, namely offset (Fig. 5.1a), raster (up and down milling) (Fig. 5.1b), single direction raster (up or down milling) (Fig. 5.1c and d) [149]. Since it is desired to test the up milling and down milling separately, single direction raster instead of raster are chosen in this research, together with offset tool path.

As illustrated in Fig. 5.1a, for the offset type of tool path, the micro endmill begins the machining at the outside of the workpiece, and then continues spirally towards the middle. During machining, the direction of the endmill varies frequently. For the single direction raster tool paths (Fig. 5.1c and d), the micro endmill starts from one side of the workpiece and moves in parallel directions across the surface. During machining, the direction of the cutter does not change.

Toh [150] tested these three types of tool paths in macro scale milling in terms of tool life by using  $\varnothing$  10 mm 6-flute square endmills to machine AISI H13 with

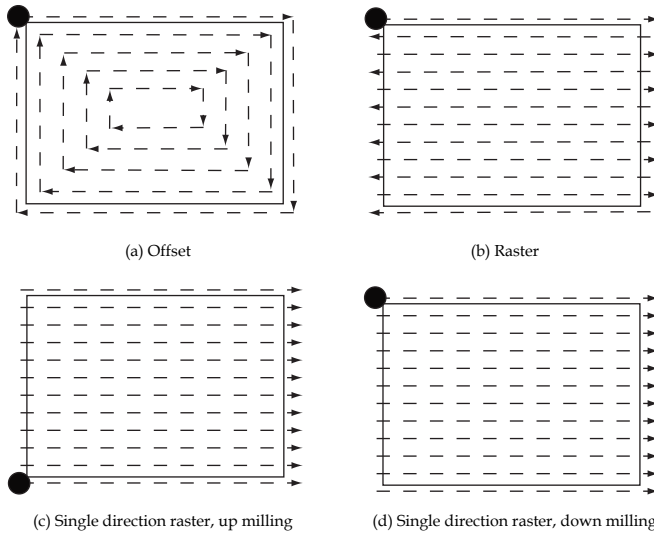


**Fig. 5.1:** Illustration of fundamental tool paths.

52 HRC. He observed that offset strategy gave the shortest tool life among the three types of tool paths. This is explained as a result of the abrupt nature of the strategy at the tool entrance and exit positions. Besides, it was found that tool life was about 15% higher when conducting up milling rather than down milling. This was explained that the force in the direction normal to cutting direction is lower in up milling than in down milling, which results in a lower temperature.

The knowledge in macro scale milling is used to design the experiments in this research. According to the first input variable, tool paths, the tests were divided into two sets: the first set is to compare single direction up milling and single direction down milling; the second set is to compare offset strategy and the single direction raster tool paths. As a result, for each set of experiments, the input variable has two levels.

The second input variable,  $a_e$ , also has two levels: the low level is  $a_e <$  tool cutting radius and the high level is  $a_e >$  tool cutting radius. The risk of less replication is that the fitted model can have a large experimental error. To minimize this error, the distance between the two levels of  $a_e$  and the high level is increased on purpose [146]. Since the cutting diameter of the tested micro endmills is 0.5 mm, the two levels of  $a_e$  are chosen to be 0.12 mm, and 0.38 mm.

For the first set of experiments,  $2^2$  factorial **experimental design** is used; two rounds of experiments under each combination of factors are conducted, therefore, there are 8 tests in total. For the second set of experiments, simple

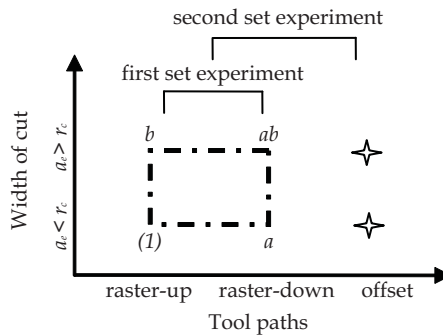


Fig. 5.2: Illustration of the experimental design.

comparative experiment is adopted; no replication is conducted, since the data from the first set of experiments can be borrowed, so only 2 additional tests are required.

The experimental design is chosen as such because it was observed in macro scale milling that the offset strategy showed a significant difference from the single direction raster strategy. If it is found during tests that the observations in micromilling are significantly different from that in macro scale milling, additional tests will be added to investigate the process further. The whole experimental design is illustrated in Fig. 5.2.

Followed [146], some conventions for the  $2^2$  factorial experiments are introduced: the two input factors are referred to  $A$  (tool paths) and  $B$  ( $a_v$ ).  $AB$  stands for the interaction. The low and high levels of input variables are denoted by '-' and '+'. The treatment combinations are represented by lowercase letters, as shown in the Fig. 5.2. Therefore  $a$  stands for the combination of  $A$  at the high level and  $B$  at the low level,  $b$  stands for  $A$  at the low level and  $B$  at the high level,  $ab$  stands for both  $A$  and  $B$  at the high level, and  $(1)$  is used to represent both variables at the low level.

**Experimental setup:** The cutting tools used in the experiments were manufactured from the same batch. The workpiece material was AISI H11 with 54 HRC. The machine tool was the KERN EVO located at Cranfield University.

The static runout at the end of tool shaft was controlled to be better than  $1 \mu\text{m}$ . Tool overhang length (distance between the tool tip and the tool holder end) was kept about 35 mm for each test. MQL was used in all experiments.

The tool wear was checked by a SEM microscope. The workpiece surface quality was checked by the Talysurf CCI white light interferometer. The cutting force was measured by the Kistler MiniDym 9256C2.

**Table 5.1:** Cutting conditions.

Test Nr.	Tool path	$a_e$ (mm)	$v_c$ (m/min)	$a_p$ (mm)	$f_z$ (mm)	MR (mm <sup>3</sup> )	Machining time (s)
1, 6	single direction raster, up milling	0.12	47.1	0.1	0.007	20	238
3, 7	single direction raster, up milling	0.38	47.1	0.1	0.007	20	75
4, 8	single direction raster, down milling	0.12	47.1	0.1	0.007	20	238
2, 5	single direction raster, down milling	0.38	47.1	0.1	0.007	20	75
9	offset, down milling	0.12	47.1	0.1	0.007	20	238
10	offset, down milling	0.38	47.1	0.1	0.007	20	75

**Table 5.2:** Summary of measured tool wear, unit:  $\mu\text{m}$ .

Factor		Combination	Replicate		Average
A	B		I	II	
-	-	A low, B low	38	30	34.0
+	-	A high, B low	48	57	52.5
-	+	A low, B high	35	29	32.0
+	+	A high, B high	96*	40	40.0
Offset	-		72		72.0
Offset	+		49		49.0

\* Strange result, excluded from further analysis

The cutting conditions are listed in the Table 5.1. All the cutting conditions, except the tool paths and  $a_e$ , are fixed. For a fair comparison, the material removal (MR) was kept the same, 20 mm<sup>3</sup>, for every test.

The spindle speed was chosen to be 30000 rpm, which gives a relatively small motion error according to a former test done by researchers at Cranfield University. The choice of  $f_z$  took into account the MCT effect and tool premature breakage. When  $f_z$  is chosen to be 7  $\mu\text{m}$  the MCT only influences about 11% of the tool immersion angle at most.

### 5.3.2 Results in terms of tool wear

The tool wear in the first and second set of experiments will be introduced separately.

**The first set of experiments:** The results of tool wear measurements are summarized in Table 5.2. In general, the repeatability of the measurements was acceptable. However, tool wear in test Nr. 2 was 96  $\mu\text{m}$ , about 2.4 times higher

**Table 5.3:** Analysis of Variance for the Experiment.

Source	SS	df	MS	F	Prob>F
A	351.125	1	351.125	15.52	0.0170*
B	105.125	1	105.125	4.65	0.0974**
AB	55.126	1	55.125	2.44	0.1936
Error	90.500	4	22.625		
Total	601.875	7			

\*Significant at the 5% and 10% level.

\*\*Significant at the 10% level.

than that in test Nr. 5, which was conducted under the same cutting conditions. The cutting tool used in test Nr. 2 was checked, and it was found that premature breakage happened on the cutting edges. This was confirmed by the measured force data: the resultant force in test Nr. 2 was about 1.5 times higher than that in test Nr. 5. Therefore, test Nr. 2 was excluded from further analysis.

The average main effect of  $A$  can be calculated as:

$$A = \frac{1}{2} \{[ab - b] + [a - (1)]\} \quad (5-1)$$

$$= (40 - 32 + 52.5 - 34) / 2 = 13.25$$

The average main effect of  $B$  can be calculated as:

$$B = \frac{1}{2} \{[ab - a] + [b - (1)]\} \quad (5-2)$$

$$= (40 - 52.5 + 32 - 34) / 2 = -7.25$$

The interaction effect  $AB$  can be calculated as:

$$AB = \frac{1}{2} \{[ab - b] - [a - (1)]\} \quad (5-3)$$

$$= (40 - 32 - 52.5 + 34) / 2 = -5.25$$

The effect of  $A$  (tool path) is positive; this means that increasing  $A$  from the low level (up milling) to the high level (down milling) will increase tool wear. The effect of  $B$  ( $a_e$ ) is negative; this means that increasing  $a_e$  will have an effect of decreasing tool wear. The interaction effect appears to be small relative to the two main effects.

Analysis of Variance (ANOVA) was conducted to determine which variables are likely to be important; the result is summarized in Table 5.3.

The ANOVA table consists of the information about the variability due to the differences among the input variable  $A$ ,  $B$ , and their interaction  $AB$  [151]. As it is

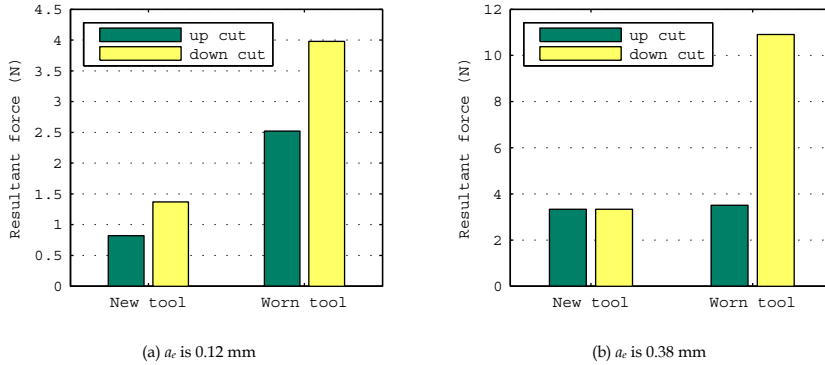


Fig. 5.3: Comparison of measured resultant forces in up milling and down milling.

seen in Table 5.3 it contains six columns: the first column is the source of the variability; the second column is the sum of squares (SS); the third column is the degrees of freedom (df); the fourth column is the mean squares, which is calculated by  $SS/df$ ; the fifth column shows the  $F$  statistics, which are the ratios of the mean squares; the sixth column presents the  $p$ -values for the  $F$  statistics. The  $F$  statistics determines whether the observed relationship between the input and output variables happens by chance; the  $p$ -value is the probability of obtaining an  $F$  statistic at least as extreme as the one that was actually observed, assuming that the null hypothesis is true.

It can be seen in Table 5.3 that the  $p$ -values for factor  $A$  is 0.017, which means an  $F$  statistics as extreme as the observation (15.52) would occur by a chance of less than 17 in 1000 times if all the levels of  $A$  have the same influence on tool wear. When the critical value is set to be 0.05, since the  $p$ -value (0.017) is smaller than the critical value, it can be concluded that  $A$  (tool path) has a significant effect on tool wear.

The same analysis was conducted on the variable  $B$  and the interaction  $AB$ . It is found that  $B$  ( $a_e$ ) is significant at the critical level of 0.10, and the interaction  $AB$  is not significant. The ANOVA result confirms the initial interpretation of the results.

The reasons for the observations that tool wear is less when up milling and bigger  $a_e$  are used can be explained from the following aspects.

- Cutting forces: It was found that the resultant force is much lower in up milling than that in down milling, as shown in Table 5.3, no matter which level of  $a_e$  is considered. Higher forces increase the chance of chipping, and speed up the wear rate.

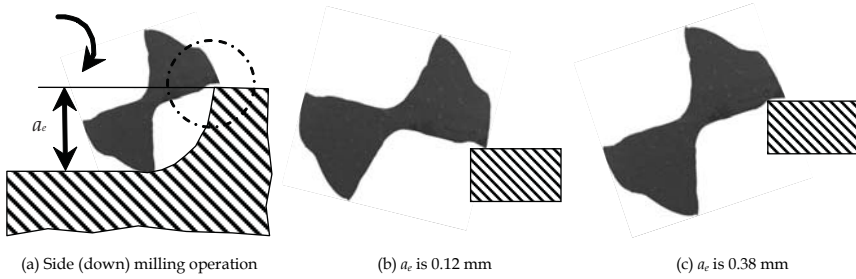


**Fig. 5.4:** Illustration of the initial contact point when different  $a_e$  is used.

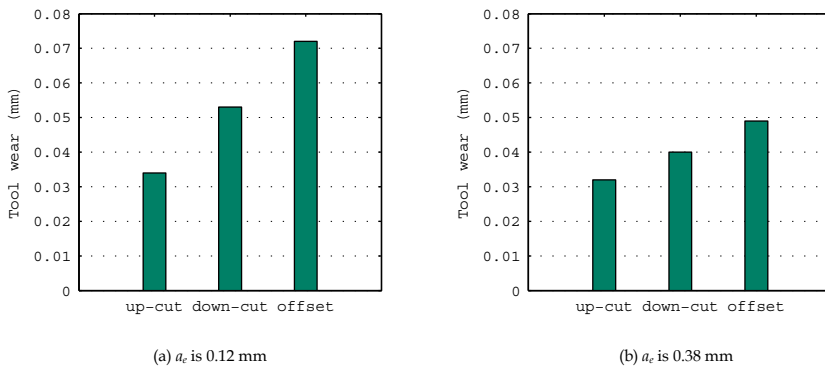


**Fig. 5.5:** Comparison of the tool wear when different tool paths are used.

- **Machining time:** As shown in Table 5.1 the machining time is about 3 times shorter when  $a_e$  is 0.38 mm instead of 0.12 mm when the same amount of material is machined. This means the contact time between the cutting tool and the workpiece is shorter when a bigger  $a_e$  is used. This decreases the tool wear rate.
- **Initial contact point between the tool and workpiece:** As illustrated in Fig. 5.4, for down milling, when  $a_e$  is 0.12 mm, the geometrical centre of the micro endmill is outside the workpiece, the initial contact point between the tool and the workpiece is at the very end of the cutting edge. While when  $a_e$  is 0.38 mm, the tool centre is inside the workpiece, the initial contact point is away from the edge, which is less prone for the edge chipping. This effect has been studied in macro scale milling [152].

**The second set of experiments:** The result of in terms of tool wear is shown in Fig. 5.5. From these figures it can be seen that the offset tool path showed the highest wear magnitude among all the three types of tested tool paths. This observation is consistent with that in conventional high speed hard milling

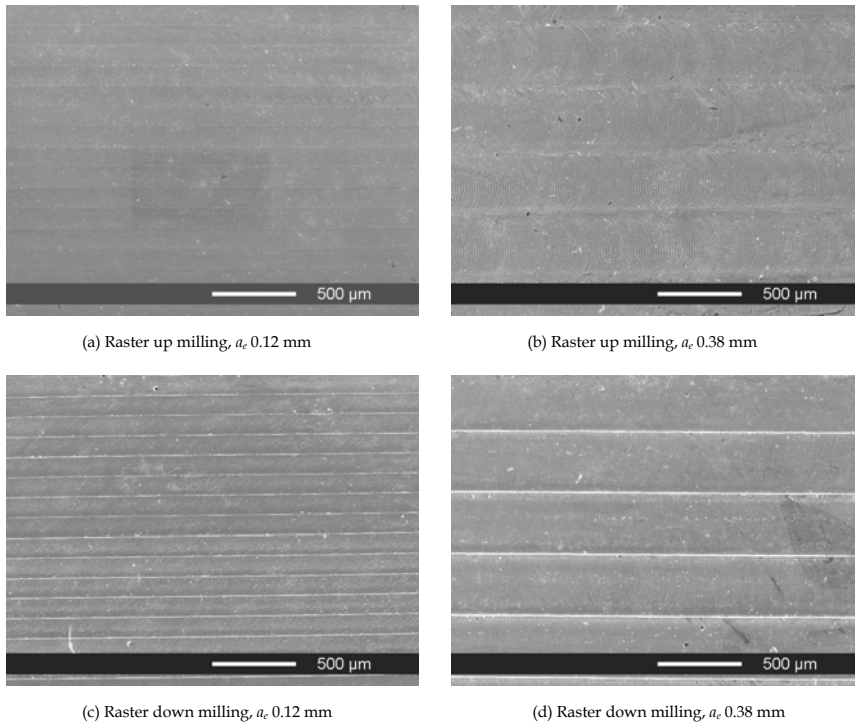


**Fig. 5.6:** Machined surfaces under different conditions.

[150]. One possible explanation is that in the offset tool path, the cutting tool has to change cutting directions often and abruptly. The load on the tool fluctuates frequently due to the tool path and the machine dynamics.

In summary, in the experiments to test the influence of tool path on wear of micro square endmills, similar observations are seen as those in macro scale milling [150]. To achieve less tool wear, raster up milling and bigger  $a_e$  are preferable.

However, it does not mean the bigger the  $a_e$  is, the longer the tool life will be. This study only indicates the general trend of the influence of the  $a_e$  on tool wear. In order to find an optimum value of  $a_e$  in terms of tool wear, a further study with more levels of  $a_e$  can be conducted. It is not included in this work.

### 5.3.3 Results in terms of surface finish

Again the results and analysis are presented separately for two sets of experiments.

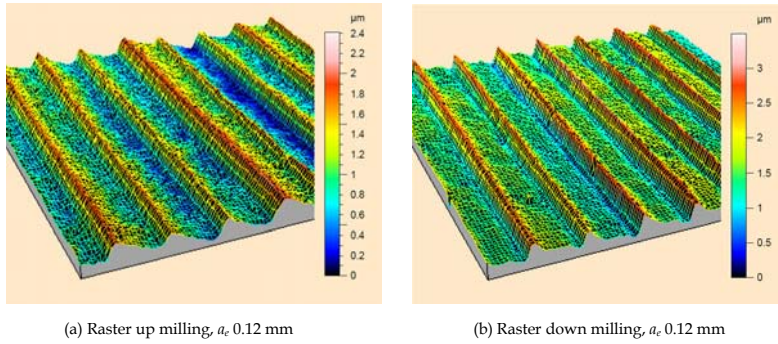


**Fig. 5.7:** 3D view of the machined surfaces by different tool paths.

**The first set of experiments:** The machined surfaces by the new cutting tools under different combination of tool paths and  $a_e$  were first visually checked by means of SEM. Some examples are shown in Fig. 5.6. Two types of tool marks can be seen on the surfaces: the tool marks in the feed direction (horizontal direction in the figures) correspond to the applied  $f_z$ . Tool marks in the cross feed direction (vertical direction in the figures) correspond to the applied  $a_e$ .

Furthermore, the following aspects can be concluded in Fig. 5.6:

- The boundary between 2 consecutive tool marks in the cross-feed direction is much smoother in up milling (Fig. 5.6a and Fig. 5.6b) than that in down milling (Fig. 5.6c and Fig. 5.6d). This is confirmed by the 3D view of the machined surface measured by the WLI, as shown in Fig. 5.7. This is probably due to the fact that the force in down milling is higher than that in up milling, see Fig. 5.3. The micro endmills bent more when down milling was conducted, which left deep groove patterns on the surface. This will increase the roughness of the surface.
- It is also noticed that in up milling, the roughness in the feed direction and the cross feed direction looks similar; while in down milling, the roughness in the cross feed direction looks higher than that in the feed direction. This is confirmed by quantitative measurement.
- When different  $a_e$  is used, the surface appears different (e.g. Fig. 5.6c and Fig. 5.6d). However, it is difficult to judge from these photos which surface will have higher roughness. In order to evaluate the surfaces accurately, quantitative criteria have to be used.

The surface quality was evaluated by WLI; a  $20\times$  lens was used, and the field of view was about  $0.85 \times 0.9 \text{ mm}^2$ . To avoid the error in surface measurement due to the measurement direction, the amplitude parameter  $Sa$  is used. Amplitude

**Table 5.4:** Summary of measured  $S_a$ , unit:  $\mu\text{m}$ .

Factor		Combination	Replicate		Average
A	B		I	II	
-	-	A low, B low	0.35	0.38	0.365
+	-	A high, B low	0.41	0.47	0.440
-	+	A low, B high	0.52	0.69	0.605
+	+	A high, B high	1.54*	0.73	0.73
Offset	-		0.44		0.44
Offset	+		1.19		1.19

\*Strange result, excluded from further analysis

**Table 5.5:** Analysis of Variance for the surface finish.

Source	SS	df	MS	F	Prob>F
A	0.01921	1	0.01921	4.79	0.0938*
B	0.13520	1	0.13520	33.73	0.0044**
AB	0.00151	1	0.00151	0.38	0.5722
Error	0.01603	4	0.00401		
Total	0.17195	7			

\*Significant at the 10% level.

\*\*Significant at the 5% and 10% level.

parameters are a class of surface finish parameters characterizing the distribution of heights [153].  $S_a$  is the arithmetic mean deviation of the surface. The results of measurements are summarized in Table 5.4. Again, test Nr. 2 gave a strange result ( $S_a$  1.54  $\mu\text{m}$ ), and it was excluded from further analysis.

The average main effect of  $A$  on  $S_a$  can be calculated as:

$$A = \frac{1}{2} \{[ab - b] + [a - (1)]\}$$

$$= (0.73 - 0.605 + 0.44 - 0.365) / 2 = 0.1$$

The average main effect of  $B$  can be calculated as:

$$B = \frac{1}{2} \{[ab - a] + [b - (1)]\}$$

$$= (0.73 - 0.44 + 0.605 - 0.365) / 2 = 0.265$$

The interaction effect  $AB$  can be calculated as:

$$AB = \frac{1}{2} \{[ab - b] - [a - (1)]\}$$

$$= (0.73 - 0.605 - 0.44 + 0.365) / 2 = 0.025$$

The effect of  $A$  (tool path) is positive; this suggests that increasing  $A$  from the low level (up milling) to the high level (down milling) will deteriorate the

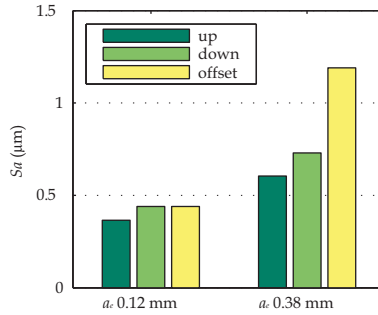


Fig. 5.8: Comparison of achieved  $S_a$  by different tool paths.

surface finish. The effect of  $B$  ( $a_e$ ) is also positive; this suggests that increasing  $a_e$  will have an effect of decreasing surface quality. The interaction effect appears to be small relative to the two main effects.

ANOVA is conducted in terms of surface finish, and the result is listed in Table 5.5. From the ANOVA result, the  $p$ -value of variable  $A$  is smaller than 0.1, and  $p$ -value of variable  $B$  is smaller than 0.05, while the  $p$ -value of interaction is much bigger than 0.1. Therefore, it can be concluded that  $a_e$  and tool paths have the statistically significant effect on the surface finish.

**The second set of experiments:** The surface  $S_a$  achieved by the offset strategy is compared with the surfaces machined by the other two types of tool paths. The result in Fig. 5.8 shows that the offset strategy in general gives the worst surface finish no matter which  $a_e$  value was chosen. This is because the offset strategy was basically down milling and the direction of the force applied on the tool changed frequently during machining due to the change of the cutting direction.

In summary, it is observed that the combination of the single direction raster up milling tool path and a smaller  $a_e$  gives the best surface finish. One possible reason is that the force in this combination is smaller which results in less bending of the tool during machining.

## 5.4 Study of $v_c$ , $a_p$ , and $f_z$

In this group of experiments, the input variables are  $v_c$ ,  $a_p$ , and  $f_z$ , the output variables are tool wear and surface finish.

It should be pointed out that these experiments are not designed to increase the understanding to the fundamental cutting mechanism of micromilling. The

purposes are rather to identify the significant variables and find out the optimum machining parameters which give the minimum tool wear or better surface finish under the given experimental conditions.

### 5.4.1 Design of experiments and experimental conditions

**Experimental design:** The effect of some machining parameters has been discussed briefly in Chapter 4. It is seen in Fig. 4.13a that  $f_z$  has an effect on the tool wear and it seems that the relationship between  $f_z$  and tool wear is rather high-order than a first order relationship. This implies that there exists a possibility to minimize the tool wear by adjusting the machining parameters.

According to the purpose of the experiments, Central Composite Design (CCD) was chosen in this group of experiments. CCD is an efficient design method for fitting second-order response surface equation [147]. The general expression for a central composite design is described by the model

$$E(y) = \beta_0 + \sum_{i=1}^k \beta_i x_i + \sum_{i=1}^k \beta_{ii} x_i^2 + \sum_{i < i'} \beta_{ii'} x_i x_{i'} \quad (5-4)$$

where  $E(y)$  is the expected response,  $x_i$  is the  $i^{\text{th}}$  input variable,  $\beta_0$  is intercept,  $\beta_i$  is the coefficient for the linear term,  $\beta_{ii}$  is the coefficient for the quadratic term,  $\beta_{ii'}$  is the coefficient for the interaction, and  $k$  is the number of input variables.

The experiments include three parts:

- Factorial points: to fit a first-order surface.
- Center points: to provide measure of error variance.
- Axial points: to fit the second-order surface.

The number of center points and the value of the axial points should be chosen carefully to give the design certain properties such as orthogonality (simplify the computation and make the estimates uncorrelated with each other), rotatability (let the estimated response independent on the design orientation), and uniformity of precision [147]. There are guidelines available for the choice of the design parameters in [147].

In this work, there are 3 input variables, and each variable has 2 levels, so there are 8 ( $2^3$ ) factorial points. Besides, 6 center points and 6 axial points are chosen to make the design a uniform precision design. Therefore, there are 20 ( $8 + 6 + 6$ ) experiments altogether.

An advantage of this experimental design is that if the quadratic coefficients are not significant, a first order equation can still be used.

**Table 5.6:** Coding of the input variables.

Coded design variables	Input variables		
$x_i$	$v_c$ (m/min)	$a_p$ (mm)	$f_z$ (mm)
-1.6818	20.7	0.02	0.002
-1	31.4	0.04	0.004
0	47.1	0.07	0.007
1	62.8	0.10	0.010
1.6818	73.5	0.12	0.012

The sequence of experiments is randomized to minimize possible system errors.

The selection of levels for  $a_p$  and  $f_z$  was based on former experiments, taking into account tool premature breakage and MCT effect, and covering the possible application range. The maximum  $v_c$  is limited by the achievable spindle speed. The coding of the input variables and corresponding values are listed in Table 5.6 and Table 5.7.

**Experimental conditions:** All the endmills were manufactured from the same batch to avoid large geometrical deviations. It is shown in former experiments that micro endmills with small wedge angles (large positive radial rake angles or relief angles) will show severe tool wear, the tested endmills were examined and selected carefully before the experiments to minimize tool pre-damage and big positive rake angles.

The workpiece material was AISI H11 with 54 HRC. The machine tool was KERN EVO located at the Mondragon University in Spain. As introduced in Chapter 3, this machine showed errors in the setting of workpiece coordinate due to thermal elongation of the spindle; to minimize the possible influence of this error, the tool wear results were corrected by normalizing the wear value by MR. MQL was used for all experiments.

In order to minimize the influence of complex workpiece geometries and machine tool errors on tool wear, simple slot milling was conducted. To minimize the influence of runout, the relative position between the tool holder and the spindle was kept the same for each test. The static runout at the end of the tool shaft was controlled to be better than 1  $\mu\text{m}$ . For a fair comparison, the same nominal amount of workpiece material (20  $\text{mm}^3$ ) was planned at each different combination of cutting conditions. The real MR was corrected by measuring the depth of the milled slots.

The tool wear was measured by the JEOL JSM-6300 SEM. The bottom surface roughness of milled slots was measured by the Talysurf and the WYKO NT 3300 WLI.

Table 5.7: Experimental conditions and tool wear.

Exp. Nr.	Coded values			Actual values			Response
	$x_1$	$x_2$	$x_3$	$v_c$ (m/min)	$a_p$ (mm)	$f_z$ ( $\mu\text{m}$ )	Tool wear/MR ( $\mu\text{m}/\text{mm}^3$ )
1	-1	-1	-1	31.4	0.04	4	4.05
2	1	-1	-1	62.8	0.04	4	6.98
3	-1	1	-1	31.4	0.10	4	4.41
4	1	1	-1	62.8	0.10	4	3.65
5	-1	-1	1	31.4	0.04	10	4.56
6	1	-1	1	62.8	0.04	10	2.89
7	-1	1	1	31.4	0.10	10	3.71
8	1	1	1	62.8	0.10	10	2.23
9	0	0	0	47.1	0.07	7	3.89
10	0	0	0	47.1	0.07	7	4.04
11	0	0	0	47.1	0.07	7	3.69
12	0	0	0	47.1	0.07	7	4.52
13	0	0	0	47.1	0.07	7	4.14
14	0	0	0	47.1	0.07	7	2.86
15	-1.6818	0	0	20.7	0.07	7	3.51
16	1.6818	0	0	73.5	0.07	7	5.28
17	0	-1.6818	0	47.1	0.02	7	3.09
18	0	1.6818	0	47.1	0.12	7	1.33
19	0	0	-1.6818	47.1	0.07	2	5.79
20	0	0	1.6818	47.1	0.07	12	3.95

## 5.4.2 Results in terms of tool wear

**Overview of the data:** The results of the tool wear measurement are shown in Table 5.7. It is seen that tool wear varied from 1.33 to 6.98  $\mu\text{m}/\text{mm}^3$ , depending on the combination of machining parameters.

Before conducting further analysis, the quality of the data was checked by means of 4-plot, namely Run sequence plot, Histogram plot, Lag plot, and Normal probability plot [145]. If the four underlying assumptions hold, then probabilistic predictability can be achieved: The ability to make probability statements not only about the process in the past, but also about the process in the future. The 4-plot showed that the process was in statistical control. Therefore, these data can be used for further analysis. The detailed 4-plot is included in the Appendix D.

**The model:** The experimental results given in Table 5.7 have been used to calculate the coefficients of the quadratic model, (5-4), by means of the least square method. After calculation, the model is

**Table 5.8:** Analysis of Variance for the tool wear.

Source	SS	df	MS	F	Prob>F
Total	28.5893	19			
Regression	23.4604	9	2.6067	8.27	0.0158*
Lack of fit	3.5527	5	0.7105	2.25	0.1971
Pure error	1.5762	5	0.3152		

\*Significant at the 5% level.

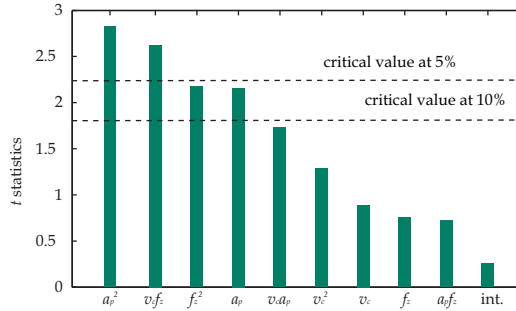


**Fig. 5.9:** *t* statistics of the coefficients for the regression model.

$$\hat{y} = 0.94 + 0.81 \times 10^{-1} v_c + 0.95 \times 10^2 a_p - 0.33 f_z + 0.98 \times 10^{-3} v_c^2 - 0.60 \times 10^3 a_p^2 + 0.46 \times 10^{-1} f_z^2 - 0.93 v_c a_p - 0.14 \times 10^{-1} v_c f_z + 0.20 \times 10^1 a_p f_z \tag{5-5}$$

where  $\hat{y}$  is the estimated yield.

The coefficient of determination,  $R^2$ , is normally used to measure how well the found regression fits the observed data. In this case, the  $R^2$  is 0.821, which shows that about 82.1% of the variation in yield (tool wear) is accounted by the model.

The result of ANOVA analysis is shown in Table 5.8, which shows the statistical significance of the regression by comparing the mean square of regression against the estimated value of the pure error. The  $p$ -value for the  $F$ -regression is smaller than the critical value 0.05, while the  $p$ -value for the  $F$ -lack-of-fit is bigger than 0.05, therefore the yield of the experiments can be well described by the proposed quadratic function.

The significance of the coefficients in (5-5) was tested by conducting  $t$  statistics. If the  $t$  observed value of the coefficient is greater than the critical value at a significance level, it can be concluded that this coefficient is statistically significant, and this coefficient is useful in estimating the value of tool wear. The result of  $t$  statistics is plotted in Fig. 5.9. It is seen that  $a_p$  and  $f_z$  have a greater effect on yield than  $v_c$ .

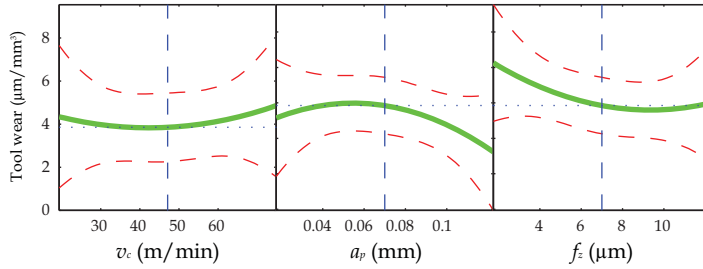


**Fig. 5.10:** Study of the effect of each input variable on tool wear by using the regression model.

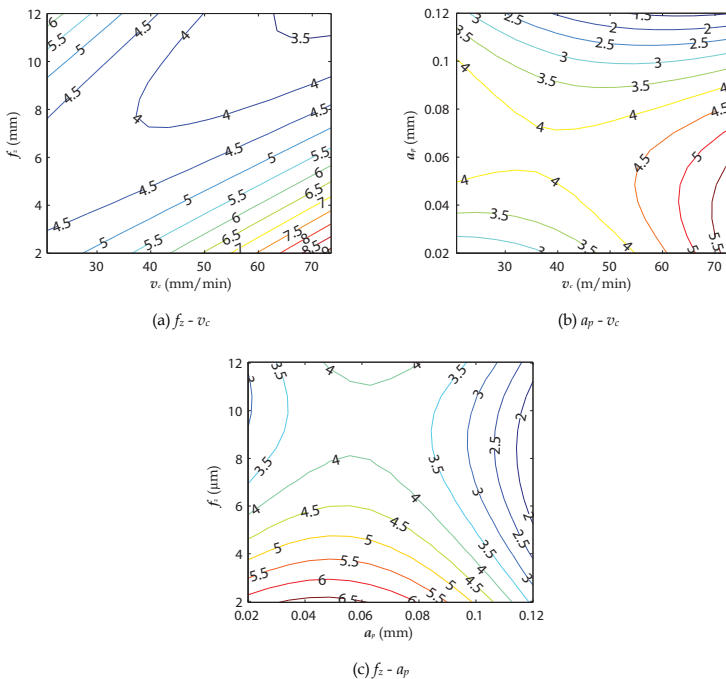


**Fig. 5.11:** Interaction effect of input variables on tool wear.

The regression model is used to study the effect of each input variable on the yield. In Fig. 5.10 each plot is the effect of one input variable by fixing the other two input variables at the center positions. For example, the first plot shows the variation of the tool wear with the change of  $v_c$  when  $a_p$  is 0.07 mm and  $f_z$  is 0.007 mm. The 95% confidence intervals are also plotted on this figure with dashed lines. It can be seen again in this figure that within the tested process window,  $v_c$  does not have significant effect on the tool wear; the tool wear first increases with the increase of  $a_p$ , and then decreases when  $a_p$  is further increased;

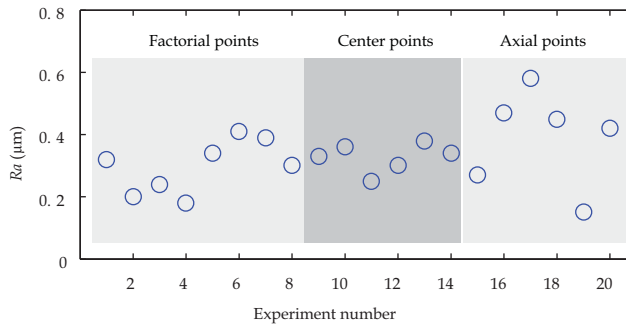


Fig. 5.12: Summary of the  $R_a$  values from 20 tests.

for  $f_z$ , it is seen there exists an optimum value of  $f_z$  which gives the minimum tool wear.

The optimum  $f_z$  value and the achieved tool wear can be calculated by taking differentiation of (5-5) with respect to  $f_z$ . For example, when  $v_c$  and  $a_p$  are fixed at 47.1 m/min and 0.07 mm respectively, the calculated  $f_z$  is 0.0094 mm, and the tool wear is 3.82  $\mu\text{m}/\text{mm}^3$ .

In Fig. 5.11, each plot shows the interaction of two input variables by fixing the third variable at the center position. By using these plots, it is possible to plan the machining parameters in the areas that the tool wear magnitude is minimized.

The reasons for the observed trend can be explained from several aspects. As described in the Section 5.4.1, the MR was kept the same for each test, therefore the higher  $v_c$  and  $a_p$  are, the shorter the machining time will be. It is possible that the tool wear will increase when further increasing the  $v_c$ ; however, due to the limitation of the available spindle speed, it was not possible to test tool performance at a high speed range. This should be included in future research. When increasing  $a_p$ , the unit force on the cutting edge is kept the same, but the machining time is short, so it is beneficial for the tool wear. However, increasing  $f_z$  has different effect. Initial increase of  $f_z$  enhanced the MRR; further increase of  $f_z$  over a critical value led to the load on the tool edge being higher than the TRS of the tool material, which resulted in severe wear at the cutting edges.

It has to be pointed out that the error in the  $a_p$  due to the thermal elongation of the spindle could have an influence on the interpretation of the results although the wear magnitude has been normalized by the real MR in each test. However, the experimental design method has been proved to be useful for the planning of machining parameters in micromilling.

Table 5.9: Analysis of Variance for the  $R_a$ .

Source	SS	df	MS	F	F tabulated 5% level
Total	0.2097	19			
Regression	0.1369	9	0.0152	7.09*	4.77
Lack of fit	0.0621	5	0.0124	5.78*	5.05
Pure error	0.0107	5	0.0021		

\*Significant at 5% level.

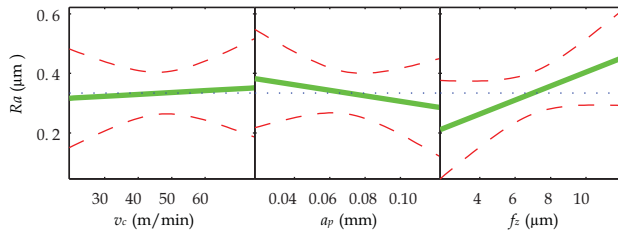


Fig. 5.13: Study of the effect of each input variable on  $R_a$ .

### 5.4.3 Results in terms of surface finish

The roughness of the bottom surfaces of the milled slots in each test was measured in order to investigate the relationship between the input variables and the surface quality. Only the first slot in each test was used; therefore, it is assumed that the surface was formed when the tool was new.

Because slot milling operation was conducted, only tool marks corresponding to the applied  $f_z$  show up on the machined surface. The roughness,  $R_a$ , was measured by the WYKO WLI. An overview of the result is given in Fig. 5.12.

A quadratic model was first proposed to describe the relationship between the input variables and the response ( $R_a$ ). The coefficients of the quadratic model were fitted by the least square method. After regression, the model is:

$$\hat{y} = 0.30 + 0.15 \times 10^{-2} v_c - 0.73 \times 10^{-1} a_p + 0.54 \times 10^{-1} f_z - 0.21 \times 10^{-4} v_c^2 + 0.51 \times 10^2 a_p^2 - 0.39 \times 10^{-2} f_z^2 - 0.27 \times 10^{-1} v_c a_p + 0.42 \times 10^{-3} v_c f_z + 0.56 \times 10^{-1} a_p f_z \quad (5-6)$$

The coefficient of determination,  $R^2$ , is 0.653, which shows that the model only explains 65.3% of the variability in the roughness. The ANOVA analysis, in Table 5.9, confirms that the lack of fit of this model is significant. Therefore, the relationship between machining parameters and surface finish in this research cannot be explained by this quadratic model. Detailed examination of the data shows that the roughness values at the center points varied substantially. This

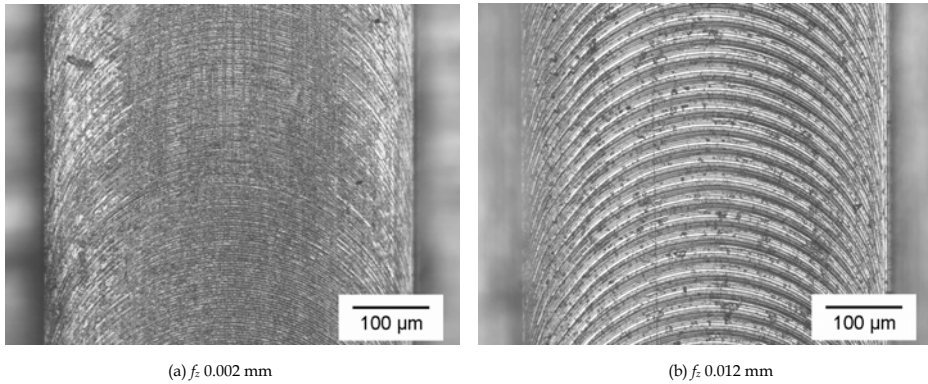


**Fig. 5.14:** Microscopic pictures of the milled surface under different  $f_z$ .

means some factor is missing, which has an important influence to the surface formation. Further experiments are needed to find out the reason.

In this work, linear regression was conducted instead to study the general trend of the input variables on the roughness. The variation of  $Ra$  with each input variable at a fixed value (center points) of the other two input variables is plotted in Fig. 5.13. The 95% confidence intervals are also plotted on this figure.

Although it seems that  $v_c$  and  $a_p$  have an effect on  $Ra$ , the effect is not significant when the 95% confidence interval is taken into account. A clear relation can be observed between  $f_z$  and  $Ra$ . In general,  $Ra$  increases with the increase of  $f_z$ . For example, when  $f_z$  changes from 2 to 12  $\mu$ m,  $Ra$  increases from 0.22 to 0.45  $\mu$ m.

This increase of surface roughness with the increase of  $f_z$  is mainly due to the increase of the distance between tool marks when a bigger  $f_z$  is used. This can be seen clearly from the pictures of the milled surfaces machined by different  $f_z$ , as shown in Fig. 5.14. This observation is same as the practical knowledge in macro scale milling.

In summary, when planning the machining parameters in micromilling, in order to achieve a good surface finish, a smaller  $f_z$  should be used. However, a smaller  $f_z$  means the MRR will be lowered if all other parameters are fixed, which is not economical for industrial applications. A trade-off between the surface finish and the productivity has to be made according to the situation.

## 5.5 Discussion

In this chapter, the effect of machining parameters and tool paths on tool wear

and workpiece surface finish is studied by means of DOE.

The experiments were divided into two groups:

- The first group of experiments was designed to test three fundamental tool paths (single direction up milling, single direction down milling, and offset strategy) and  $a_e$ . The  $2^2$  factorial design and simple comparative experiments were used.

It is observed that single direction up milling performs best among the three types of tool paths in terms of tool wear. This observation is consistent with the observation in conventional hard milling. Besides, a bigger  $a_e$  is preferable for a longer tool life because the machining time is short and the initial contact point between the tool and the workpiece is away from the edge.

For surface finish, up milling and smaller  $a_e$  are preferable because the cutting force in down milling is higher. This will cause bending of micro endmills during machining, leaving a deep groove-pattern on the machined surface.

- The second group of experiments was designed to test  $v_c$ ,  $a_p$ , and  $f_z$ . A quadratic relation was proposed based on a previous observation; in detail, Central Composite Design method was used.

For tool wear, a regression model was found by means of least square method. The  $R^2$  value was 0.821; the ANOVA analysis confirms the regression was statistically significant at 5% level. This model was used to study the effect of each input variable on tool wear. Optimum combination of machining parameters can be found to achieve minimum tool wear.

For surface roughness, it was found that the quadratic model was not accurate enough; therefore, the main effect of the input variables on  $Ra$  was studied by means of linear regression. It was found that  $f_z$  has the most significant effect on  $Ra$ : surface roughness increases with the increase of  $f_z$ . This observation is consistent with the practical knowledge in macro scale milling.

It has to be pointed it out that the error in the setting of  $a_p$  could influence the interpretation of the results although the tool wear data have been normalized by the real MR.

As discussed before, the observation in micromilling is experimental conditions dependent. Therefore, compared with the specific observations, it is more preferable and meaningful to find a widely applicable method to plan the micromilling process. In this research, the DOE method has been proved to be valid and can be used for such purposes.

# Chapter 6 Design of micro endmills

In this chapter, the design of micro square endmills is presented. In Section 6.1, the motivation and approach are introduced. The design guidelines are described in Section 6.2. In Section 6.3, the tool geometry is theoretically designed by means of a 3-section cantilever beam model and a FEM tool model. The newly designed micro square endmills were manufactured and validated through experiments; these two aspects are introduced in Section 6.4 and 6.5, respectively. In Section 6.6 the advantages and disadvantages of the new design is discussed.

## 6.1 Motivation and approach

**Motivation:** It has been discussed in Chapter 3 that the geometry of the tested commercial micro square endmills is derived from the geometry of macro endmills, and it has been proved both experimentally and theoretically that such geometry led to severe wear at the cutting edge corners of micro endmills at the early stage of machining. As a result, the tool life was shortened significantly and the workpiece quality was not reaching the requirements. In order to achieve a reliable tool life the performance of the micro endmills must be improved significantly. One way to do this is through proper design of the tool geometry.

Some work has been done to improve the geometry of micro endmills as is observed in literature. Fang et al. [35] compared three different types of geometries for the cutting part of micro endmills in terms of stiffness and tool life, namely traditional geometry, semi-circle (cross-section) based geometry, and triangle based geometry. They found that the semi-circle based design has higher rigidity and wear resistance over the other two, and is more suitable for micromachining of soft materials (e.g. brass) and endmills smaller than 0.2 mm in cutting diameter. Uhlmann et al. [14] designed micro endmills with the objective to improve the stability of the endmill. With FEM analysis, it could show that stress on the cutting part of the tool could be improved by shortening

tool cutting part and introducing a continuous change-over into the taper section. The newly designed tools were tested on tool steel PM X190CrVMo 20 with 62 HRC. The workpiece surface roughness ( $R_z$ ) was used as the tool life criterion; however, wear on the cutting edges was not discussed.

Current work in literature was merely focused on the improvement of tool strength in order to prevent tool breakage and less on the wear of cutting edges and its possible remedy.

It has been observed in this research that the main tool failure type is the wear of the cutting edges; premature tool breakage seldom happened on the tested  $\varnothing$  0.5 mm endmills. Therefore, the focus of tool design in this research will be to improve the wear resistance at the cutting edge corners.

**Approach:** The choice of tool geometry depends on many aspects; three main factors, which are relevant to this research, are as follows:

- **Workpiece materials:** As described in Chapter 1 micro square endmills showed different dominant wear types in machining low strength materials and high strength materials. This implies that the tool geometry should be designed depending on the workpiece material.
- **Product geometry:** The tool geometry is also required by the geometry of the product. For example, to machine a deep groove will require cutting tools with a long underneck length; while to machine a surface the tool should be capable of making a good surface finish.
- **Operations:** Different operations require different characteristics of tools. During the roughing operation, the endmill should be robust enough to remove a bulk of material in a short time. While in the finishing stage, the endmill should be able to keep its shape during machining to guarantee a good accuracy of the workpiece.

In this work, the current micro endmills show an acceptable surface finishing capability; however, the tool life is too short to conduct a reliable cut. Therefore, in a first stage it is desired to design the tool geometry to reduce the tool wear and achieve a reasonable tool life especially in roughing and reroughing operations. Besides, the design process will target on hard milling applications because hardened tool steels are the workpiece materials. Furthermore, because the goal of this research is to gain fundamental understanding of the process, simple slot milling and side milling tests are conducted where the achievable aspect ratios (underneck of the tool) are not a limiting factor.

It is not the purpose of this research to deliver commercially ready-to-use cutting tools; rather, it is preferable to generate knowledge about how the geometrical features of the micro endmill will influence its performance. The

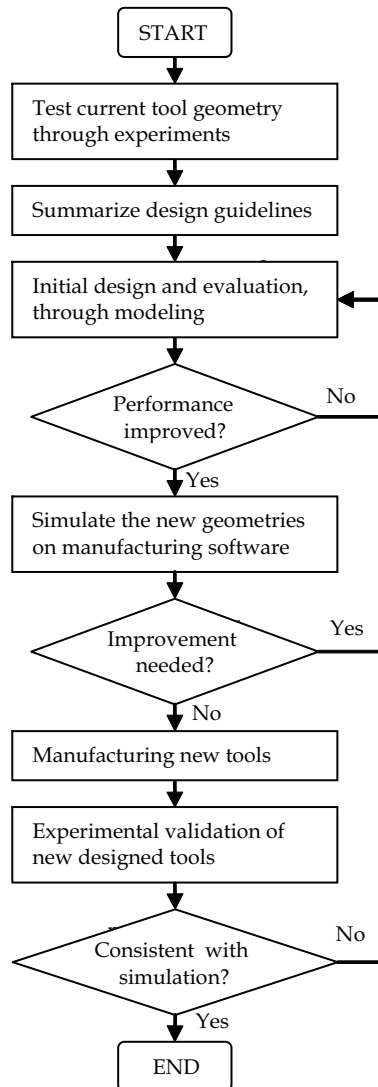


**Fig. 6.1:** Process of designing the micro endmill.

approach should be widely applicable and can be used by industries to design the tool properly when the requirements from the application are clearly defined.

The flow chart in Fig. 6.1 summarizes the whole design process; it is briefly explained as follows:

- The guidelines for the endmill design are generated based on experimental observations. In this research, the strength at the edge corners and the stiffness of the tool will be the main aspects to be improved.
- Theoretically study the influence of tool geometrical features on its performance. After knowing this, the values for these features can be chosen adaptively according to the practical requirements. In this research, the design is divided into two parts, namely the neck part and the cutting part, according to their different contributions to the total tool performance. The design of the neck geometry is done by means of a 3-section cantilever beam model; the design of the cutting part is done by FEM analysis.
- Simulate the theoretical design on tool manufacturing software. This step is as important as the theoretical tool design. The limitation of the tool manufacturing process can be checked at this stage. Further improvements may be needed. Afterwards, the newly designed endmills are manufactured.
- Validate the new design through experiments in comparison with the commercial tool geometry. In this research, the validation tests are done under different cutting conditions, with different types of materials, and on several machines. Besides tool stiffness, tool wear and tool life, the quality of workpieces is also used as an evaluation criterion.

The whole design process is demonstrated on  $\varnothing$  0.5 mm square endmills. However, the generated knowledge and developed method will be applicable for the design of smaller endmills and ball-nose endmills.

## 6.2 Design guidelines

Based on the experimental observations with the commercial micro endmills, the following guidelines are derived in this research:

- **High stiffness:** Because of the small dimension of micro endmills, the stiffness of the tool is low. This will result in the bending of the tool during machining. Low stiffness can also lead to vibration of the tool and chatter.
- **Elevated strength at the cutting edge corners:** The dominant wear type of commercial tools is wear at the edge corners, which is the main reason for the limiting tool life. To improve tool life and achieve a reliable process, the strength at the edge corners must be improved.
- **Simple geometry:** It is observed that due to the limitation of the manufacturing process (grinding), complex features cannot be realized accurately on the micro endmills. As a result, there will be some deviations of the real tool geometry from the design; the designed geometrical features

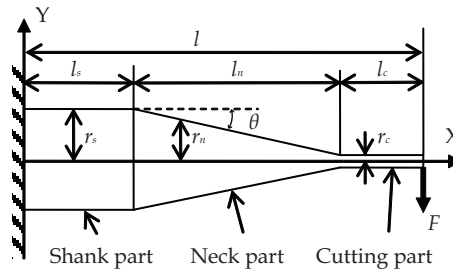


Fig. 6.2: Schematic overview of the micro endmill geometry.

cannot be fully achieved.

- **Runout compensation:** Due to runout, the two cutting edges of the micro endmill showed uneven wear. Once one edge fails due to overloading, the tool has to be changed. It will be preferable if the runout can be evenly distributed on the cutting edges of the endmill.
- **Avoidance of stress concentrations:** Due to the special geometry of micro endmills, there are several discontinuities in the cross section of the tool body. The transitions among these parts have to be smoothed.

## 6.3 Design of micro square endmills

As described in the last section, the main improvements of the new tool will be the stiffness and strength at the edge corners. From preliminary analysis, these two aspects are mainly related to the neck part and the cutting part of the tool, respectively. Therefore, the design of the micro endmill is divided into two parts, the neck part and the cutting part.

### 6.3.1 Design of the neck part

The typical micro endmill geometry is illustrated in Fig. 6.2. It composes three parts, which have been introduced in Chapter 3. Some commercial tools also have an undercut at the end of the cutting part near the neck part in order to avoid possible contact between the tool and workpiece. It is not drawn in this figure, and not considered in this research. The reason for this decision will be explained later.

**Examination of four possible geometries:** The neck geometry in Fig. 6.2 is a conical shape, which is a traditional shape for commercial tools. However, it

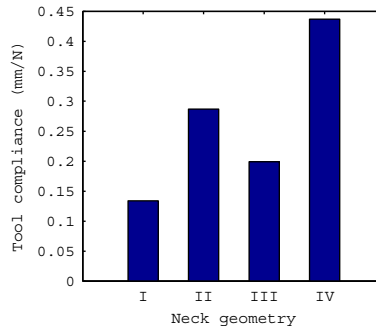


**Fig. 6.3:** Calculated tool compliance of 4 types of neck geometries: I conical; II parabolic; III fourth power; IV exponential. Simulation conditions:  $r_s$  1.5 mm,  $r_c$  0.05 mm,  $l_c$  1 mm.

does not need to be limited to the conical shape as long as the neck fulfills the required functions (to bridge the shank part and the cutting part). Therefore, before designing the neck part, 3 other possible geometries, namely full parabolic shape (Shape II), fourth power shape (Shape III), and exponential shape (Shape IV), were compared on the tool stiffness, in comparison with the conical shape (Shape I). The method and results are shortly introduced as follows.

The 4 types of neck geometries were first described by mathematical equations in Matlab, and then exported to Ansys for FEM analysis. For a fair comparison,  $l$ ,  $l_c$ ,  $r_s$  and  $r_c$  were kept same for all tools. The variables are the neck shape,  $l_n$ , and  $l_s$ . To exaggerate the difference among these scenarios, the analysis was done on  $\varnothing$  0.1 mm endmills with 1 mm underneck length, the calculated tool compliance is shown in Fig. 6.3.

It is seen from Fig. 6.3 that the conical shape has the highest stiffness among all the tested geometries. This is because there is more material presented at the neck part for this geometry than any other geometry. Besides, the conical shape is simple and easy to manufacture. Therefore, it was chosen as the basic neck geometry for the newly designed micro endmills.

**Study of geometrical features that influence tool stiffness:** Using Euler beam model the analytical model of the tool with a tapered neck part is described. The equations are derived in Equation 6-1 and 6-2 and a Matlab routine was written for design purpose. By using this model, the value of each geometrical feature and their effect on the tool stiffness can be tested.

As described in Chapter 1, the cantilever beam model has been widely used in the modeling of micro endmills, where the neck geometry is approximated as a beam with a constant cross section. While in this work, a beam with a variable

cross section is used for the neck part, this is close to the reality.

For the convenience of simulation, some assumptions have to be made. First, the tool is rigidly connected to the machine at the shank end; the stiffness of the machine including tool clamping is considered to be infinite. Second, tool geometrical deviations from the manufacturing process are not considered. Third, the fillet between the cutting part and the neck part is omitted for simple computations. Fourth, for the cutting part, an equivalent cutting radius ( $r_{c,eq}$ ) is used instead of the nominal value in order to take into account the effect of flutes. The equivalent cutting radius is calculated from the area of the cross section of the cutting part in the CAD model. Fifth, undercut part is not considered. At last, the cutting length is assumed to be equal to the underneck length. These omitted features are not dominant features on the tool body. They will influence the tool performance to a certain extent; however, the general tool performance is mainly decided by the three main parts. As long as the general behavior of the micro endmill is of concern, these assumptions can be made.

Referring to Fig. 6.2, the deflection  $\delta(x)$  at the tool tip under a force  $F$  can be calculated by using the cantilever beam theory:

$$EI(x) \frac{\partial^2 \delta(x)}{\partial x^2} = -M \quad (6-1)$$

where

$$M = F(l-x), \quad I(x) = \frac{\pi r^4(x)}{4}, \quad r(x) = \begin{cases} r_s & 0 \leq x \leq l_s \\ r_s - (x-l_s) \tan \theta & l_s < x < l_s + l_n \\ r_c & l_s + l_n \leq x \leq l \end{cases}$$

After solving differential equations,

$$\delta(x) = \begin{cases} \frac{F}{6EI_s} x^3 - \frac{FL}{2EI_s} x^2 & 0 \leq x \leq l_s \\ -\frac{F}{2ab^3(1-bx)} - \frac{c}{6ab^2(1-bx)^2} + c_1''x + c_2'' & l_s < x < l_s + l_n \\ \frac{F}{6EI_c} x^3 - \frac{FL}{2EI_c} x^2 + c_1'''x + c_2''' & l_s + l_n \leq x \leq l \end{cases} \quad (6-2)$$

where  $a = \frac{\pi}{4} E(r_s + l_s \tan \theta)^4$ ,  $b = \frac{\tan \theta}{r_s + l_s \tan \theta}$ ,  $c = Fl - F \frac{r_s + l_s \tan \theta}{\tan \theta}$ ,  $c_1''$ ,  $c_2''$ ,  $c_1'''$ ,  $c_2'''$

are constants and can be calculated when the tool geometry and material are defined. The stiffness of the endmill is calculated by dividing the applied force over the displacement at the tool tip.

The specifications of commercial tools are used for simulation. The conditions and results are shown in Fig. 6.4. In the catalogue of the commercial tool, two values for the cutting length are available, namely 0.8 mm and 3mm; both of

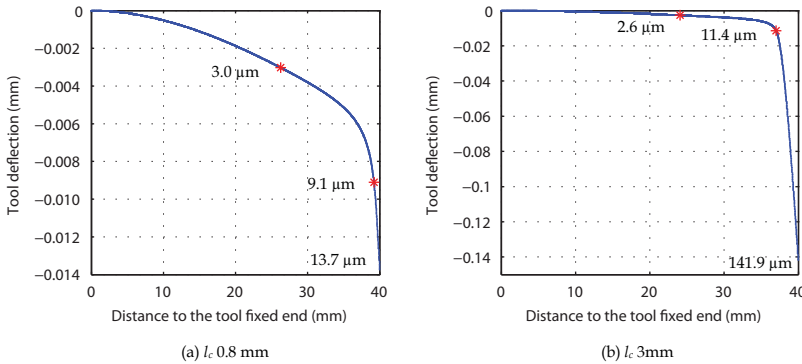


**Fig. 6.4:** Simulated deflection of micro endmills. The transition between different parts of the tool is marked by a star. Simulation conditions:  $l = 40$  mm  $r_s$  is 3 mm,  $r_c = 0.25$  mm,  $r_{c,eq} = 0.21$  mm,  $\theta = 12^\circ$ ; 10 N force.

them were used in the simulation.

It is seen in Fig. 6.4a that when  $l_c$  is 0.8 mm the total deflection at the tool tip is about 13.7  $\mu\text{m}$  under a 10 N force; therefore, the stiffness of the tool is 0.73 N/ $\mu\text{m}$ . This total deflection can be decomposed into contributions from the 3 parts of the tool. The deflection at the end of the shank part is 3.0  $\mu\text{m}$ , which is 21.9% of the total deflection; the corresponding values for the neck part and cutting part are 6.1  $\mu\text{m}$  (44.5%) and 4.6  $\mu\text{m}$  (33.6%), respectively.

It is seen that when the cutting part is short (e.g. 0.8 mm), the neck part is the main contributor to the low tool stiffness. The reason is that the length of the neck (12.9 mm) is much longer than that of the cutting part. This analysis shows that special attention has to be paid to the neck geometry in order to improve the tool stiffness

When the cutting length is 3 mm, the tool stiffness is calculated to be 0.07 N/ $\mu\text{m}$ . In this case, the cutting length will contribute to 92.0% of the total tool deflection, as shown in Fig. 6.4b. Therefore, unless required by the product geometry, micro endmills with short cutting lengths should be chosen in micromilling to minimize possible tool bending.

Because the stiffness of the micro endmill is so low, the tool will bend during machining. The magnitude of bending is normally higher than the value of the undercut (normally several micrometers). Therefore an undercut on micro endmills cannot avoid the possible contact between the tool and workpiece. On the contrary, it will weaken the tool and lower the tool stiffness. Based on these reasons, the undercut section becomes irrelevant and is therefore omitted.

**Improvement of the neck geometry:** There are two possibilities to improve the

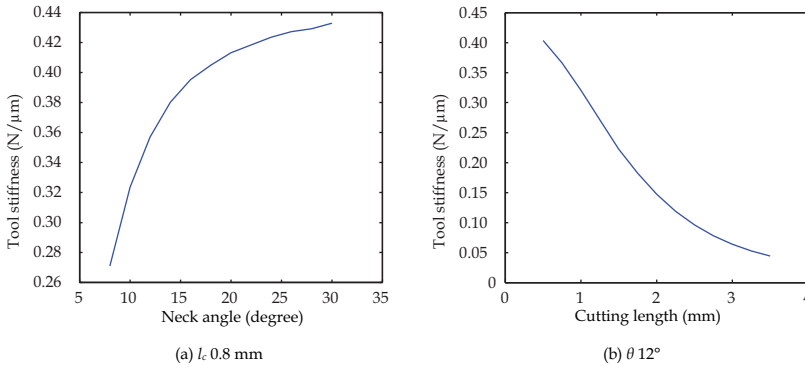


**Fig. 6.5:** Simulated effect of neck angle and cutting length on the tool stiffness. Simulation conditions:  $l$  60 mm,  $r_s$  is 3 mm,  $r_c$  0.25 mm, equivalent  $r_c$  0.21 mm.

tool stiffness, namely to optimize the neck angle and to shorten the cutting length. The effect of these two geometrical features on tool stiffness was further studied by the developed model. The results in Fig. 6.5 show that the larger the neck angle is, the higher the tool stiffness. However, when the neck angle is over  $20^\circ$ , the slope of the curve in Fig. 6.5a is getting smaller, which means further increasing the angle does not significantly increase the tool stiffness. For the cutting length, the shorter it is, the higher the tool stiffness.

Although the theoretical trend is clear, the choice of practical values for these two geometrical features is limited by manufacturability. For example, the neck angle is constrained by the available size of the grinding wheel. The minimum underneck length of the tool is constrained by the highest AR of the product.

### 6.3.2 Design of the cutting part

The geometry of the cutting part is relatively complex due to the existence of cutting edges and helix angle. The main geometrical features on the cutting part include the rake angles (radial and axial), relief angles (radial and on the end face), helix angle, and core radius, as shown in Fig. 6.6.

The objective of designing the cutting part is to improve the strength of the cutting edge corners. For this purpose, the aforementioned geometrical features will be tested. Because these features are not coupled, they can be tested separately. In the end the design of the cutting part will be based on the analysis of each geometrical feature.

The design of the cutting part was done by means of FEM analysis. First, the geometry of the cutting part was drawn in SolidWorks. Then, by using the

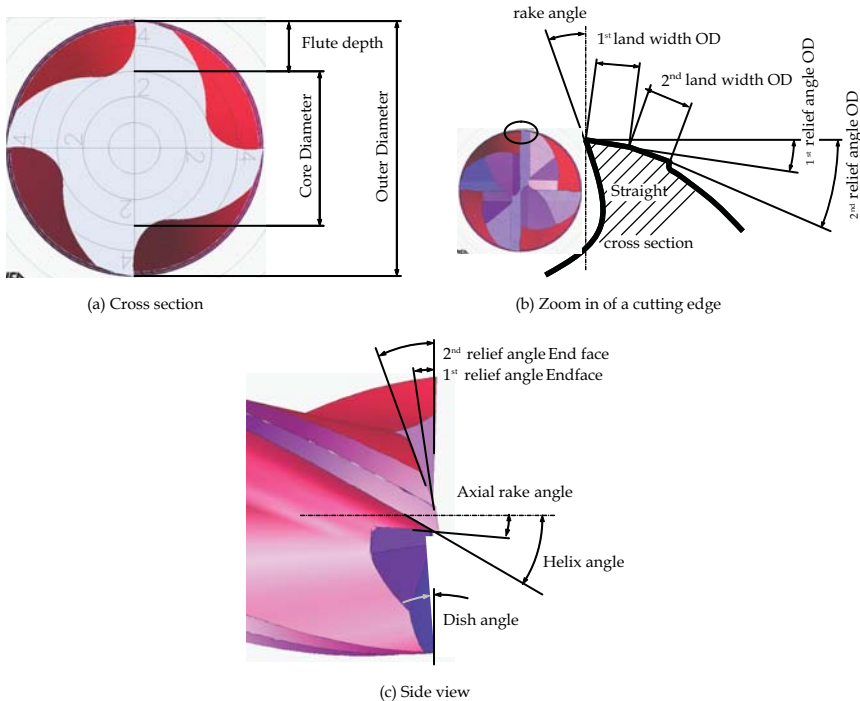


**Fig. 6.6:** Illustration of the endmill geometry [154].

configuration function of SolidWorks, the value of each geometrical feature can be varied easily, and its effect can be tested in COSMOSWorks. Static study was conducted. The methods to apply the force and meshing are same as those introduced in Chapter 4.

First, the effect of radial rake angle was tested. Three levels of rake angles are chosen, namely  $-8^\circ$ ,  $0^\circ$ , and  $+8^\circ$ . The  $-8^\circ$  and  $8^\circ$  rake angles are illustrated in Fig. 6.7. The  $+8^\circ$  angle is commonly used on commercial macro and micro endmills. It is clearly seen in Fig. 6.8 that the rake angle has very significant effect on the maximum stress at the cutting edge corner. Among all the three values, the  $+8^\circ$  tool has the maximum stress; the  $-8^\circ$  tool has the minimum stress level. This means that the cutting edge corner is weakened by using the positive rake angle. When the localized stress from cutting process is higher than the rupture strength of the carbide, the cutting edge corner will chip off. This is the reason why the commercial tools show severe reduction of cutting diameter at the very early stage of machining. Therefore, a negative rake angle is preferable for micro square endmills in hard milling applications. It is also a common practice to use negative rake angles on endmills for macro scale hard milling [9].

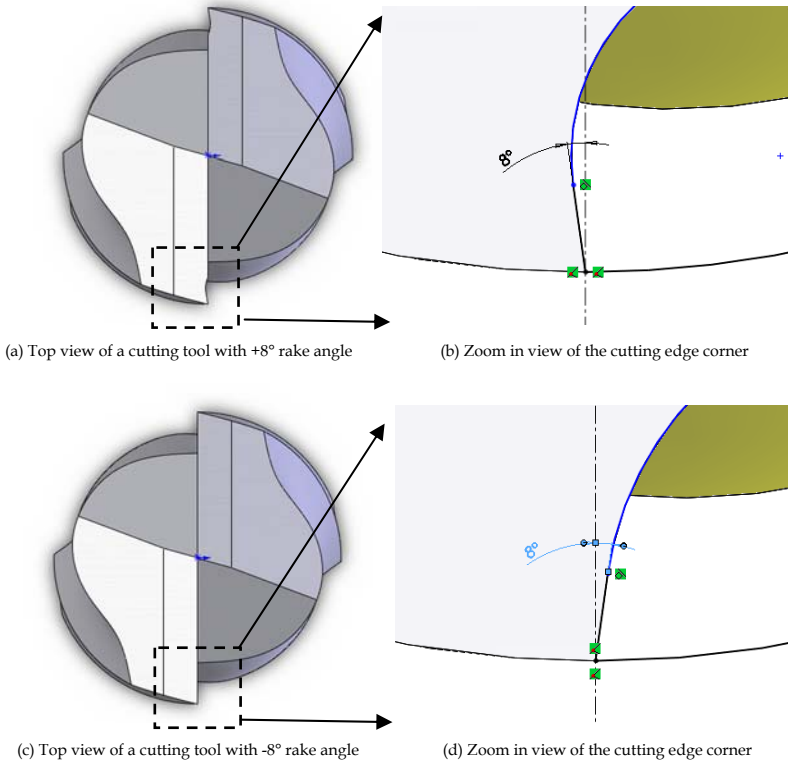


**Fig. 6.7:** Illustration of +8° and -8° radial rake angles.

Similar analysis was done to test the effect of helix angle, core radius, radial relief angle, and axial relief angle. Their results are shown in Fig. 6.9. It is seen that among these geometrical features, the helix angle and the end face relief angle have more significant effect on the maximum stress on the tool than the core radius and the radial relief angle. The smaller the helix angle and the end face relief angle are, the lower the maximum stress level will be. Because the actual  $a_p$  is relatively small in machining, a small helix angle will not influence the chip removal significantly. The tested tools in experiments showed no wear on the cutting edges at the end surface, which means in micromilling that the chip removal is mainly done by side cutting edges. Therefore, a smaller end face relief angle can be chosen as long as the end face does not contact the workpiece during machining. Although the core radius has no significant effect on the maximum stress level, a big core radius will increase the stiffness of the micro cutting tool to a certain extent.

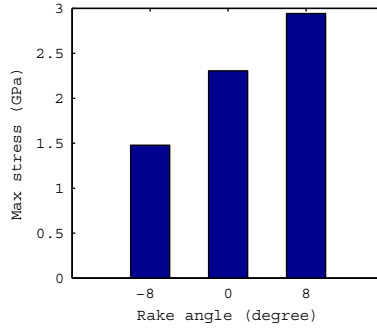
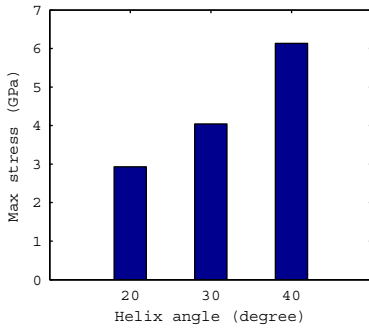
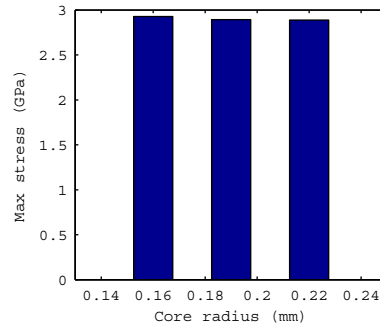


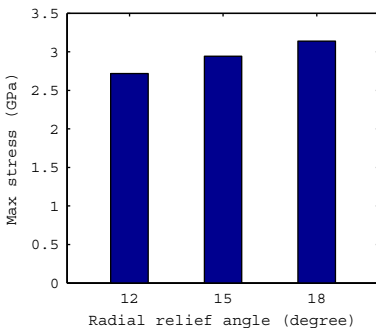
**Fig. 6.8:** Maximum stress at three levels of radial rake angles. Conditions:  $l_c$  0.8 mm,  $r_c$  0.25 mm, radial relief angle 15°, end face relief angle 15°, core radius 0.18 mm, helix angle 20°.



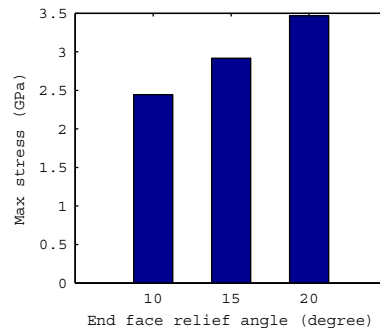
(a) Core radius 0.18 mm, radial relief 15°, end face relief 15°



(b) Radial relief 15°, end face relief 15°, helix angle 20°



(c) Core radius 0.18 mm, helix angle 20°, end face relief 15°



(b) Radial relief 15°, radial relief 15°, helix angle 20°

**Fig. 6.9:** Effect of geometrical features on the maximum stress on the tool edge corners. Conditions:  $r_c$  0.25 mm,  $l_c$  0.8 mm, rake angle 8°, radial relief land 0.1 mm.

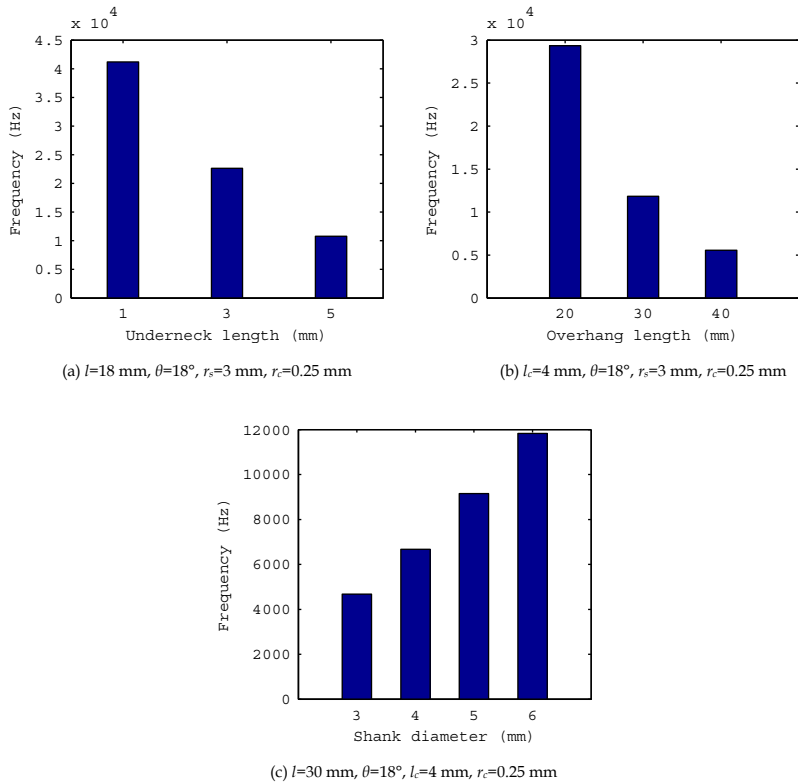


**Fig. 6.10:** Influence of tool geometrical features on its natural frequency.

### 6.3.3 Other aspects

The dynamic behavior of the micro endmill is important because vibrations could damage the tool and deteriorate the workpiece quality. The natural frequencies of micro endmills were studied under different combination of geometrical features. The tested features include the underneck length, overhang length (length from tool tip to the end of tool holder), and shank diameter; the results are shown in Fig. 6.10a, 11b, and 11c respectively.

It is seen that the minimum natural frequencies of micro endmills are about 5 times higher than that of the cutting frequency (e.g. 1000 Hz). The shorter the underneck length and the overhang length are, the higher the natural frequency of the tool will be. For the shank diameter, the bigger the diameter is, the higher the natural frequency.

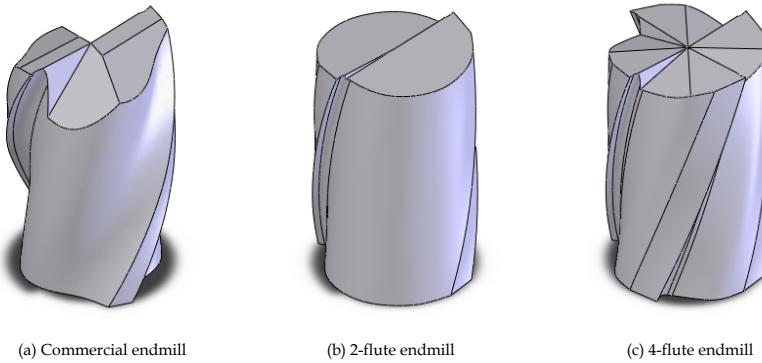


**Fig. 6.11:** CAD drawing of the cutting part of the newly designed 2-flute and 4-flute endmills in comparison with the commercial endmill.

**Table 6.1:** The chosen values of some geometrical features.

	Commercial tool	New design 2-flute	New design 4-flute
Cutting diameter (mm)	0.5	0.5	0.5
Cutting length (mm)	0.8	0.5	0.5
Nr. of flutes	2	2	4
Core radius (mm)	0.175	0.19	0.19
Rake angle (°)	+8	-8	-8
Radial relief angle (°)	10	10	10
Radial relief land (mm)	0.075	0.06	0.06
End face relief angle (°)	10	7	7
Helix angle (°)	30	20	20
Neck angle (°)	12	18	18
Shank diameter (mm)	6	6	6

These results will be directions on how to design micro endmills in order to have a higher natural frequency and to avoid possible vibrations.

### 6.3.4 The complete new tool design

In the previous sections, the geometrical features of a micro endmill have been analyzed to show their influence on the tool performance in terms of stiffness and stress distribution at the edge corner. In this section, some values will be given to these features to give the endmill desired performance.

As discussed before, it is not the purpose in this research to deliver commercially ready-to-use endmill geometry since the endmill geometry should be chosen accordingly for different applications. Rather, it is to generate knowledge about tool design and to demonstrate the method for new tool

**Table 6.2:** Summary of FEM simulation results.

	Commercial tool	New design 2-flute	New design, 4-flute
Applied force (N)	10	10	5
Max stress (GPa)	3.00	1.58	1.00
Max deflection ( $\mu\text{m}$ )	9.3	3.4	1.7
Calculated stiffness (N/ $\mu\text{m}$ )	1.1	2.9	2.9

design.

Because hard milling is the targeting application, the selection of the values for tool geometrical features is to give the tool a higher stiffness and high strength at the edge corner in comparison with the commercial tool geometry.

To improve tool stiffness, conical shape is chosen as the neck geometry. According to Fig. 6.5 and Fig. 6.9, a higher neck angle, a shorter tool cutting length, and a bigger core radius are chosen.

To improve the strength of cutting edge corners, according to Fig. 6.8 and Fig. 6.9, a negative rake angle, a smaller helix angle, and a smaller end face relief angle are chosen.

The values of the chosen geometrical features are listed in Table 6.1. The CAD drawings of the cutting part of the newly designed endmills are shown in Fig. 6.11, together with the commercial micro endmill.

Besides 2-flute endmills, 4-flute is also used in the new design. As described before, asymmetric tool wear was commonly observed on the different cutting edges of the tested 2-flute commercial micro endmills due to runout. By adopting 4 cutting edges, the runout effect can be compensated to a certain extent among the two pairs of cutting edges.

The performance of the newly designed endmills was first theoretically evaluated by means of FEM analysis in comparison with the commercial tool; the results are shown in Table 6.2. A 10 N force was applied on the commercial tool and the newly designed 2-flute tool, while a 5 N force on the 4-flute endmill because the chip load by using this type of tool can be roughly 2 times lower than the others without sacrificing the MRR.

As expected, the theoretical results show that both the newly designed 2-flute endmill and the 4-flute endmill perform better than the conventional endmill in terms of the maximum stress level at the cutting edge corners and the total tool stiffness. This means that the direction of tool geometry adjustment is correct according to the purpose of tool design.

Therefore, the new geometries can be tested in experiments.

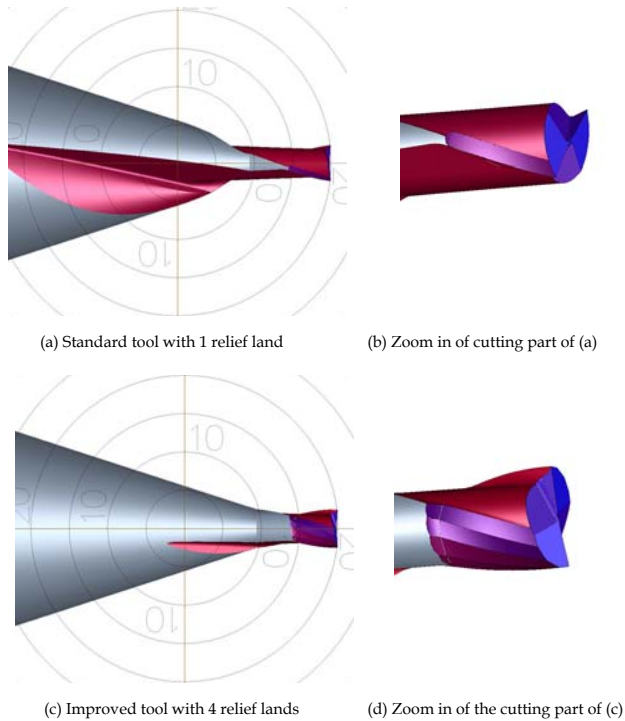


**Fig. 6.12:** Minimizing the extra cut at the tool body by adjusting the number of relief lands.

## 6.4 Manufacturing of the newly designed tools

The newly designed endmills were simulated on the manufacturing software in a tool company to check the possibility of realizing the designed features. The main improvement after the test was that 4-relief lands instead of 1-relief was used on the newly designed endmill in order to minimize the extra cut at the tool neck part. This is explained in detail in Fig. 6.12.

Due to the relative big size of the grinding wheel, some tool substrate material at the neck part will be removed when forming the cutting edges. This effect is shown in Fig. 6.12a and Fig. 6.12b, where the simulated tool has 1-relief land as normally. This extra cut will unavoidably lower the stiffness of the micro endmill. To compensate this effect, a solution is proposed; a 4-relief land is used, as shown in Fig. 6.12c and Fig. 6.12d. From the comparison between Fig. 6.12a and Fig. 6.12c, it can be seen that the extra cut has been reduced significantly by adopting this solution.



Fig. 6.13: Setup for stiffness measurement.

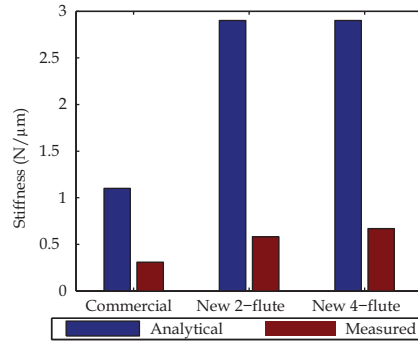


Fig. 6.14: Comparison of stiffness results.

## 6.5 Experimental validation

The newly designed  $\varnothing$  0.5mm square endmills were manufactured and validated through experiments in comparison with commercial  $\varnothing$  0.5 mm square endmills. First the static stiffness of the three types of tools was measured and compared. Then the newly designed endmills were used in machining of hardened tool steels to test their wear behavior.

### 6.5.1 Tool stiffness

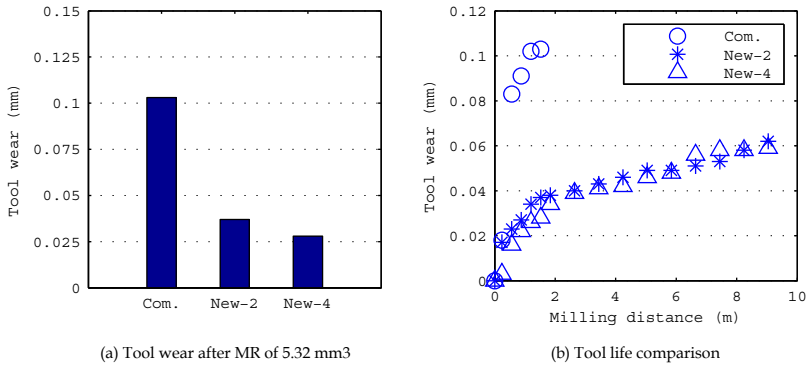
The setup for the tool stiffness measurement is shown in Fig. 6.13. The shank part of the endmill was rigidly clamped to a mechanical clamping device. Known static loads were applied at the tool tip end gradually, and the displacement of the tool tip was read out by the Keyence microscope. The resolution of the microscope is about  $0.37 \mu\text{m}/\text{pixel}$ .

The experimental measured stiffness of three types of endmills is shown in Fig. 6.14 together with the theoretical stiffness calculated by the cantilever beam model. It shows that the newly designed endmills are about 2 times stiffer than the commercial tool. The experimentally measured stiffness for the commercial endmill is  $0.3 \text{ N}/\mu\text{m}$ . The measured stiffness of the newly designed 2-flute and 4-flute endmill is  $0.6 \text{ N}/\mu\text{m}$  and  $0.7 \text{ N}/\mu\text{m}$ , respectively.

It can also be seen in Fig. 6.14 that the relative relation between the stiffness of the commercial tool and the newly designed tools has been predicted by the cantilever beam model with a good accuracy. However, there is a difference in the absolute value. There could be many reasons for this difference, such as the

**Table 6.3:** Summary of cutting conditions for tool wear/life tests.

	Commercial tool	New design 2-flute	New design 4-flute
Spindle speed (rpm)	30000	30000	30000
Cutting speed (m/min)	47.1	47.1	47.1
Feed per tooth ( $\mu\text{m}$ )	6	6	3
Feed rate (mm/min)	360	360	360
Depth of cut (mm)	0.07	0.07	0.07
Width of cut (mm)	0.5	0.5	0.5
MRR (mm <sup>3</sup> /min)	12.6	12.6	12.6

**Fig. 6.15:** Experimental results of tool wear and tool life tests.

error in the assumption of tool substrate material properties, simplification in the tool geometry when developing the cantilever beam model, and manufacturing error such as the extra cut at the neck part. Furthermore, the Euler Bernoulli beam tends to underestimate the stiffness when the ratio between length and radius of the beam is lower than 10. However, for a qualitative study, the theoretical results are sufficient.

## 6.5.2 Tool wear and tool life

Experiments were designed and conducted to test the wear performance of the three types of endmills under different cutting conditions with different types of workpiece materials and on different machine tools.

The first set of experiments was designed to compare three types of tools under one set of cutting conditions. The tests were done on the Fehlmann Picomax 60HSC machine. The workpiece material was AISI H11 with 56 HRC. The cutting conditions are listed in Table 6.3. MQL was used for all tests. For a fair

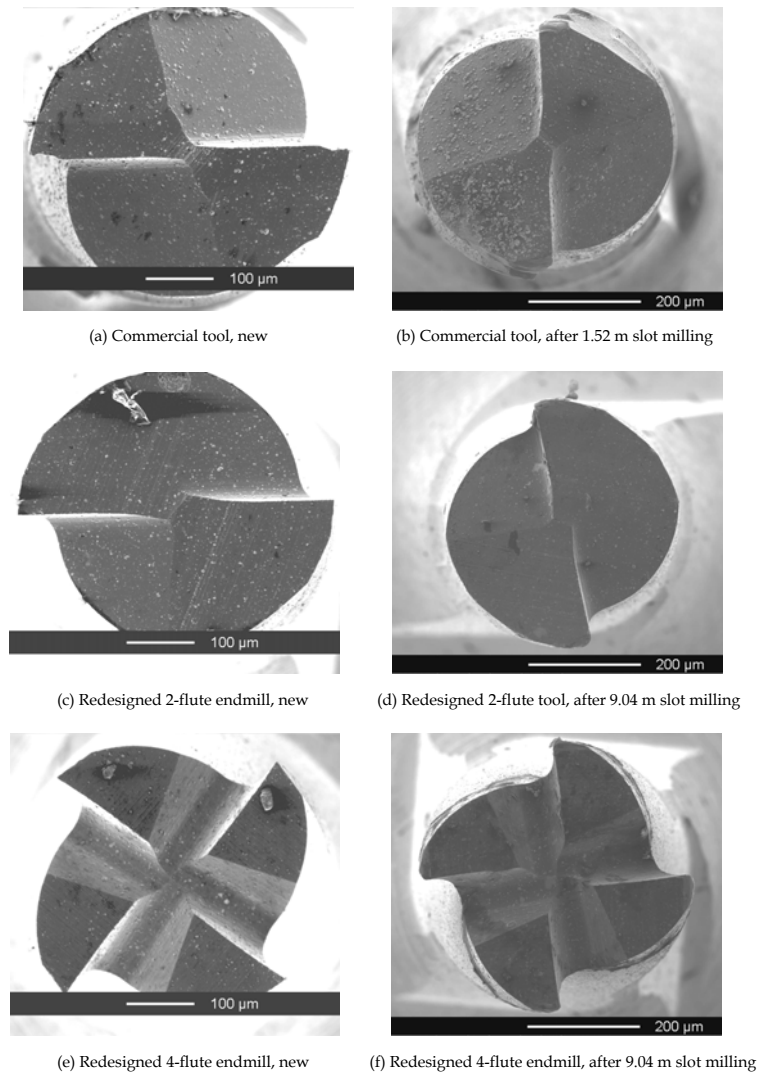


**Fig. 6.16:** Top views of new and worn tools.

comparison, the total MRR was kept same for each type of tools.

The tool life criterion was set to be 10% reduction of the tool diameter. The tool wear, workpiece form accuracy and burr formation were observed by the FEI Quanta 600 SEM and the Keyence microscope. The cutting force was monitored by the dynamometer Kistler 9256C2. No chatter was found in machining.

The tool wear and tool life test results are shown in Fig. 6.15. In Fig. 6.15a, after

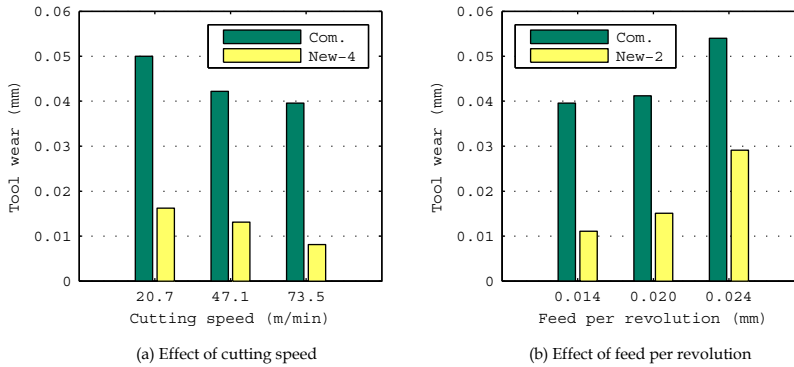


**Fig. 6.17:** Comparison of tool wear under different conditions. The MR by each tool was kept same as  $20 \text{ mm}^3$ , workpiece material AISI H11.

MR of  $5.32 \text{ mm}^3$ , the commercial micro endmill had a wear of  $103 \mu\text{m}$ ; it was 20.7% of the tool nominal cutting diameter and was over the tool life criterion already; while the wear of the newly designed 2-flute and 4-flute endmills were  $37.5 \mu\text{m}$  and  $28 \mu\text{m}$ , respectively.

Because the commercial tool has reached the tool end of life criterion, the machining with it was stopped. The tests with two newly designed tools were continued until the tool life criterion was reached. The Fig. 6.15b shows that the newly designed tools had about 6 times longer tool life than the commercial tool. In Fig. 6.16 the top views of the new and worn tools are shown. It is clearly seen that the newly designed endmills still kept good shape after slot milling of 9.04 m; while the two cutting edge corners of the commercial tool were totally gone after slot milling of 1.52 m.

The second set of experiments was designed to test the influence of cutting conditions on the tool performance. The MR was kept the same for each type of tool. The experiments were done on the KERN EVO machine. The results in Fig. 6.17 show that the wear of the newly designed endmills was much less than that of the commercial tools under all test conditions.

The third set of experiments was designed to test the newly designed tools in machining of hard to machine materials. For this purpose, AISI D2 (50 HRC) was used as the workpiece material. The experiments were done on the KERN EVO machine. As shown in Fig. 6.18, the wear magnitude of each type of tool is much higher than when machining other materials (e.g. AISI H11); however, the newly designed endmills still showed significant less wear than the commercial tool.

The last experiments also show that when the strength of the workpiece

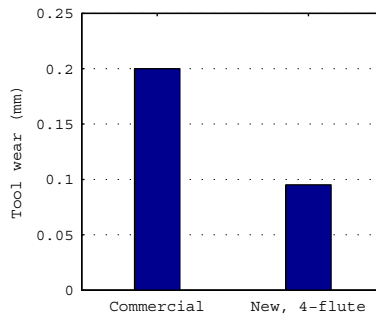


**Fig. 6.18:** Tool wear in machining of AISI D2 with 50 HRC. MR was kept same as  $20 \text{ mm}^3$  for each tool.

material is very high, the reduction of tool wear only by improving the tool geometry is limited. To solve this problem, new tool material should be used for micro endmills with higher hardness and wear resistance.

Besides, it was observed in experiments that the wear (reduction of the cutting diameters) on the two pairs of cutting edges of the 4-flute endmill was about the same in magnitude. It means that the wear was more evenly distributed in the two directions of the 4 cutting edges; the newly designed 4-flute endmill could compensate the runout effect to a certain extent.

### 6.5.3 Workpiece quality

It has been discussed before that the workpiece quality is closely related with the tool conditions in micromilling. Since the tool wear has been reduced by the new designs, the workpiece quality is also improved in terms of form accuracy and burr formation.

The slots shown in Fig. 6.19a and Fig. 6.19b were machined by the commercial tool and the newly designed 2-flute tool, respectively. These two tools have machined the same amount of material under same nominal cutting conditions. It is clearly seen that the burr volume on both edges of the slots by the commercial tool was much bigger than that by the newly designed tool. Burr formation is closely related with the tool condition. When the cutting edge corners of the commercial tool broke, the material removal process became more ploughing, instead of shearing. As a result, the workpiece material could not be removed as chips, instead it attached to the edge of the slots forming burrs. Because the wear of the newly designed endmill has been reduced, the cutting edges of the new endmills could keep its original shapes; therefore, the material removal could be guaranteed.

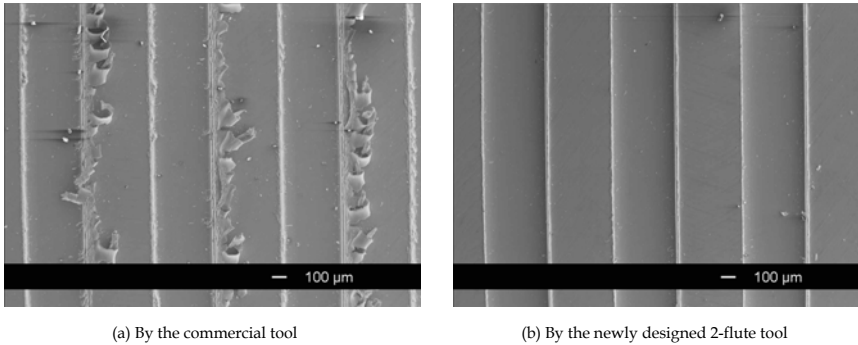


**Fig. 6.19:** Top views of machined slots by the commercial endmill and the newly designed 2-flute endmill after MR of  $5.32 \text{ mm}^3$ .

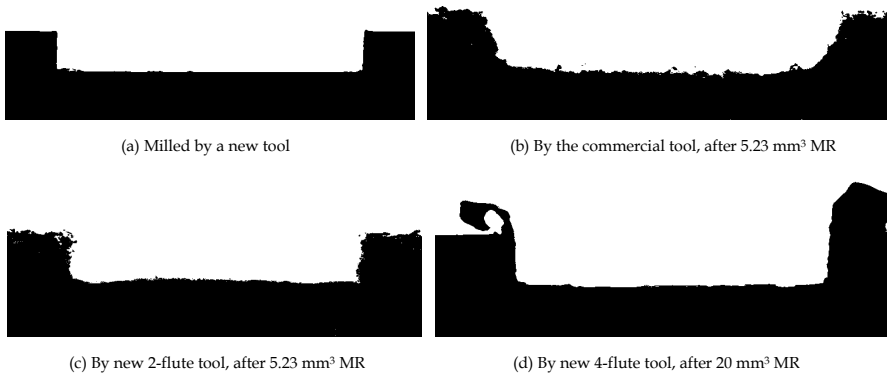


**Fig. 6.20:** Side views of the milled slots after MR of  $5.32 \text{ mm}^3$ , (a) by the commercial tool, (b) by newly designed 2-flute endmill.

The same reasoning can be applied for the improvement of the form accuracy, as shown in Fig. 6.20.

### 6.5.4 Force data

The milling forces generated by the three types of micro endmills were collected and compared. The average forces in the cross feed direction are shown in Fig. 6.21 as an example. It is seen that the initial force of the newly designed 4-flute endmill is the lowest among the three types of tools and the initial force on the newly designed 2-flute tool is the highest. This is as expected because the  $f_z$  on this 4-flute tool was half the value of the other two types of tools, and the newly designed 2-flute tool has a negative rake angle, which results in a bigger force.

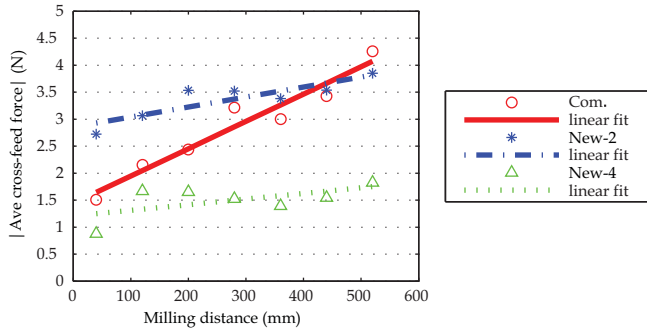


**Fig. 6.21:** Comparison of the average cross feed forces by three types of endmills. Conditions:  $v_c$  73.5 m/min,  $a_p$  0.07 mm,  $a_e$  0.5 mm, feed per revolution 0.014 mm.

With the increase of tool wear, the average forces for the 3 types of endmills increased. It is seen in Fig. 6.21 that the slope of the commercial endmill is the biggest among all three types of tools, which means the condition of the commercial tool changed rapidly during machining. However, the slopes of the force curves of the two newly designed endmills are much smaller, which means the tool conditions were relatively stable during cutting.

## 6.6 Summary

In this chapter, new guidelines for the design of micro square endmills for hard milling applications were introduced and experimentally verified successfully.

The procedures used in this research to design the micro cutting tool include:

- Experimental investigation of commercial tools;
- Derivation of design guidelines based on the experimental observations;
- Study of the geometrical features of micro endmills by means of a cantilever beam model and a FEM model;
- Design of the tool geometry based on the theoretical analysis, and verification of the new design theoretically;
- Simulation of the newly designed geometries on the tool manufacturing software; further improvement of the tool geometry if necessary;
- Manufacturing and experimental validation of the newly designed endmills.

Since hardened tool steels are chosen as the workpiece material in this research,

the objectives of the new design are set to improve the tool stiffness and strength of the cutting edge corners. The experimental validation results show that the newly designed geometries have achieved the predefined objectives. Compared with commercial micro endmills, the newly designed endmills have higher stiffness, less wear, and therefore longer tool lives. The workpiece quality has been improved accordingly in terms of form accuracy and burr formation; this is because the cutting edges of the newly designed endmills can keep the original shape.

The disadvantage of the newly designed endmills is that they cannot be used for drilling operations. This is because a relatively small end face relief angle was used on the new tool in order to strengthen the cutting edge corners. Furthermore, due to the usage of negative rake angle, the cutting force is higher than using the commercial tools.

The newly designed endmills can be used for roughing, and reroughing operations. When the deflection of the machined micro geometries is not an issue, the new tools can also be used for finishing operations.

Although the method and generated knowledge are demonstrated on  $\varnothing 0.5$  mm square endmills, the knowledge about how to improve tool geometry is applicable on the design of smaller endmills and ball nose endmills.

# Chapter 7 Machining of micro ribs with high aspect ratios

The selection of cutting conditions in terms of tool wear and surface finish has been discussed in Chapter 5. This chapter will be designated to the discussion of choosing machining parameters and tool paths for the machining of micro features, in which case the bending of the micro cutting tool and the machined micro features is important.

In Section 7.1, the motivation, objective and approach are introduced. In Section 7.2, the selection of example geometry is described. The selection of machining parameters and tool paths are discussed in Section 7.3 and Section 7.4, respectively, applying results from cutting force modeling and FEM workpiece modeling. In Section 7.5, the dynamic behavior of thin ribs is studied. The machining of thin ribs is presented in Section 7.6; the results and analysis are shown in Section 7.7. This chapter ends with a discussion in Section 7.8.

## 7.1 Motivation, objective, and approach

**Motivation:** Micro features with high AR are the most commonly seen geometries in literature [155, 156] that were machined by micromilling. These thin features can be applied as electrodes for the EDM process or components in micro moulds for micro injection molding [156].

One challenge when machining such features by micromilling is that the cutting force will bend or damage the product, if not well controlled. The cutting force is related to the machining parameters. In literature, it is seen that micro features with high ARs were mainly machined by trial-and-error methods. The features were machined by a set of conservative machining parameters to avoid tool failure; this resulted in extremely long machining time. And no discussion was given how and why those conditions were chosen; knowledge about machining parameters gained by using such a method is hardly transferable to the machining of different types of geometries.

The effect of cutting force on machined features also depends on tool paths. At this moment, tool paths are normally generated using commercial CAM packages which are developed for conventional machining. It has been reported in many papers [108, 157] that micromilling needs specially designed strategies.

In summary the current methods to choose cutting conditions cannot guarantee a successful micromilling of thin features.

**Objective:** For aforementioned reasons, it was decided in this work to develop an approach towards knowledge-based techniques to machine micro features. The selection of the cutting conditions should be based on theoretical guidelines instead of trial-and-error. Besides, the quality of the products can be predictable and ensured. Furthermore the results will be repeatable.

Machining of thin features is a benchmark reflecting the capability of the micromilling process. Therefore, the achieved AR will be used as the criterion to evaluate the results in this work. Because there is no good solution available to measure the dynamic cutting diameter of the micro endmill, the dimensional accuracy of machined micro features is not used as the evaluation criterion in this research.

**Approach:** The selection of cutting conditions is a part of the process planning. By definition [158], process planning includes all the processes that transforms raw material into the final product, including activities from the start as derivation of design requirements to the final quality control of the product. Since the focus of this research is to the micromilling process, only the selection of machining parameters and tool paths is relevant here.

For the convenience of demonstration and evaluation, a typical micro geometry is chosen as the running example. The developed approach includes the following aspects:

- Theoretical study and selection of machining parameters;
- Theoretical study and selection of tool paths;
- Analysis and modeling towards the static and dynamic behavior of thin features during machining under theoretically selected conditions;
- Experimental validation of the developed approach.

The above aspects will be introduced in detail in the following section.

## 7.2 Selection of the example geometry

The machining of micro features is influenced by many factors like software and data translation errors, machine errors, machining errors, measurement

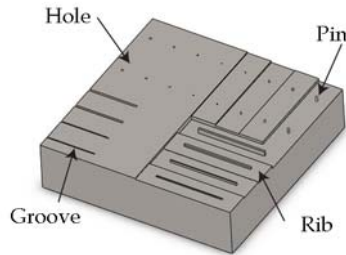


Fig. 7.1: Illustrations of typical micro features.

errors, etc [159]. Since it is of interest to test the process capability, the selection of the example geometry should be based on the principle that all the error sources other than the machining process will have minimal effect to the final results.

Micro parts are normally composed of four basic types of geometries, ribs, pins, grooves, and holes, as shown in Fig. 7.1. Machining of these geometries is influenced by different factors. For instance, machining of a pin requires circular interpolations of the machine axes, in which case the quality of the pin will heavily depend on the performance of the controller of the machine. When machining micro holes, the micro endmill has to be used as a drill, which has a special requirement on the tool geometry. The achievable dimension of micro grooves relies on the dimension of the micro tools.

Compared with the other three types of features, micro ribs have a simple geometry, which can minimize the errors from sources other than the cutting tool and the process. Therefore, micro ribs with high ARs are well suitable to serve the purpose of this research, to test the capability of the process. That is the reasons the ribs are chosen as the test geometry and used as the running example.

### 7.3 Selection of machining parameters

The objective of selecting machining parameters is to control the cutting force during machining to minimize bending or prevent damage of the micro cutting tool and the machined micro features. For this purpose, the relationship between the machining parameters and the cutting force has to be studied; this is done by using a micromilling force model.

In this section, firstly, the typical force signature and repeatability of force

measurements are studied. Secondly, the strategy of force modeling is defined. Then the development of the force model is described, including the calibration and validation methods. Finally, analysis is done with this force model to study the relationship between machining parameters and the force, and to discuss how to choose machining parameters for this study.

### 7.3.1 Study of micromilling forces

Machining forces are an important performance indicator for micromilling because it is related to the applied machining parameters, workpiece machinability, cutting tool conditions, etc. After proper processing, it is possible to use the force signals to monitor the process, such as to predict remaining tool life time or to avoid premature tool breakage. The reason to model forces in this research is to control the force magnitude to prevent bending or damage of the ribs.

Before modeling the forces, the typical force signals in micromilling were studied, and also the factors that influence the forces.

A typical example of the measured micromilling forces is given in Fig. 7.2. Since the forces in the feed and the cross feed directions show similar patterns, and the force in the axial direction is much lower for a new tool compared with the other two direction, only the force in the feed direction is shown here as an example.

From this figure, the following aspects can be concluded:

- The frequencies occurred in this example include: spindle frequency (about 500 Hz), the tool passing frequency (about 1000 Hz), and their harmonics, as shown in Fig. 7.2b. The relatively high energy at the spindle frequency is due to the runout from the process. The peaks around 5000 Hz are due to the structure resonance of the force sensor and workpiece clamping device.
- As in macro scale milling the force in micromilling is composed of a static and a dynamic component, as shown in Fig. 7.2c. The static (DC) component is the average force, -1.05 N in this example, during the period of the measurement; it defines the bending of the cutting tool and the machined micro rib. The dynamic component is the variation of the force around the average force due to the nature of the milling process; it will influence the texture of the machined surface.
- Also can be seen in Fig. 7.2c that there are two peaks and two valleys in each spindle revolution. This is because the micro endmill has 2 cutting edges. However, they have different magnitudes due to runout.

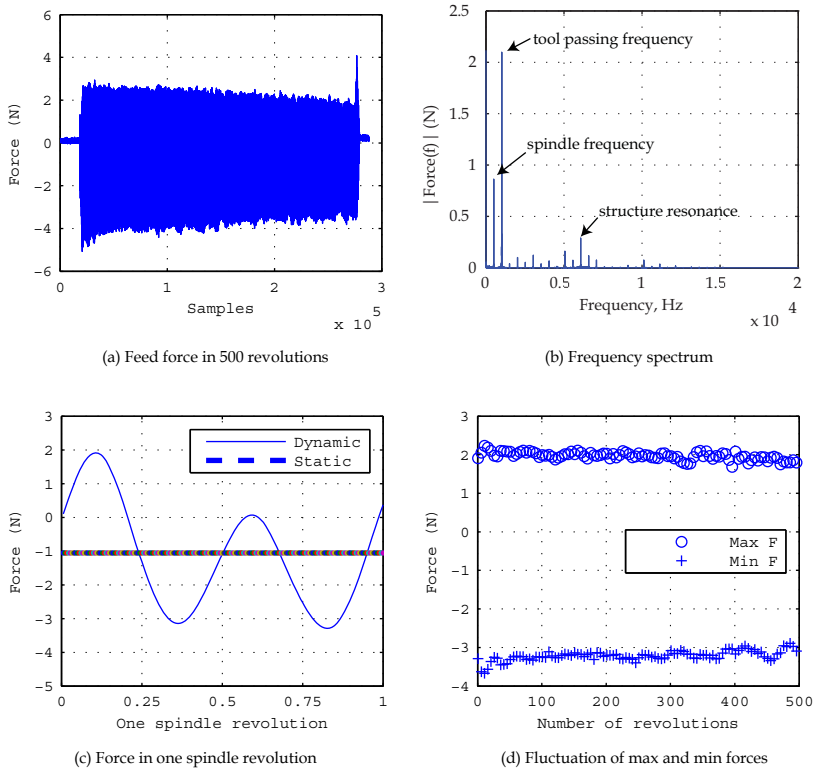


**Fig. 7.2:** An example of micromilling forces in the feed direction. Cutting conditions: workpiece AISI H11 WITH 54 HRC,  $v_c$  47.1 m/min,  $f_z$  0.007 mm,  $a_p$  0.07 mm, slot milling.

- The figure in Fig. 7.2d shows that the cutting forces were not constant during machining. The band of the fluctuation is about  $\pm 0.27$  N (10-15% of the average value) for the maximum and minimum forces in this example. There could be several reasons for this fluctuation, such as the inhomogeneous property of the workpiece material, change of the cutting tool conditions (e.g. BUE chip clogging), etc. Compared with macro scale milling the ratio between the force fluctuation and the average force is much higher in micromilling due to the low magnitude of the forces.

The processing of force signals showed that the repeatability of the force measurement is strongly influenced by the runout, cutting tool conditions, and workpiece property. They will be discussed here shortly.

**Runout:** As explained in former chapters, runout has a more significant effect on the micromilling process. Due to runout the two cutting edges of the micro endmill will have different loads, which result in different force magnitude.

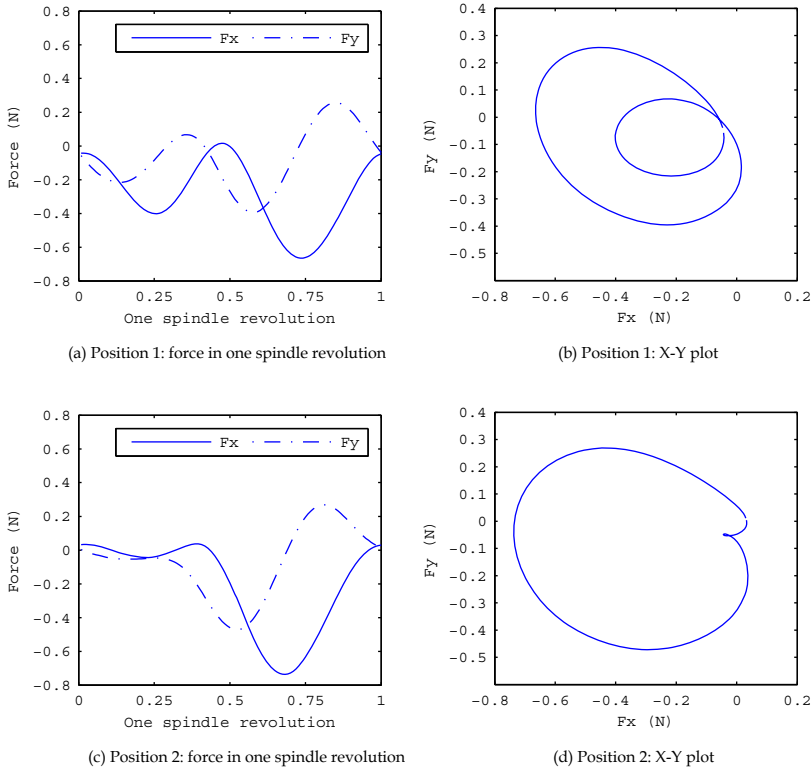


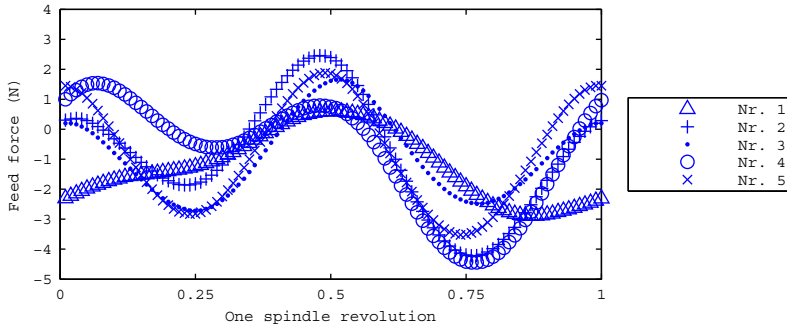
**Fig. 7.3:** Influence of runout on force profiles. Cutting conditions: workpiece brass,  $v_c$  37.7 m/min,  $f_z$  0.005 mm,  $a_p$  0.05 mm, slot milling.

Once the runout (magnitude or angle) changes, the chip loads on the two edges will change. This is one of the reasons why the repeatability of the dynamic force is low.

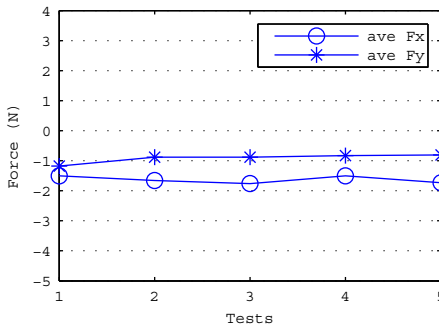
Experiments were done to verify this assumption. It is known that the connection between the tool holder and the spindle is one of the sources for runout. Therefore, when the relative position between the holder and spindle changes, the runout should change, so does the force profile. Experiments were designed based on this principle.

The procedure for the experiments is as follows:

- A micro endmill was inserted into the tool holder, and then the tool holder was loaded into the spindle.
- The relative position between the spindle and the tool holder was marked; this position is called Position 1.



(a) Comparison of forces in the feed direction



(b) Comparison of average forces

	Ave F (N)	$\sigma$ (N)	%
$F_x$	-1.63	0.12	7.6
$F_y$	-0.91	0.15	16.3

**Fig. 7.4:** Comparison of force signals from 5 tests. Cutting conditions: 5 cutting tools from the same batch, workpiece AISI H11 WITH 54 HRC,  $v_c$  47.1 m/min,  $f_z$  0.007 mm,  $a_p$  0.07 mm, slot milling.

- The tool was used to cut a slot in a piece of brass, and the forces were measured. Brass was chosen in this test instead of steel in order to minimize the influence of tool wear.
- After the first cut, the tool holder was unloaded, rotated 60 degree clockwise and inserted back to the spindle again. This position is called Position 2.
- Another slot was machined at this position with the exact same conditions as those used in machining of the first slot.
- In order to get a reliable result, the above described experiments were repeated by another new tool.
- The force signals at different positions are analyzed to check the effect of runout. Because similar observations were observed, only the results from the first tool are shown here as an example, in Fig. 7.3.

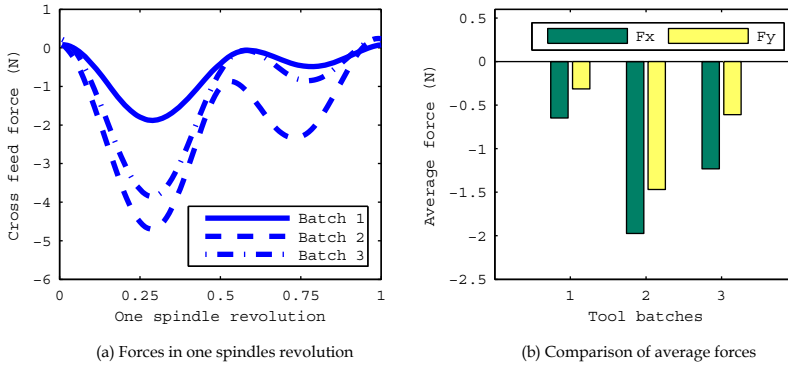


**Fig. 7.5:** Variation of force signals due to the deviations of tool geometries. Cutting conditions: M261,  $v_c$  37.7 m/min,  $f_z$  0.006 mm,  $a_p$  0.04 mm, slot milling.

It is clearly seen in these figures that the dynamic forces at the two positions look significantly different. The magnitudes of the forces on the two cutting edges changed once the relative position between the tool holder and the spindle changed. These results proved that runout indeed is one of the reasons for the low repeatability of the dynamic forces. It also implies that there exists an optimum position where the runout effect is smallest; however, this position has to be found experimentally due to the lack of suitable tools.

Although the force profiles for those two positions changed, the average force remained relatively constant. The average  $F_x$  and  $F_y$  at the Position 1 is -0.28 N and -0.07 N respectively; the average  $F_x$  and  $F_y$  at the Position 2 is -0.21 N and -0.07 N.

Further experiments were done with cutting tools from the same batch. Altogether 5 tests were done with 5 new tools from the same batch under the same nominal cutting conditions. The results are shown in Fig. 7.4. It is seen that the dynamic force profile in one spindle revolution differed from test to test; but the average force was again relatively constant.

From the analysis, it is clear that it is not possible to model the dynamic force accurately because there is no means to measure, predict, and control runout at the tool tip accurately. However, the average force can be modeled with a relatively good accuracy.

**Cutting tool geometry:** As described in Chapter 3 micro endmills from different batches will show deviations in geometry although they have the same nominal specifications. This subtle change in geometry will change the cutting forces.

Experiments were done with tools from 3 different batches under the same

nominal cutting conditions. The Fig. 7.5 shows the comparison of forces in the cross feed direction collected from these 3 tests. It is seen that not only the dynamic components of the forces are different, as shown in Fig. 7.5a, but also the static components, as shown in Fig. 7.5b.

This test shows that it is important to use tools from the same batch in comparison experiments in order to draw a reliable conclusion.

**Workpiece properties:** It is known from experiments that the harder the workpiece material, the quicker the wear of the micro tools will be. In order to model the force, signals have to be collected when the tools are new. This is challenging in this research due to the extremely short lives of tested commercial cutting tools. To solve this problem, one possible solution is to use workpiece material with relatively lower hardness.

### 7.3.2 Strategy for force modeling

From the above analysis, it can be concluded that the dynamic force cannot be modeled accurately due to the factors such as runout, tool geometrical deviations, workpiece material properties, etc. However, the average force can be modeled with a relatively good accuracy if former discussed factors can be controlled well.

Since the purpose of this study is to investigate the bending of the micro endmill and micro ribs, which is determined by the static component of the force, it was decided in this research to only model the average micromilling force. The modeling strategy is defined as follows:

- A force model is developed to study the relation between machining parameters and the average forces.
- Only the forces in the feed and cross feed directions are modeled. The axial force is much lower in magnitude compared with the forces in the other 2 directions, and it is irrelevant to the bending of the machined thin feature, therefore it will not be modeled.
- To avoid the possible deviations of the tool geometry, only one tool is used for all the tests, including calibration and validation tests. By using this strategy, this tool will unavoidably wear out at the end of the tests. This will result in the fact that the developed model will predict a force slightly higher than the reality. This is safe, hence it is acceptable.
- To prevent premature breakage of the cutting edge corners, the selected micro endmill should have a relatively big wedge angle (e.g. zero or negative radial rake angle and small relief angle).

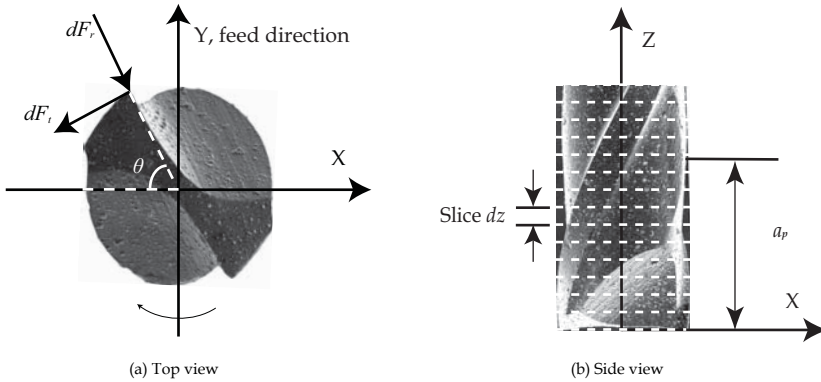


**Fig. 7.6:** Illustration of the coordinate system for the force model.

- To minimize the tool wear, M261 with 46 HRC will be used as the workpiece material, instead of AISI H11 with 54 HRC. M261 will also be used as the material for the thin ribs. Because the bending of the rib is proportional to the strength of the workpiece material, it is in theory more difficult to machine thin ribs with high ARs on M261.
- Furthermore, the cutting length in each test will be kept short enough to avoid unnecessary tool wear, but long enough to collect the stable force data.
- Tool wear is not considered in this model. The machining of thin ribs will be done with new tools to keep the absolute force magnitude low.

Again, this force model is mainly used for qualitative study. Once it is calibrated, it can be used to study the relationship between machining parameters and the average micromilling forces; this will give indications about how selection of machining parameters can be made in order to control the process forces.

### 7.3.3 The average force model

**The mechanistic force model:** To build a relationship between the average force and the machining parameters, a mechanistic force model is chosen. The mechanistic model is an empirical model, which has a certain structure and the force coefficients are obtained experimentally [121, 160-162].

The Cartesian coordinate system of the force model is illustrated in Fig. 7.6. The direction X is the cross feed direction, Y is the feed direction, Z is along the tool axial direction with  $Z=0$  at the free end of the endmill. In order to include the effect of the helix angle, the axial  $a_p$  is divided into slices. The force in each slice

is calculated separately; the total force applied on the tool is the integration of the forces of all the slices.

For each slice, the elemental forces are the tangential force  $dF_t$  and the radial force  $dF_r$ , as shown in Fig. 7.6a. The relation between these elemental forces and process parameters (instantaneous chip thickness  $h$  and elemental depth of cut  $dz$ ) at a rotational angle  $\theta$  can be expressed as:

$$dF_t(\theta) = (K_{tc}h(\theta) + K_{te})dz \quad (7-1)$$

$$dF_r(\theta) = (K_{rc}h(\theta) + K_{re})dz \quad (7-2)$$

where  $K_{tc}$  and  $K_{rc}$  are the cutting force coefficients,  $K_{te}$  and  $K_{re}$  are the edge force coefficients.

For the calculation of the instantaneous chip thickness  $h(\theta)$ , a tool path model has to be chosen. There are two types of tool path models, namely the circular model and the trochoidal model. Trochoidal tool path is more close to the reality; however, it is complex in calculation and the accuracy is only improved at the entry and exit parts of the cut when extremely small  $a_e$  is used. To model the average force in micromilling the circular model is accurate enough; therefore, it is chosen for this study. According to the circular tool path model the chip thickness at the immersion angle  $\theta$  is:

$$h(\theta) = f_z \sin(\theta) \quad (7-3)$$

These elemental forces can be resolved into the X and Y directions by using the transformation:

$$dF_x(\theta) = +dF_r(\theta) \cos \theta - dF_t(\theta) \sin \theta \quad (7-4)$$

$$dF_y(\theta) = -dF_r(\theta) \sin \theta - dF_t(\theta) \cos \theta \quad (7-5)$$

By integrating the elemental forces along the axial depth of cut and adding the forces on all the flutes ( $N$ ) that are involved in cutting, the total instantaneous forces on the cutter at immersion  $\theta$  are:

$$F_x(\theta) = \sum \sum_{a_p}^N dF_x,$$

$$F_y(\theta) = \sum \sum_{a_p}^N dF_y \quad (7-6)$$

**Model calibration and validation:** The force coefficients in (7-1) and (7-2) have to be calibrated. There are several possible methods available; the mechanistic approach introduced in [121] is used in this work. Since it is a well developed method, it will only be introduced here briefly.

In short, the method to calibrate the force coefficients is to equate the measured average force per tooth ( $\overline{F_{xc}}$ ,  $\overline{F_{xe}}$ ,  $\overline{F_{yc}}$ , and  $\overline{F_{ye}}$ ) to the analytically derived

**Table 7.1:** Machining parameters for model calibration and validation.

	Tests Nr.	Spindle speed (rpm)	$a_e$ (mm)	$a_p$ (mm)	$f_z$ ( $\mu\text{m}$ )
Calibration	1-5	24000	0.5	0.04	2, 4, 6, 8, 10
	6-10			0.06	2, 4, 6, 8, 10
	11-15			0.08	2, 4, 6, 8, 10
	16-20			0.10	2, 4, 6, 8, 10
Validation	1	24000	0.5	0.05	5
	2			0.03	9
	3			0.07	7
	4			0.09	5

**Table 7.2:** Model validation.

Test Nr.		Measurement (N)	Prediction (N)	Error (%)
1	Ave $F_x$	-1.15	-1.23	7.2
	Ave $F_y$	-0.79	-0.74	6.8
2	Ave $F_x$	-1.50	-1.34	10.4
	Ave $F_y$	-0.87	-0.79	8.7
3	Ave $F_x$	-2.19	-2.05	6.6
	Ave $F_y$	-1.64	-1.46	10.9
4	Ave $F_x$	-1.79	-1.82	1.5
	Ave $F_y$	-1.38	-1.47	5.9

average force by using the following relations:

$$K_{tc} = -\frac{4\overline{F_{xc}}}{Na_p}, K_{te} = -\frac{\pi\overline{F_{xe}}}{Na_p} \quad (7-7)$$

$$K_{rc} = -\frac{4\overline{F_{yc}}}{Na_p}, K_{re} = -\frac{\pi\overline{F_{ye}}}{Na_p} \quad (7-8)$$

The calibration experiments have to be specially designed. A series of full slot milling experiments have to be conducted under different combination of  $f_z$  and  $a_p$ . The cutting force signals of each test will be collected. To minimize the influence of runout, the measured average force per tooth can be calculated by dividing the total force per spindle revolution over the number of teeth of the cutting tool.

The experiments were done on the Mikron HSM700 machine. Full slot milling was conducted for both calibration and validation purposes. Side milling was not used because the accuracy of the  $a_e$  cannot be guaranteed due to runout and tool deflection. Each slot was 10 mm long. The force signals in the middle of the cut were used for analysis in order to avoid possible excitation at the entry and exit parts of the cut. No lubrication was used during cutting since the high pressure air will also exert a force on the cutting tool. The machining

parameters were chosen to cover the greatest possible cutting area, as shown in Table 7.1.

After calibration, the relation between the cutting coefficients and the machining parameters can be expressed as:

$$K_{tc} = -5.41 \cdot 10^4 \times a_p + 1.06 \cdot 10^4 \text{ N/mm}^2, K_{te} = 4.26 \cdot 10^1 \times a_p + 5.41 \text{ N/mm} \quad (7-9)$$

$$K_{rc} = -2.38 \cdot 10^4 \times a_p + 6.98 \cdot 10^3 \text{ N/mm}^2, K_{re} = 1.53 \cdot 10^2 \times a_p - 7.24 \text{ N/mm} \quad (7-10)$$

For the validation of the force model, the cutting forces under the conditions of the validation tests were calculated using the force model, and compared with the measured forces in experiments which were conducted under the same conditions. The results are shown in Table 7.2.

It is seen that the error between the predicted force and the measured force in all the calibration tests is smaller than 15%. This accuracy is acceptable for this study. As described in Section 7.3.1, the micromilling forces fluctuate during machining; 15% is still within the range of the observed fluctuation.

Therefore, the developed model is ready to be used for further analysis.

### 7.3.4 Analysis with the force model

The relation between the milling force and machining parameters was studied by means of the validated force model. According to the requirements of the application, the objective would be to control the average force in the direction normal to the rib lower than a pre-defined level by adjusting the machining parameters.

If the longitudinal direction of the rib is along the Y direction in the coordinate system, as shown in Fig. 7.6, the average force in the X direction is the interest of this analysis because it will influence the bending of the rib. Therefore, all the analysis presented in this section will be done on the average X force. Besides, the micro endmill is supposed to have 2 cutting edges. The values of each parameter were varied within the possible application range.

**Main effect of machining parameters:** The main effect of a cutting parameter means how this parameter will influence the average force when all the other parameters are fixed. Three parameters are tested, namely  $f_z$ ,  $a_p$ , and  $a_e$ . The value of  $v_c$  is fixed to achieve a minimum motion error according to the property of the machine tool; therefore, it is not included here. The results are shown in Fig. 7.7a, b, and c respectively.

From the Fig. 7.7, the following aspects can be observed:

- The force in down milling is always higher than that in up milling, which

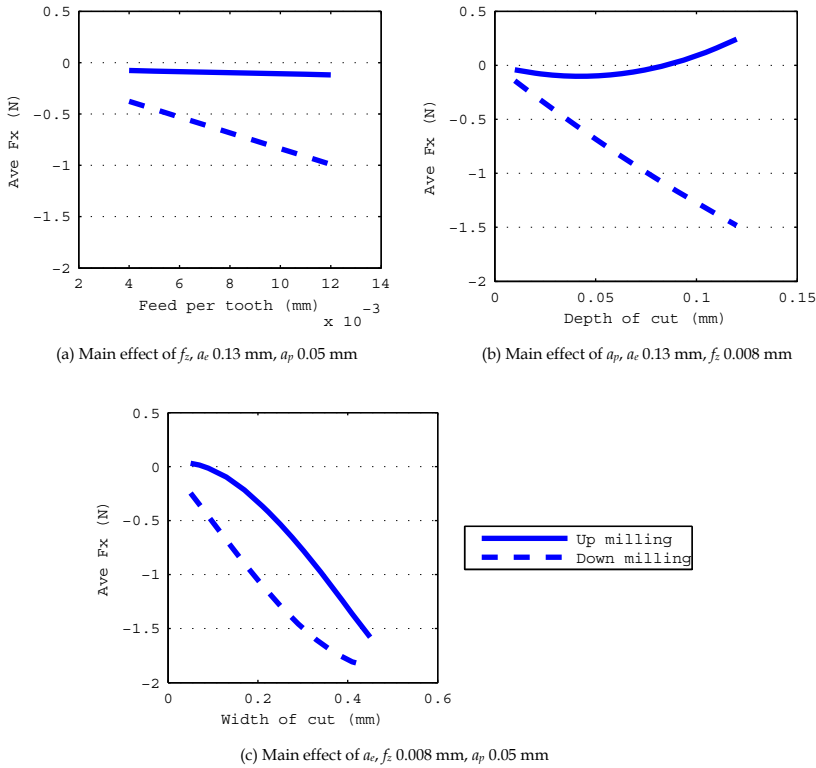


**Fig. 7.7:** Main effect of machining parameters on the average force in the cross feed direction.

means up milling should be chosen for the machining of the thin rib in order to control the force level.

- For up milling, the force magnitude will increase with the increase of  $f_z$  and  $a_c$ . However, the effect of  $f_z$  is not as significant as  $a_c$ .
- For up milling, within a certain level, increase of  $a_p$  does not increase the force. This means that a bigger  $a_p$  can be used to improve the productivity without affecting the workpiece quality. In practice, people are apt to use small  $a_p$  in order to lower the force magnitude; it is not correct from the results of this analysis.
- For down milling, the force will increase with the increase of all three parameters. Among them, again  $a_c$  has the most significant effect.

Although small  $a_c$  gives lower force for both up and down milling, the  $a_c$  value cannot be chosen too small otherwise the MCT effect will become dominant,

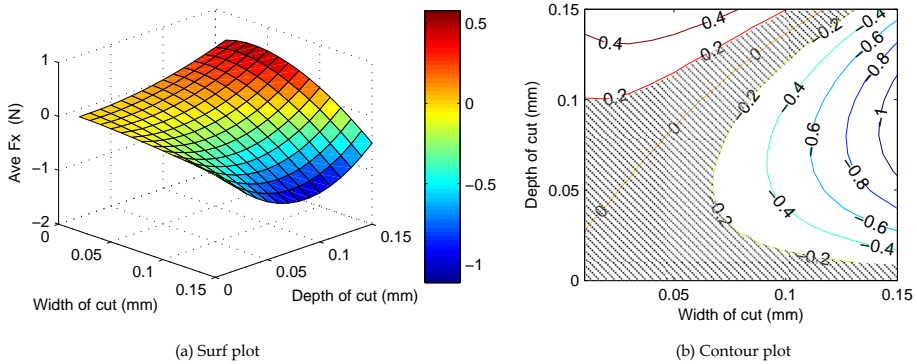


**Fig. 7.8:** Effect of  $a_p$  and  $a_e$  on the average  $F_x$ ,  $f_z$  is fixed at 0.008 mm.

which is not desired.

**Interaction between machining parameters:** For this analysis, only up milling is assumed. Because  $f_z$  is not as significant as the other two parameters, its value is fixed,  $a_e$  and  $a_p$  are varied to test their interaction effect on the average X force. The results are shown in Fig. 7.8.

From this figure, it is clear that there exists an area where the combination of  $a_e$  and  $a_p$  will produce a force lower than a pre-defined level when all the other parameters are fixed. For example, if the desired absolute force level is set to be 0.2 N, any point (different combination of  $a_e$  and  $a_p$ ) in the shadowed area in Fig. 7.8b would fulfill the requirement.

Again it has to be pointed out that this graph should be used to give a qualitative indication about how to choose machining parameters to control the force level. The accuracy of the force prediction should take into account the fluctuation of the force signals.

**Deflection of the micro endmill:** When machining thin ribs, not only the rib will bend under the micromilling force, but also the micro cutting tools. If the deflection of the tool is too big, the dimensional accuracy of the rib cannot be guaranteed.

The deflection of the micro endmill can be calculated by knowing the stiffness of the tool and the force magnitude. For the tested  $\varnothing$  0.5 mm micro endmills, the tool stiffness was measured to be 0.4 N/ $\mu$ m. The stiffness of the machine tool is assumed to be 5 times higher than that of the cutting tool. If the average  $F_x$  is controlled to be smaller than 0.2 N, the deflection of the tool will be lower than 1  $\mu$ m. This is acceptable.

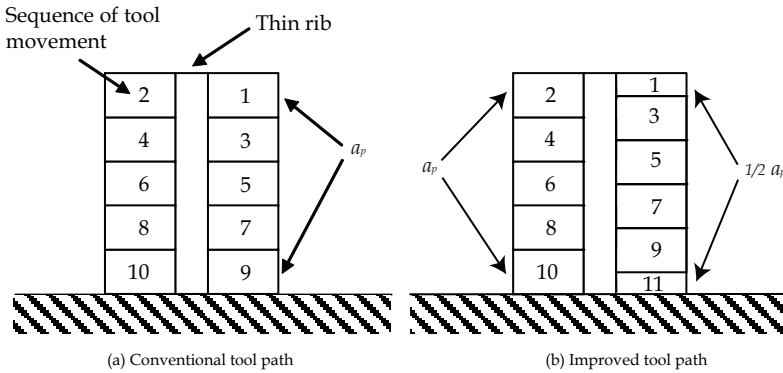


**Fig. 7.9:** Illustration of the conventional and the improved tool path. Up milling is assumed, tool moves into the paper at odd sequence, and out of the paper at even sequence.

## 7.4 Selection of tool paths

Tool path is another important factor that should be considered when planning the machining of micro ribs. In this section, first a conventional tool path is studied, which is commonly used in commercial CAM softwares when machining features like thin ribs; and then the tool path is improved especially for the machining of thin ribs. Afterward, the effectiveness of these two paths is compared by means of a FEM model of the micro rib.

### 7.4.1 Conventional tool path and improved tool path

The principle of the conventional tool path, Constant level  $Z$ , is demonstrated in Fig. 7.9a. In this drawing, up milling is assumed. To machine the rib, the cutting tool will start from the right side of the workpiece (Sequence 1), move in the direction away from the observer to remove a certain depth of material ( $a_p$ ); then the tool will move to the other side (Sequence 2), move in the direction towards the observer to remove the same amount of material as that in Sequence 1. Then the tool will move down to the position of Sequence 3. These movements will be repeated until all the materials are removed.

By using this tool path, the surfaces at both sides of the rib will be at the same level after an even number of tool movement sequences. It is clear in this figure that at the odd sequences of tool movements, the rib is supported by the material from the other side of the workpiece; however, at the even sequences, there is no support from the other side at all, which will result in bending of the

rib under the milling force.

The conventional tool path works well when the bending of the rib is not crucial. However, when the width of the rib is small enough and the designed AR is high, its drawback will become critical for the success of the machining.

To solve this problem, an improved tool path is proposed, as shown in Fig. 7.9b. The difference between the conventional tool path and the improved one can be clearly seen in this figure. For the improved tool path, again the cutting tool starts from the right side of the rib, however, it will only remove part of an  $a_p$  (50% for example) in Sequence 1. Then the tool moves to another side and machine full  $a_p$  in Sequence 2. After even number of tool sequences, the surfaces at both sides of the rib are not at the same level. The advantage of the improved tool path is that there is always support to the rib during machining, which is believed to serve the purpose to reduce the bending of the rib.

#### 7.4.2 FEM model of the rib

The effectiveness of the 2 types of tool paths is checked by means of a FEM model of the rib.

The rib is designated to be 25  $\mu\text{m}$  thick and 500  $\mu\text{m}$  high. The workpiece material is M261 which is the same as the material used for the force model. Its Young's Modulus is 210 GPa, density 0.0078  $\text{g}/\text{mm}^3$ . The FEM analysis was done by COSMOSWorks. Because it is a comparison study, the force magnitude is assumed to be 1 N for a full  $a_p$  (0.1 mm), and also 1 N for half an  $a_p$  since the force model predicts that the force will not increase significantly when the  $a_p$  is smaller than 0.1 mm, as shown in Fig. 7.7b. The direction of the force is normal to the rib and pushes the rib away. The location of the force is near the side edge of the rib, which represents the worse case among all the scenarios and will bend the rib most.

#### 7.4.3 Results and analysis

Analysis was done to each sequence of tool movements for both tool paths. The results are shown in Fig. 7.9 and Table 7.3; only the maximum deflection of the rib was recorded.

For the conventional tool path, when there is material support from the other side, the deflection of the rib is small ( $< 1 \mu\text{m}$ ) under the simulation conditions. However, when there is no support from the other side, the deflection of the rib is relatively big and increased rapidly when the force location approaches to the bottom of the rib. At the last tool movement (Sequence 10), the deflection of the

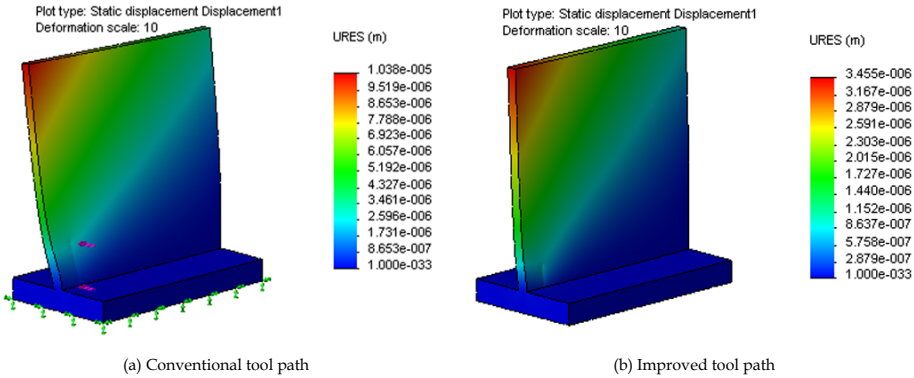


**Fig. 7.10:** Deflection of the rib at the last tool movement sequence, both for the conventional tool path and the improved tool path.

**Table 7.3:** Maximum deflections of the ribs for the two tool paths, Unit:  $\mu\text{m}$ .

Sequence	1	2	3	4	5	6	7	8	9	10	11
Path Con.	0.6	4.5	0.5	6.9	0.4	8.2	0.3	9.3	0.2	10.4	-
Path Imp.	0.6	1.3	1.6	1.9	2.0	2.1	2.2	2.3	2.3	2.4	3.5

rib is 10.4  $\mu\text{m}$ . When the strength of the rib is too low to withstand the force, the rib will break.

For the improved tool path, because there is always support at the other side of the rib, the increase of the deflection is more gradual and mild, and there is no clear difference between the odd and the even sequence. The deflection of the rib at the last movement (Sequence 11) is about 3.5  $\mu\text{m}$ , about 3 times lower than that when the conventional tool path is used.

This study shows that the quality of the micro rib can be improved by proper selected tool paths.

## 7.5 Behavior of the thin ribs

The rib model was used to test the behavior of the thin rib under different conditions.

**Dynamic behavior:** If the eigen-frequency of the rib is close to the frequency of the cutting process, the rib will start to vibrate. This will violate the dimensional accuracy or even break the rib. Therefore, the modal analysis was conducted to study the different structural resonances of a rib with different combination of width and height.

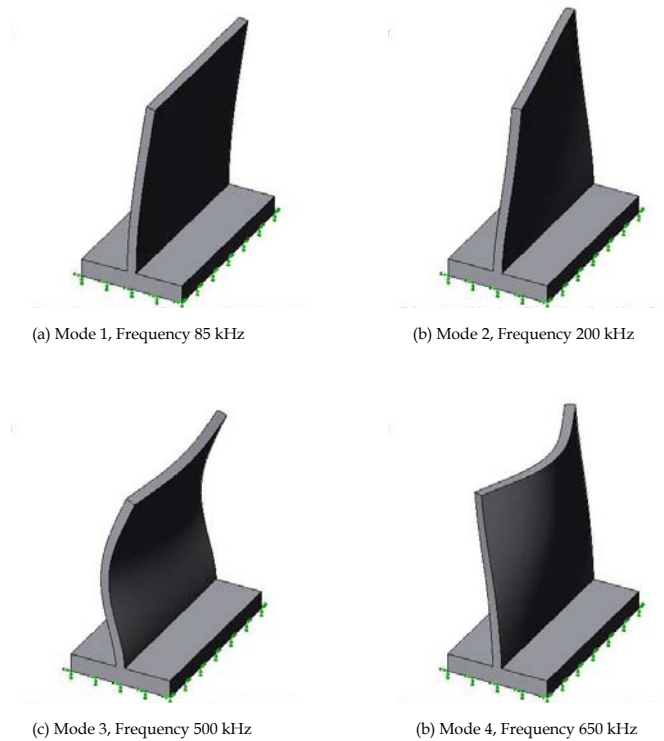


**Fig. 7.11:** Frequency study of the rib, width 25  $\mu\text{m}$ , AR 20.

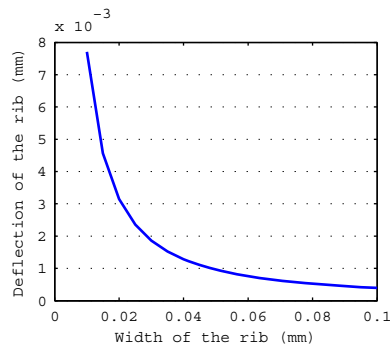


**Fig. 7.12:** Rib width VS rib deflection.

The first 4 mode shapes of a rib ( $L \times W \times H = 500 \times 25 \times 500 \mu\text{m}^3$ ) are shown in Fig. 7.11 as an example. The frequency of the first mode is 80 kHz. Suppose the spindle speed is 30000 RPM, and the micro endmill has 2 cutting edges; the cutting frequency will be 1000 Hz. The resonance frequencies are significantly

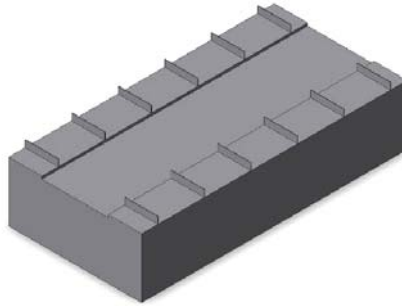


Fig. 7.13: CAD drawing of the workpiece with 12 ribs.

far away from the cutting frequencies. Therefore it can be concluded that the rib is unlikely to be excited by the cutting process.

**Width of the rib:** The relation between the width of the rib and its deflection was studied. The method to apply the force is the same as that introduced in Section 7.4. Only the improved tool path is used for this analysis. The results are shown in Fig. 7.12. It is seen that the deflection of the thin rib increased as a power relation with the decrease of the width of the rib. When the rib is 25  $\mu\text{m}$  wide, the deflection of the rib is about 2.1  $\mu\text{m}$  under 1 N force.

In order to achieve a good dimensional accuracy when the rib width is small, the force magnitude has to be controlled well together with other measures (such as runout). This can be done by calculating the maximum allowable force once the dimensional accuracy and rib stiffness is known. For example, if a rib of  $500 \times 25 \times 500 \mu\text{m}^3$  has to be machined, and the dimensional accuracy is set to be 2  $\mu\text{m}$ . From the FEM model, the stiffness of the rib at extremity is about 0.48 N/ $\mu\text{m}$ . The maximum allowable average force will then be 0.96 N.

## 7.6 Machining of micro ribs

Experiments were conducted to machine micro ribs with high ARs with conditions (machining parameters and tool paths) selected through theoretical analysis as introduced in former sections.

The machine tool is KERN EVO. The workpiece material is Böhler M261 with 46 HRC. On the  $20 \times 10 \text{ mm}^2$  surface of the workpiece 12 ribs will be machined, as shown in Fig. 7.13.

The machining of the ribs includes three operations, namely roughing, re-

roughing, and finishing operations. The function of each operation and the used tools and cutting conditions are introduced here briefly.

- **Roughing:** A  $\varnothing$  4 mm square endmill was used to remove the bulk material in the middle of the workpiece, as shown in Fig. 7.13. The groove in the middle is mainly for easy observations; therefore the allowance is not important at this stage.
- **Re-roughing:** A  $\varnothing$  3 mm square endmill was used to remove the material between 2 adjacent ribs, leaving enough allowance for the next operation. It is important to achieve the allowance accurately; otherwise the chip load for the micro endmills in the next operation will be higher than expected, and so will be the forces.
- **Finishing:** This is the operation that will form the ribs to their final shapes.  $\varnothing$  0.5 mm endmills with positive rake angles were chosen. The advantage of using such tools is that the generated force will be lower than that by using tools with negative rake angles; this is desired in order to keep the force level low. The disadvantage would be that the tool will wear out quickly. Low pressure air was used to blow away the chips during machining.

The 12 ribs on one workpiece were machined with different combinations of tool paths and parameters, and several repetitions to get a statistically reliable result. Ribs with lower ARs (for example  $50 \times 500 \mu\text{m}$ ) were first machined. Afterward the AR was increased gradually either by decreasing the width of the rib or by increasing the height of the rib to explore the capability of the process. In the end, 5 pieces (altogether 60 ribs) were machined in total.

Table 7.4 lists some of the designed ribs values, the cutting conditions, and the results. For all these tests, the spindle speed was fixed at 30000 rpm, which gave a relatively small spindle motion error according to a preliminary test. The feed rate was fixed at 420 mm/min.

All the Numerical Control (NC) codes were written manually to have a full control to the movement of the cutting tool. The total machining time for one workpiece was less than 1 hour. The machining time for one rib in the finishing operation was less than 30 seconds.

## 7.7 Results and analysis

The machined ribs were studied by means of the SEM and the WLI. The experimental results were compared with the theoretical analysis to check the effectiveness of the developed method.

**Table 7.4:** Example of designed ribs, cutting conditions and results

Designed value		Cutting conditions				Results		
Width ( $\mu\text{m}$ )	Height ( $\mu\text{m}$ )	$a_p$ ( $\mu\text{m}$ )	$a_c$ ( $\mu\text{m}$ )	Tool Path	Up/Down milling	Status	Width ( $\mu\text{m}$ )	AR
50	500	100	100	Con., new	Up	Successful	61	8
30	500	100	100, 200	Con., new	Up, Down	Successful	41	12
20	500	100	100, 200	Con., new	Up, Down	Successful	30	17
15	500	50	80	Con., new	Up	Successful	23	22
12	500	50	80	Con., new	Up	Successful	14	36
10	500	50	80	Con.	Up	Successful	15	33
10	500	50	80	New	Up	Successful	14	36
8	500	100	80	Con.	Up	Failed	-	-
8	500	100	80	New	Up	Successful	10	50
6	500	100	80	Con.	Up	Failed	-	-
6	500	100	80	New	Up	Successful*	8	63
16	800	40, 80	70, 80, 90	New	Up	Successful	21	38
12	800	40, 80	70, 80, 90	New	Up	Successful	15	53

Note: \* Successful in strategies, but the quality of the rib was not good.

\*\*The error in the rib width is due to the uncertainty in the tool dynamic cutting diameter.

### 7.7.1 General observations

In summary, the machining of micro ribs was successful; all the planned micro ribs could be realized under the chosen cutting conditions. No manual intervention was needed during machining; therefore, the trial-and-error method was avoided. Besides, ribs machined with the same nominal cutting conditions showed similar quality; this means that the repeatability of the process was good. Therefore, the results can be used for further analysis.

The achieved highest AR was about 63 (rib width about 8  $\mu\text{m}$ , rib height 500  $\mu\text{m}$ ); the machined ribs are shown in Fig. 7.14, the corresponding cutting conditions are shown in Table 7.4. From this figure, the overall shape of this rib was acceptable; the designed height was achieved. The small rip at the up corner was due to friction with a piece of chip which was attached to the tool for a short while during machining. This rib is the thinnest rib that was machined in experiments. The successful machining of such thin ribs showed that the cutting process was well under control and the chosen cutting conditions (parameters and tool paths) were appropriate. It shows that the micromilling process is capable of machining such micro features with high ARs when the process conditions are well planned.

However, it can also be seen in Fig. 7.14 that the quality of the rib is not good. The body of the rib became twisted. This is probably because the rib is so thin

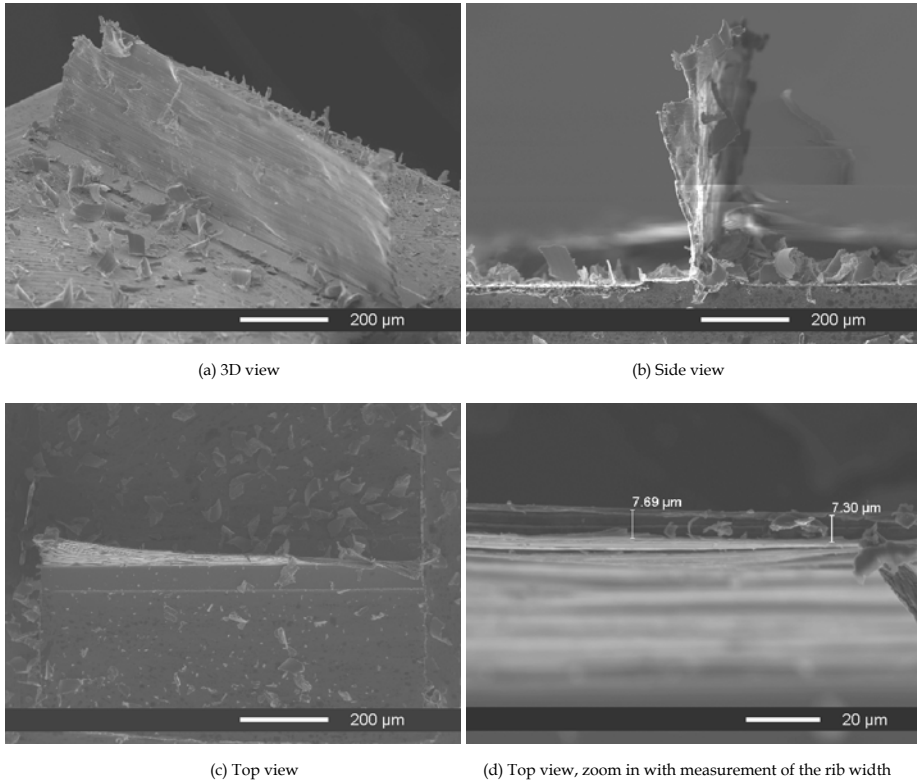


**Fig. 7.14:** The rib with an AR of 63 (width about 8  $\mu\text{m}$ , height 500  $\mu\text{m}$ ).

that it is not strong enough to withstand the force along the longitudinal direction of the rib ( $F_y$ ).

This means that when the rib is thick enough, the plastic deformation (chip formation) is local; when the rib is too thin, the plastic deformation will be more global. Therefore, when machining ribs in such a scale, the force not only in the cross feed direction but also in the feed direction should be considered.

Besides, it is seen in Fig. 7.14 that the quality of the machined surface is not very satisfactory. To improve the surface quality, the microstructure of the workpiece material should also be considered.

The rib in Fig. 7.15 has an AR of 54 (rib width about 15  $\mu\text{m}$ , height 800  $\mu\text{m}$ ). It is seen in this figure that the quality of this rib is good in both the shape and the surface quality. The rib is straight both seen from the side view in Fig. 7.15a and the top view in Fig. 7.15b. Fig. 7.15d shows the zoom-in view of the machined surface; it is rather smooth. The surface roughness was measured by the WLI; it

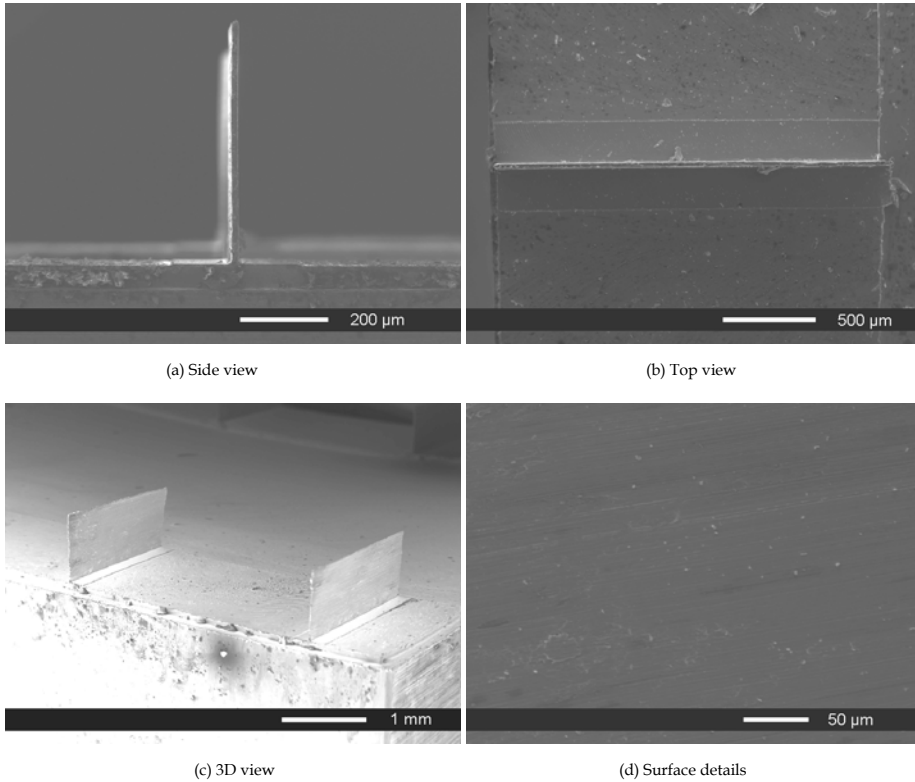


**Fig. 7.15:** The rib with an AR of 54 (width 15  $\mu\text{m}$ , height 800  $\mu\text{m}$ ).

is better than 0.3  $\mu\text{m}$  ( $Ra$ ).

In this work, the achievable AR was limited by the maximum underneck length of the micro cutting tools, which was 0.8 mm. Since the quality of the rib was very good under the chosen cutting conditions, it is believed that micro ribs with even higher AR can be machined successfully if tools with bigger underneck length are available.

**The error in the rib width:** It is seen in Table 7.4 that there is always a difference between the designed rib width and achieved rib width in practice. One of the main reasons for this error is that the dynamic cutting diameter of the micro endmill could not be measured accurately in this research due to the lack of suitable instrument/method. Because of this reason, as described before, the dimensional accuracy is not used as the criterion to evaluate the results in this research.

Other possible reasons for the error in the rib width include the positioning

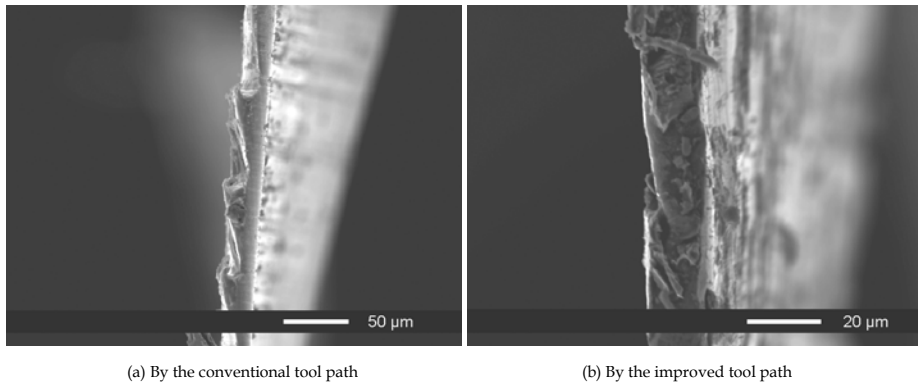


**Fig. 7.16:** Side views of the ribs machined by the two tool paths.

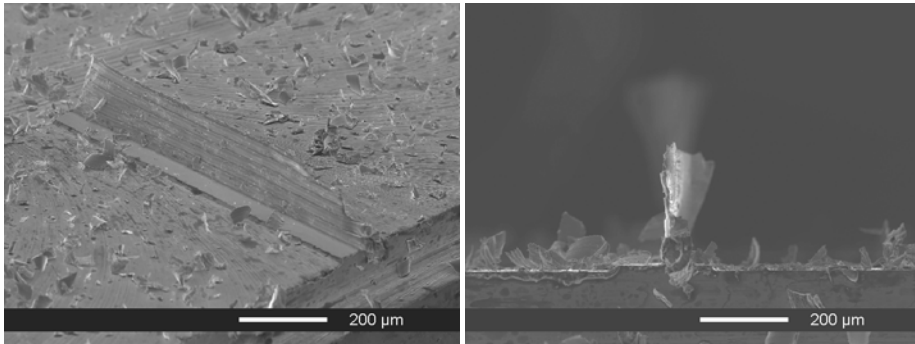
accuracy of the machine tool, process runout, bending of cutting tools and thin ribs, etc.

## 7.7.2 Tool paths

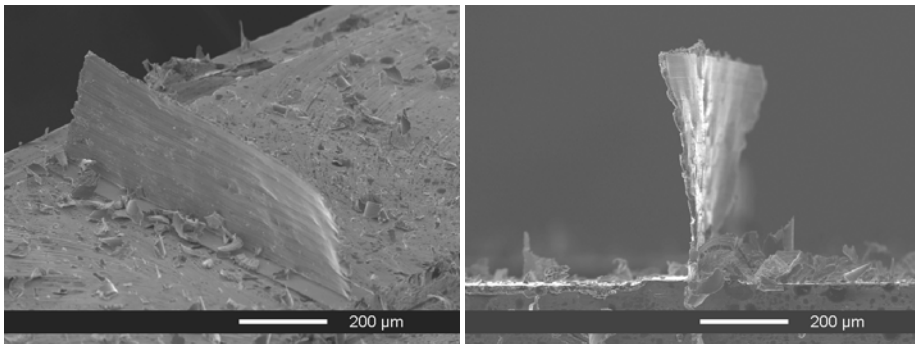
The ribs machined by the 2 types of tool paths are compared. Through tests, it was observed that the new improved tool path outperformed the conventional tool path in the aspect of keeping the shape of the rib, especially when the rib width was smaller than  $10\ \mu\text{m}$ . When the rib is within this range, the quality of the rib by using the conventional tool path was deteriorated, and then failed. While the ribs machined by using the improved tool path could always be machined successfully under the tested conditions.

The Fig. 7.16 is the zoom-in view of the side walls of the ribs machined by both types of tool paths. The width of the rib is about  $14\ \mu\text{m}$ . The rib machined by the conventional tool path, Fig. 7.16a, shows a saw-toothed shape on one side of the rib. The distance between two saw-teeth is  $50\ \mu\text{m}$ , which is equal to the applied  $a_p$ . This side is the even sequences of the tool movements, refer to Fig. 7.9a; there was no support from the other side during machining. On the contrary the rib machined by the improved tool path, shown in Fig. 7.16b, did not show this problem due to the support from the other side of the rib all the time during machining.

When the rib width was further decreased to be about  $8\ \mu\text{m}$ , the conventional tool path failed to machine the rib, as shown in Fig. 7.17a; the rib broke in the middle. The left height of the rib is about  $271\ \mu\text{m}$ . The rib made by the improved tool path, shown in Fig. 7.17b, could achieve the designed height,  $500\ \mu\text{m}$ , successfully.



(a) By the conventional tool path, 3D and side view, rib broke during machining



(b) By the improved tool path, 3D and side view, rib height is about 500  $\mu\text{m}$

**Fig. 7.17:** Ribs machined by two tool paths. The designed rib height is 500  $\mu\text{m}$ .

In summary, the experimental results confirmed the theoretical analysis that the improved tool path is more suitable for the machining of thin ribs compared with the conventional tool path.

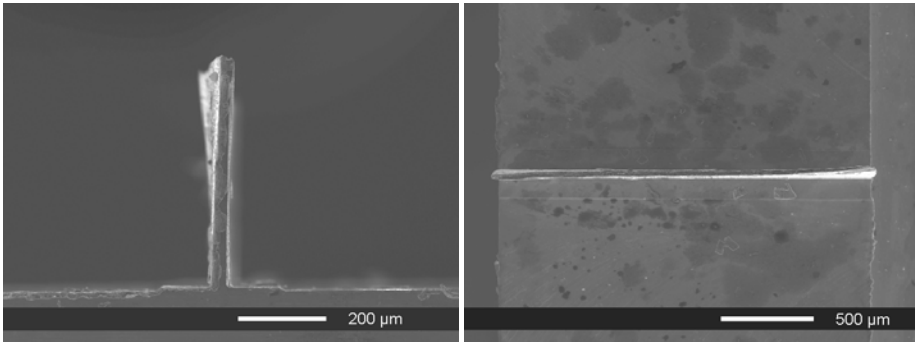
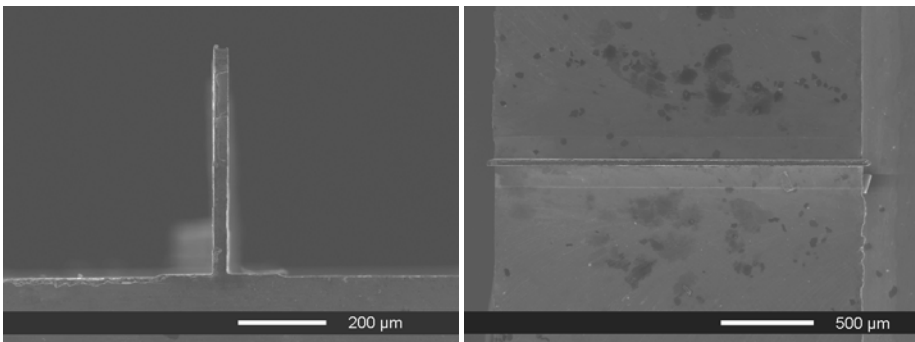
### 7.7.3 Cutting conditions

The fact that no premature breakage happened during machining, except those ribs (width  $< 10 \mu\text{m}$ ) by using the conventional tool path, indicates that the force level was well controlled by using the machining parameters selected by the force model.

**Cutting forces:** The measured cutting forces were compared with the theoretically predicted values. They showed good consistency, as shown in Table 7.5.

**Table 7.5:** Comparison of measured and predicted forces.

Rib Width ( $\mu\text{m}$ )	Cutting conditions			Ave $ F_x $ (N)	
	$a_p$ ( $\mu\text{m}$ )	$a_c$ ( $\mu\text{m}$ )	Up/Down milling	Measured	Predicted
30	100	100	Up	0.15	0.15
30	100	100	Down	0.84	0.92
19	80	70	Up	0.09	0.09
15	40	80	Up	0.05	0.02
10	50	80	Up	0.10	0.18

(a) Side view and top view of a rib (width  $30\ \mu\text{m}$ , height  $500\ \mu\text{m}$ ) machined by down milling(b) Side view and top view of a rib (width  $30\ \mu\text{m}$ , height  $500\ \mu\text{m}$ ) machined by up milling**Fig. 7.18:** Ribs machining by down milling and up milling, other conditions are same.

**Up and down milling:** As shown in Table 7.4, when machining ribs with a width of  $30\ \mu\text{m}$ , both up and down milling were used. The measured force in down milling was  $0.84\ \text{N}$ , which is about 5.6 times higher than that in up milling. This trend has been predicted by the force model accurately, as shown in Table 7.5. Because the rib was relatively thick, this force did not break the rib during machining; however, the quality of the rib has been deteriorated

compared with the one machined in up milling. In Fig. 7.18, the ribs machined under down milling and up milling were shown in comparison. It is seen that the rib machined by down milling, Fig. 7.18a, has deformed at both free ends; while the rib machined by up milling, Fig. 7.18b, kept good shape.

## 7.8 Discussion

In this chapter planning of machining parameters and tool paths in terms of machining micro features were studied. This could be a first approach towards a knowledge-based method to plan cutting conditions for the machining of micro features with high ARs.

For the purpose of demonstration, thin ribs with high ARs were chosen as the running example. The reason to choose the thin rib is that its simple geometry serves to minimize the influence from error sources other than the machining process.

The developed method includes the following aspects:

- Firstly, a force model was taken from literature to study the relation between machining parameters and the average forces. Based on this model, the machining parameters can be chosen to keep the force magnitude lower than a pre-defined value.
- Secondly, the effect of different tool paths was studied by means of a FEM model. The principle to choose tool paths for machining of thin ribs is to provide support to the structure during machining. Based on the FEM analysis, an improved tool path was proposed especially for the machining of thin ribs.
- Afterwards, the behavior of the thin rib under different conditions was studied. The dynamic study shows that the eigen-frequency of the thin rib is much higher than the cutting frequency from the process; the ribs will not be excited during machining.
- In the end, experiments were conducted to verify the theoretical analysis. The experimental results were consistent with the theoretical study. The highest AR achieved in this work was 63. The achievable AR is limited by the underneck length of the cutting tool.

The experimental results also show that when machining micro ribs thinner than 10  $\mu\text{m}$ , measures should be taken to avoid global deformation (e.g. by controlling force in the feed direction or using high strength material). Besides, the properties of the workpiece material should also be taken into account to improve the surface quality.

Although the developed method is demonstrated on the example geometry, thin ribs, it can be extended to machine other types of geometries. However, just like different application needs different type of cutting tools, the developed method have to be improved adaptively when a new geometry is to be machined.



# Chapter 8 Conclusions and recommendations

To fulfill the requirements in the market on developing alternative micromachining technologies for the machining of micro dies and moulds, investigations have been conducted in this research on micromilling technology in machining of hardened tool steels.

## 8.1 Background, project goal and approach

According to the literature survey, the fundamental cutting mechanism of micro orthogonal cutting is rather well understood. The process is influenced by the scaling effect: the undeformed chip thickness in micro scale cutting can be comparable in magnitude with the cutting edge radius of the cutting tool, and the grain size of the workpiece material. The detailed information is introduced in Chapter 1.

Micromilling is an interrupted process in nature. The instantaneous chip thickness varies with the rotation of the cutting tool; therefore, the whole tool passing period is divided into a shearing-dominant region and a ploughing-dominant region. For tools as small as  $\varnothing 0.3$  mm, the shearing-dominant region can be as big as 90% of the total tool immersion for a new tool. Therefore, it can be concluded that the general behavior of micromilling in this research is still mainly determined by the shearing period under the given experimental conditions.

Based on the literature survey and initial micromilling tests the general goal of this research is defined as to develop and describe a reliable micromilling process for precision machining of hardened tool steels. It was observed that the lives of the commercial micro endmills were too short to conduct a reliable cutting. Therefore, it was decided to improve the tool life first, and then to improve the performance of the process.

According to the practical situation (e.g. variation in tool quality), some

working approaches were defined, as introduced in Chapter 2. The main approaches include to conduct qualitative and comparative study and to pay more attention to the research method instead of specific observations.

In this research experiments were mainly done by using  $\varnothing$  0.5 mm square endmills on several predefined types of hardened tool steels. The gained knowledge and developed methods can be extended to micro endmills of different sizes and shapes and different types of workpiece materials.

## 8.2 Conclusions

From this research, the main conclusions can be summarized as follows:

- The micromilling process is influenced by the scaling effect.

The scaling down of the process geometry not only influences the cutting mechanism in micromilling (e.g. percentage of the shearing and ploughing periods), but also has an effect on the wear/life of micro endmills and the quality of the machined workpiece.

The scaling effect on tool wear is not shown on the types of tool wears; actually no new wear type was observed in this research when micromilling hardened tool steels by using commercial micro square endmills compared with macro scale milling, as discussed in Chapter 4. The reason that the tool wear was a serious issue in this research was because of the increasing ratio between the wear magnitude and the tool cutting geometry and the process geometry. As a result, once the tool wears out in micromilling, the geometry of the micro endmill will change greatly, so will be the process. When the tool is worn out, the effect cutting edge radius increases, the ploughing dominant period will increase.

Similarly, for the quality of the machined workpiece, the burr formation becomes a crucial issue in micromilling because the burr volume becomes relatively big compared with the size of micro features.

- The performance of micro endmills is the decisive factor for the application of micromilling technology at this moment.

As described in Chapter 4, the life of the tested commercial micro endmill was so short (e.g. about 3 mm<sup>3</sup> in the example shown in Fig. 4.6) that it could hardly satisfy the requirements of a reliable cutting task. The causes for the poor tool performance can be from many aspects, such as the errors from the tool manufacturing process, the tool geometry, machining parameters, tool paths, workpiece material properties, and machine tools.

Detailed examination of the tested commercial tool geometry showed that it

is mainly derived from that of macro endmills. With such geometry, the cutting edge corners are the weakest points along the cutting edges under the micromilling force, which makes the tool geometry one of the direct reasons for the observed tool failure. Besides, due to the limitation of the tool manufacturing process (CNC grinding), geometrical deviations are commonly seen in the tested tools, as introduced in Chapter 3.

Before any further investigation can be conducted, it was decided to improve the tool wear and tool life first. In this research, this was done by redesigning the tool geometry adaptively for hard milling applications, and by studying the relation between cutting conditions and tool paths and choosing appropriate cutting conditions. The detailed information is presented in Chapter 5 and Chapter 6.

- Design of Experiments has been proved to be useful for the planning of cutting conditions for micromilling at this stage.

It has been seen from the literature survey that current method to choose cutting conditions is mainly based on the recommendations of tool suppliers or trial-and-error practice, none of which can guarantee a successful micromilling process.

In this research DOE has been used to understand the influence of machining parameters and tool paths on the process response (tool wear, and surface finish), as presented in Chapter 5. The used experimental design includes  $2^2$  factorial design, simple comparison design, and central composite design for different purposes. By proper design of experiments, the most significant input variables can be identified through the statistical analysis. Besides, when the influence of input variables on the output is known, the values for these input variables can be selected accordingly to achieve an optimum output performance.

As the observed results in micromilling heavily depend on the experimental conditions due to the inconsistency in the quality of cutting tools, workpiece materials, machine tools, etc., this makes it preferable and meaningful to develop a method to select cutting conditions in this research, instead of simply reporting the specific observations. And the results in this research have proved that DOE can be used for this purpose.

- When the process is well understood and controlled, the performance of the micromilling process can be significantly improved.

In literature, examples of micro products were mainly machined by the trial-and-error method. Discussion was seldom given about how to plan machining parameters, and tool paths were mainly chosen according to knowledge in macro scale milling. As a result conservative conditions were

normally chosen to avoid tool premature failure, which resulted in an extremely long machining time.

In Chapter 7, a knowledge-based method is presented to demonstrate how to plan cutting conditions theoretically for the machining of micro features with high aspect ratios. It was decided to fully avoid the trial-and-error method; the selection of machining parameters and tool paths were based on theoretical models. The experimental results confirmed the theoretical analysis. Micro ribs with a thickness of about 10  $\mu\text{m}$  and an aspect ratio over 50 could be machined successfully. Besides, by using the developed method, the capability of the micromilling process can be fully exploited.

- About application of micromilling technology:

Although a better understanding of the micromilling process has been gained through the work conducted in this project, the application of micromilling technology in mold industries is still not as straight forward as macro endmilling. As discussed in this thesis, this is partly because of the inconsistency in the quality of micro endmills, workpiece materials, machine tools, etc. The recommended cutting conditions by tool suppliers can only be used as a reference to start with; optimum setting should be found adaptively according to the real application.

In the future, when the performance/properties of micro cutting tools, machine tools, and workpiece materials become more reliable through continuous technical improvement, the performance of micromilling will also be improved accordingly.

### 8.3 Recommendations

Although the life of micro square endmills has been improved significantly in this research by redesigning the geometry, the performance of micro carbide endmills is still the most critical factor for the application of micromilling. It is also seen that when machining hard to machine materials (e.g. AISI D2) the improvement of tool life by only improving tool geometry was limited. To overcome this problem, new tool substrate material or coating has to be developed and adopted. CBN tools have been used in macro scale milling; however, their application in micromilling is not commonly seen.

Besides, in order to achieve automation of the micromilling process and improve the productivity, it is important to monitor the tool condition online. The literature survey shows that this aspect is still at the early stage. More research needs to be done.

In this research, simple machining operations (slot and side milling) were

mainly used in order to get a fundamental understanding of the process. In the next stage, methods should be developed to machine 3D freeform geometries in order to make full use of the micromilling process. And the bending of micro endmills and micro features and its compensation need more attention.

Due to time limitation, the experiments were mainly done on  $\varnothing$  0.5 mm square endmills in this research. Micro ball nose endmills are commonly used in machining of micro moulds. In further research, performance of ball nose endmills and tools smaller than  $\varnothing$  0.5 mm should be investigated to get a further understanding of the process.

The workpiece materials are predefined and limited to several types of hardened tool steels in this research. Both the literature survey and the experimental investigation in this project have shown that the workpiece properties have significant effect on the micromilling process, such as tool performance and surface finish. In future research, it is beneficial to broaden the material range to conduct further analysis in this aspect.



# Bibliography

- 1 **enablingMNT**. URL [www.enablingmnt.com](http://www.enablingmnt.com), 2009.
- 2 **Liu, X., DeVor, R.E., Kapoor, S.G. and Ehmann, K.F.** The mechanics of machining at the microscale: assessment of the current state of the science. *Journal of Manufacturing Science and Engineering*, 2004, **126**, 666-678.
- 3 **Masuzawa, T.** State of the art of micromachining. *Annals of the CIRP*, 2000, **49**(2), 473-488.
- 4 **Masuzawa, T. and Tönshoff, H.K.** Three-dimensional micromachining by machine tools. *Annals of the CIRP*, 1997, **46**(2), 621-628.
- 5 **Chae, J., Park, S.S. and Freiheit, T.** Investigation of micro-cutting operations. *International Journal of Machine Tools & Manufacture*, 2006, **46**, 313-332.
- 6 **Dornfeld, D., Min, S. and Takeuchi, Y.** Recent advances in mechanical micromachining. *Annals of the CIRP*, 2006, **55**(2), 745-768.
- 7 **Adams, D.P., Vasile, M.J., Benavides, G. and Campbell, A.N.** Micromilling of metal alloys with focused ion beam-fabricated tools. *Precision Engineering*, 2001, **25**, 107-113.
- 8 Balzer's device for making milling-cutters. *Journal of the Franklin Institute*, 1896, **142**(6), 440-442.
- 9 **Tlusty, G.**, *Manufacturing Processes and Equipment*. (Prentice-Hall, Inc., Upper Saddle River, NJ 07458, 2000).
- 10 **Union Tool INC**. URL [www.uniontool.co.jp](http://www.uniontool.co.jp), 2009.
- 11 **Torres, C.D., Heaney, P.J., Sumant, A.V., Hamilton, M.A., Carpick, R.W. and Pfefferkorn, F.E.** Analyzing the performance of diamond-coated micro end mills *International Journal of Machine Tools & Manufacture*, 2009, 1-14.
- 12 **Performance Micro Tool Company**. URL [www.pmtnow.com](http://www.pmtnow.com). 2009.
- 13 **Weule, H., Schmidt, J., Huntrup, V. and Tritschler, H.** Micromilling of ferrous materials. *Production Engineering*, 1999, **6**(2), 17-20.
- 14 **Uhlmann, E. and Schauer, K.** Dynamic load and strain analysis for the optimization of micro end mills. *Annals of the CIRP*, 2005, **54**(1), 75-78.
- 15 **Dow, T.A., Miller, E.L. and Garrard, K.** Tool force and deflection compensation for small milling tools. *Precision Engineering*, 2004, **28**, 31-45.
- 16 **Tansel, I.N., Rodriguez, O., Trujillo, M., Paz, E. and Li, W.** Micro-end-milling--I. wear and breakage. *International Journal of Machine Tools & Manufacture*, 1998, **38**, 1419-1436.

- 17 **Bao, W.Y. and Tansel, I.N.** Modeling micro-end-milling operations. Part I: analytical cutting force model. *International Journal of Machine Tools & Manufacture*, 2000, **40**, 2155-2173.
- 18 **Rahman, M., Kumar, A.S. and Prakash, J.R.S.** Micro milling of pure copper. *Journal of Materials Processing Technology*, 2001, **116**, 39-43.
- 19 **Uhlmann, E., Piltz, S. and Schauer, K.** Micro milling of sintered tungsten-copper composite materials. *Journal of Materials Processing Technology*, 2005, **167**, 402-407.
- 20 **Zhou, L., Wang, C.Y., Qin, Z. and Li, W.H.** Wear characteristics of micro-end mill in high-speed milling of graphite electrode. *Key Engineering Materials*, 2004, **259-260**, 858-863.
- 21 **Luo, X., Cheng, K., Webba, D. and Wardle, F.** Design of ultraprecision machine tools with applications to manufacture of miniature and micro components. *Journal of Materials Processing Technology*, 2005, **167**, 515-528.
- 22 **Phillip, A.G., Kapoor, S.G. and DeVor, R.E.** A new acceleration-based methodology for micro/meso-scale machine tool performance evaluation. *International Journal of Machine Tools & Manufacture*, 2006, **46**(12-13), 1435-1444.
- 23 **Zdebski, D., Allen, D.M., Stephenson, D.J., Hedge, J., Ducros, C. and Sanchette, F.** An analysis of the effects of nanolayered nitride coatings on the lifetimes and wear of tungsten carbide micromilling tools. *Proceedings of 4th International Conference on Multi-Material Micro Manufacture*, pp. 179-182, Cardiff, UK, 2008.
- 24 **Makino Machine Tool.** URL [www.makino.com](http://www.makino.com), 2009.
- 25 **Wang, W., Kweon, S.H. and yang, S.H.** A study on roughness of the micro-end-milled surface produced by a miniaturized machine tool. *Journal of Materials Processing Technology*, 2005, **162-163**, 702-708.
- 26 **Bang, Y.B., Lee, K.M. and Oh, S.** 5-axis micro milling machine for machining micro parts. *International Journal of Advanced Manufacturing Technology*, 2005, **25**, 888-894.
- 27 **Takeuchi, Y., Sakaida, Y., Sawada, K. and Sata, T.** Development of a 5-axis control ultraprecision milling machine for micromachining based on non-friction servomechanisms. *Annals of the CIRP*, 2000, **49**(1), 295-298.
- 28 **Zhou, L., Yaguchi, Y., Fujii, T., Shimizu, J. and Eda, H.** Development of a multifunctional micro-machining system and its applications. *Key Engineering Materials*, 2003, **238-239**, 3-8.
- 29 **Vogler, M.P., Liu, X., Kapoor, S.G., DeVor, R.E. and Ehmman, K.F.** Development of meso-scale machine tool (mMT) systems. *Transactions of NAMRI/SME*, pp. 653-661, 2002.
- 30 **Filiz, S., Conley, C.M., Wasserman, M.B. and Ozdoganlar, O.B.** An experimental investigation of micro-machinability of copper 101 using tungsten carbide micro-endmills. *International Journal of Machine Tools & Manufacture*, 2007, **47**, 1088-1100.
- 31 **Cheng, K., Huo, D., Wardle, F. and Nor, K.M.** Design of a 5-axis ultraprecision micro milling machine (UltraMill) and its key enabling technologies. *Proceedings of the 9th euspen International Conference*, pp. 204-207, San Sebastian, Spain, 2009.
- 32 **Chern, G.L. and Chang, Y.C.** Using two-dimensional vibration cutting for micro-milling. *International Journal of Machine Tools & Manufacture*, 2006, **46**(6), 659-666.
- 33 **Son, S.M., Lim, H.S. and Ahn, J.H.** The effect of vibration cutting on minimum cutting thickness. *International Journal of Machine Tools & Manufacture*, 2006, **46**, 2066-2072.

- 34 **Malekian, M., Park, S.S. and Jun, M.B.G.** Tool wear monitoring of micro-milling operations. *Journal of Materials Processing Technology*, 2009, 1-12.
- 35 **Fang, F.Z., Wu, H., Liu, X.D., Liu, Y.C. and Ng, S.T.** Tool geometry study in micromachining. *Journal of Micromechanics and Microengineering*, 2003, **13**, 726-731.
- 36 **Weule, H., Hüntrup, V. and Tritschler, H.** Micro-cutting of steel to meet new requirements in miniaturization. *Annals of the CIRP*, 2001, **50**(1), 61-64.
- 37 **Aramcharoen, A. and Mativenga, P.T.** Size effect and tool geometry in micromilling of tool steel. *Precision Engineering*, 2008.
- 38 **Takács, M., Verő, B. and Mészáros, I.** Micromilling of metallic materials. *Journal of Materials Processing Technology*, 2003, **138**, 152-155.
- 39 **Schmidt, J. and Tritschler, H.** Micro cutting of steel. *Microsystem Technologies*, 2004, **10**, 167-174.
- 40 **Bissacco, G., Hansen, H.N. and De Chiffre, L.** Size effects on surface generation in micro milling of hardened tool steel *Annals of the CIRP*, 2006, **55**(1), 593-596.
- 41 **Gietzelt, T., Eichhorn, L. and Schubert, K.** Micromechanical structuring of polymers, metals, and ceramics. *Proceedings of the 1st International Conference on Multi-Material Micro Manufacture*, pp. 329-332, Karlsruhe, Germany, 2005.
- 42 **Bissacco, G., Hansen, H.N. and De Chiffre, L.** Micromilling of hardened tool steel for mould making applications. *Journal of Materials Processing Technology*, 2005, **167**, 201-207.
- 43 **Karpuschewski, B., Hoogstrate, A.M. and Oosterling, J.A.J.** IOP project proposal: micro milling of dies and moulds. pp. 1-17, Delft, the Netherlands, 2004.
- 44 **Uriarte, L., Ivanov, A., Oosterling, J.A.J., Staemmler, L., Tang, P.T. and Allen, D.M.** A comparison between microfabrication technologies for metal tooling. *Proceedings of the 1st International Conference on Multi-Material Micro Manufacture*, pp. 351-354, Karlsruhe, Germany, 2005.
- 45 **Bodenhausen, J.** Micro milling of steel for the mould and die industry. (Fraunhofer Institute for Production Technology, Aachen, Germany, 2004).
- 46 **Simoneau, A., Ng, E. and Elbestawi, M.A.** Surface defects during microcutting. *International Journal of Machine Tools & Manufacture*, 2006, **46**(12-13), 1378-1387.
- 47 **Simoneau, A., Ng, E. and Elbestawi, M.A.** Chip formation during microscale cutting of a medium carbon steel. *International Journal of Machine Tools & Manufacture*, 2006, **46**(5), 467-481.
- 48 **Simoneau, A., Ng, E. and Elbestawi, M.A.** The effect of microstructure on chip formation and surface defects in microscale, mesoscale, and macroscale cutting of steel. *Annals of the CIRP*, 2006, **55**(1), 97-102.
- 49 **Liu, K. and Melkote, S.N.** Finite element analysis of the influence of tool edge radius on size effect in orthogonal micro-cutting process. *International Journal of Mechanical Sciences*, 2007, **49**(5), 650-660.
- 50 **Ng, C.K., Melkote, S.N., Rahman, M. and Kumar, A.S.** Experimental study of micro- and nano-scale cutting of aluminum 7075-T6. *International Journal of Machine Tools & Manufacture*, 2006, **46**, 929-936.
- 51 **Son, S.M., Lim, H.S. and Ahn, J.H.** Effects of the friction coefficient on the minimum cutting thickness in micro cutting. *International Journal of Machine Tools & Manufacture*, 2005, **45**, 529-535.
- 52 **Lucca, D.A., Rhorer, R.L. and Komanduri, R.** Energy dissipation in the ultraprecision machining of copper. *Annals of the CIRP*, 1991, **40**(1), 69-72.

- 53 **Ikawa, N., Shimada, S. and Tanaka, H.** Minimum thickness of cut in micromachining. *Nanotechnology*, 1992, **3**, 6-9.
- 54 **Ikawa, N., Donaldson, R.R., Komanduri, R., König, W., Aachen, T.H., McKeown, P.A., Moriwaki, T. and Stowers, I.F.** Ultraprecision metal cutting - the past, the present and the future. *Annals of the CIRP*, 1991, **40**(2), 587-594.
- 55 **Ikawa, N., Shimada, S., Tanaka, H. and Ohmori, G.** An atomistic analysis of nanometric chip removal as affected by tool-work interaction in diamond turning. *Annals of the CIRP*, 1991, **40**(1), 551-554.
- 56 **Robinson, G.M. and Jackson, M.J.** A review of micro and nanomachining from a materials perspective. *Journal of Materials Processing Technology*, 2005, **167**, 316-337.
- 57 **Shaw, M.C.** *Metal Cutting Principles*. (Oxford University Press, Inc., New York, 2005).
- 58 **Boothroyd, G., ed.** *Fundamentals of Metal Machining and Machine Tools*. (Scripta, Washington, 1975).
- 59 **Lucca, D.A., Seo, Y.W. and Komanduri, R.** Effect of tool edge geometry on energy dissipation in ultraprecision machining. *Annals of the CIRP*, 1993, **42**(1), 83-86.
- 60 **Taminiau, D.A. and Dautzenberg, J.H.** Bluntness of the tool and process forces in high-precision cutting. *Annals of the CIRP*, 1991, **40**(1), 65-68.
- 61 **Kim, C.J., Bono, M. and Ni, J.** Experimental analysis of chip formation in micromilling. *Trans. NAMRI/SME*, 2002, **30**, 1-8.
- 62 **Shimada, S., Ikawa, N., Tanaka, H., Ohmori, G., Uchikoshi, J. and Yoshinaga, H.** Feasibility study on ultimate accuracy in microcutting using molecular dynamics simulation. *Annals of the CIRP*, 1993, **42**(1), 91-94.
- 63 **Yuan, Z.J., Zhou, M. and Dong, S.** Effect of diamond tool sharpness on minimum cutting thickness and cutting surface integrity in ultraprecision machining. *Journal of Materials Processing Technology*, 1996, **62**, 327-330.
- 64 **Moriwaki, T., Sugimura, N. and Luan, S.** Combined stress, material flow and heat analysis of orthogonal micromachining of copper. *Annals of the CIRP*, 1993, **42**(1), 75-78.
- 65 **Vogler, M.P., DeVor, R.E. and Kapoor, S.G.** On the modeling and analysis of machining performance in micro-endmilling, part I: surface generation. *Journal of Manufacturing Science and Engineering*, 2004, **126**, 685-694.
- 66 **Liu, K., Li, X.P. and Rahman, M.** Characteristics of high speed micro-cutting of tungsten carbide. *Journal of Materials Processing Technology*, 2003, **140**, 352-357.
- 67 **Kim, C.J., Mayor, J.R. and Ni, J.** A static model of chip formation in microscale milling. *Journal of Manufacturing Science and Engineering*, 2004, **126**, 710-718.
- 68 **Vogler, M.P., DeVor, R.E. and Kapoor, S.G.** On the modeling and analysis of machining performance in micro-endmilling, part II: cutting force prediction. *Journal of Manufacturing Science and Engineering*, 2004, **126**, 695-705.
- 69 **Ueda, K. and Iwata, K.** Chip formation mechanism in single crystal cutting of  $\beta$ -Brass. *Annals of the CIRP*, 1980, **29**, 65-68.
- 70 **Chuzhoy, L., DeVor, R.E., Kapoor, S.G., Beaudoin, A.J. and Bammann, D.J.** Machining simulation of ductile iron and its constituents, part 1: estimation of material model parameters and their validation. *Journal of Manufacturing Science and Engineering*, 2003, **125**, 181-191.

- 71 **Chuzhoy, L., DeVor, R.E. and Kapoor, S.G.** Machining simulation of ductile iron and its constituents, part 2: numerical simulation and experimental validation of machining. *Journal of Manufacturing Science and Engineering*, 2003, **125**, 192-201.
- 72 **To, S., Lee, W.B. and Chan, C.Y.** Ultraprecision diamond turning of aluminium single crystals. *Journal of Materials Processing Technology*, 1997, **63**, 157-162.
- 73 **Min, S., Dornfeld, D., Inasaki, I., Ohmori, H., Lee, D., Deichmueller, M., Yasuda, T. and Niwa, K.** Variation in machinability of single crystal materials in micromachining. *Annals of the CIRP*, 2006, **55**(1), 103-106.
- 74 **Lee, W.B., To, S. and Cheung, C.F.** Effect of crystallographic orientation in diamond turning of copper single crystals. *Scripta Materialia*, 2000, **42**, 937-945.
- 75 **Kang, I.S., Kim, J.S., Kim, J.H., Kang, M.C. and Seo, Y.W.** A mechanistic model of cutting force in the micro end milling process. *Journal of Materials Processing Technology*, 2007, **187-188**, 250-255.
- 76 **Pérez, H., Vizán, A., Hernandez, J.C. and Guzmán, M.** Estimation of cutting forces in micromilling through the determination of specific cutting pressures. *Journal of Materials Processing Technology*, 2007, **190**, 18-22.
- 77 **Zaman, M.T., Kumar, A.S., Rahman, M. and Sreeram, S.** A three-dimensional analytical cutting force model for micro end milling operation. *International Journal of Machine Tools & Manufacture*, 2006, **46**, 353-366.
- 78 **Kaneko, J., Teramoto, K., Onosato, M. and Takeuchi, Y.** Cutting error prediction for end milling on the basis of actual depth of cut. *Proceedings of the 9th International Conference on Manufacturing Excellence (ICME2003)*, 2003.
- 79 **Li, C., Lai, X., Li, H. and Ni, J.** Modeling of three-dimensional cutting forces in micro-end-milling. *Journal of Micromechanics and Microengineering*, 2007, **17**, 671-678.
- 80 **Perez, H., Vizan, A., Perez, J. and Labarga, J.** Analysis and validation of cutting forces prediction models in micromachining. *Materials Science forum*, 2006, **526**, 13-18.
- 81 **Ko, J.H. and Heisel, U.** Mechanistic cutting force model for micro ball-end milling. *The 2nd International Conference on Micromanufacturing*, pp. 80-85, Greenville, USA, 2007.
- 82 **Newby, G., Venkatachalam, S. and Liang, S.Y.** Empirical analysis of cutting force constants in micro-end-milling operations. *Journal of Materials Processing Technology*, 2007, **192-193**, 41-47.
- 83 **Jun, M.B.G., Liu, X., DeVor, R.E. and Kapoor, S.G.** Investigation of the dynamics of microend milling—part I: model development. *Journal of Manufacturing Science and Engineering*, 2006, **128**, 893-900.
- 84 **Jun, M.B.G., Liu, X., DeVor, R.E. and Kapoor, S.G.** Investigation of the dynamics of microend milling—part II: model validation and interpretation. *Journal of Manufacturing Science and Engineering*, 2006, **128**, 901-912.
- 85 **Bao, W.Y. and Tansel, I.N.** Modeling micro-end-milling operations. Part II: tool run-out. *International Journal of Machine Tools & Manufacture*, 2000, **40**, 2175-2192.
- 86 **Bao, W.Y. and Tansel, I.N.** Modeling micro-end-milling operations. Part III: influence of tool wear. *International Journal of Machine Tools & Manufacture*, 2000, **40**, 2193-2211.
- 87 **Liu, X., Jun, M.B.G., DeVor, R.E. and Kapoor, S.G.** Cutting mechanisms and their influence on dynamic forces, vibrations and stability in micro-endmilling. 2004

- ASME International Mechanical Engineering Congress and RD&D Expo, pp. 1-10, Anaheim, California, USA, 2004.
- 88 **Vogler, M.P., DeVor, R.E. and Kapoor, S.G.** Microstructure-level force prediction model for micro-milling of multi-phase materials. *Journal of Manufacturing Science and Engineering*, 2003, **125**, 202-209.
- 89 **Park, S., Kapoor, S.G. and DeVor, R.E.** Mechanistic cutting process calibration via microstructure-level finite element simulation model. *Journal of Manufacturing Science and Engineering*, 2004, **126**, 706-709.
- 90 **Friedrich, C.R. and Kulkarni, V.P.** Effect of workpiece springback on micromilling forces. *Microsystem Technologies*, 2004, **10**, 472-477.
- 91 **Schmidt, J., Tritschler, H. and Haberer, H.** Cutting tools and material conditioning for micro end milling of tool steel. 2nd euspen International Conference, pp. 624-627, Turin, Italy, 2001.
- 92 **Aramcharoen, a. and Mativenga, P.T.** Tool wear modes in micro/mesoscale milling of hardened die steel. *CIRP 3rd International Conference High Performance Cutting*, pp. 179-188, Dublin, 2008.
- 93 **Gandarias, E., Dimov, S., Pham, D.T., Ivanov, A., Popov, K., Lizarralde, R. and Arrazola, P.J.** New methods for tool failure detection in micro-milling. *Proceedings of the 1st International Conference on Multi-Material Micro Manufacture*, pp. 371-374, Karlsruhe, Germany, 2005.
- 94 **Bissacco, G., Hansen, H.N. and De Chiffre, L.** Improving axial depth of cut accuracy in micromilling *Proceedings of 4th euspen International Conference*, pp. 386-387, Glasgow, UK, 2004.
- 95 **Jun, M.B.G., Bourne, K., DeVor, R.E. and Kapoor, S.G.** Estimation of effective error parameters in high-speed micro-endmilling. *International Journal of Machine Tools & Manufacture*, 2007, **47**(9), 1449-1454.
- 96 **Camuscu, N. and Aslan, E.** A comparative study on cutting tool performance in end milling of AISI D3 tool steel. *Journal of Materials Processing Technology*, 2005, **170**, 121-126.
- 97 **Fallbohmer, P., Rodriguez, C.A., Ozel, T. and Altan, T.** High-speed machining of cast iron and alloy steels for die and mold manufacturing. *Journal of Materials Processing Technology*, 2000, **98**, 104-115.
- 98 **Nelson, S., Schueller, J.K. and Tlusty, J.** Tool wear in milling hardened die steel. *Journal of Manufacturing Science and Engineering*, 1998, **120**, 669-673.
- 99 **Urbanski, J.P., Koshy, P., Dewes, R.C. and Aspinwall, D.K.** High speed machining of moulds and dies for net shape manufacture. *Materials and Design*, 2000, **21**, 395-402.
- 100 **Tönshoff, H.K., Arendt, C. and Ben Amor, R.** Cutting of hardened steel. *Annals of the CIRP*, 2000, **49**(2), 547-566.
- 101 **Koshy, P., Dewes, R.C. and Aspinwall, D.K.** High speed end milling of hardened AISI D2 tool steel (~58 HRC). *Journal of Materials Processing Technology*, 2002, **127**, 266-273.
- 102 **Choudhury, S.K. and Rath, S.** In-process tool wear estimation in milling using cutting force model. *Journal of Materials Processing Technology*, 2000, **99**, 113-119.
- 103 **Sarhan, A., Sayed, R., Nassr, A.A. and El-Zahry, R.M.** Interrelationships between cutting force variation and tool wear in end-milling. *Journal of Materials Processing Technology*, 2001, **109**, 229-235.

- 104 **Shao, H., Wang, H.L. and Zhao, X.M.** A cutting power model for tool wear monitoring in milling. *International Journal of Machine Tools & Manufacture*, 2004, **44**, 1503-1509.
- 105 **Arcona, C. and Dow, T.A.** An empirical tool force model for precision machining. *Journal of Manufacturing Science and Engineering*, 1998, **120**, 700-707.
- 106 **Bayoumi, A.E., Barnwal, S. and Hutton, D.V.** Prediction of flank wear and engagements from force measurements in end milling operations. *Wear*, 1993, **170**, 255-266.
- 107 **Teitenberg, T.M., Bayoumi, A.E. and Yucesan, G.** Tool wear modeling through an analytic mechanistic model of milling processes. *Wear*, 1992, **154**, 287-304.
- 108 **Dimov, S., Pham, D.T., Ivanov, A. and Fansen, K.** Micromilling strategies: optimization issues. *The Institution of Mechanical Engineers. Part B. Journal of engineering manufacture* pp. 731-736, 2004.
- 109 **Schubert, A., Schneider, J. and Eckert, U.** Influence of special milling strategies on accuracy and surface quality of microstructured forms and prototypes. *CIRP 3rd International Conference High Performance Cutting*, pp. 131-140, Dublin, Ireland, 2008.
- 110 **Tansel, I.N., Arkan, T.T., Bao, W.Y., Mahendrakar, M., Shisler, B., Smith, D. and McCool, M.** Tool wear estimation in micro-machining. Part I: tool usage-cutting force relationship. *International Journal of Machine Tools & Manufacture*, 2000, **40**, 599-608.
- 111 **Tansel, I.N., Arkan, T.T., Bao, W.Y., Mahendrakar, N., Shisler, B., Smith, D. and McCool, M.** Tool wear estimation in micro-machining. Part II: neural-network-based periodic inspector for nonmetals. *International Journal of Machine Tools & Manufacture*, 2000, **40**, 609-620.
- 112 **Tansel, I.N., Trujillo, M., Nedbouyan, A., Velez, C., Bao, W.Y., Arkan, T.T. and Tansel, B.** Micro-end-milling--III. wear estimation and tool breakage detection using acoustic emission signals. *International Journal of Machine Tools & Manufacture*, 1998, **38**, 1449-1466.
- 113 **Litwinski, K.M., Min, S., Lee, D.-E., Dornfeld, D.A. and Lee, N.** Scalability of tool path planning to micro machining. *1st International Conference on Micromanufacturing ICOMM*, Urbana-Champaign, Illinois, USA, 2006.
- 114 **Schmidt, J., Spath, D., Elsner, J., Huntrup, V. and Tritschler, H.** Requirements of an industrially applicable microcutting process for steel micro-structures. *Microsystem Technologies*, 2002, **8**, 402-408.
- 115 **Popov, K., Dimov, S., Pham, D.T. and Ivanov, A.** New solutions for improving reliability and reducing uncertainty in micro-milling. *CIRP 3rd International Conference High Performance Cutting*, pp. 159-168, Dublin, Ireland, 2008.
- 116 **Schaller, T., Bohn, L., Mayer, J. and Schubert, K.** Microstructure grooves with a width of less than 50 mm cut with ground hard metal micro end mills. *Precision Engineering*, 1999, **23**, 229-235.
- 117 **Chern, G.L., Wu, Y.J.E., Cheng, J.C. and Yao, J.C.** Study on burr formation in micro-machining using micro-tools fabricated by micro-EDM. *Precision Engineering*, 2007, **31**, 122-129.
- 118 **Lee, K. and Dornfeld, D.A.** Micro-burr formation and minimization through process control. *Precision Engineering*, 2005, **29**, 246-252.
- 119 **Lee, K. and Dornfeld, D.A.** An experimental study on burr formation in micro milling aluminum and copper. *Transactions of the NAMRI/SME*, pp. 255-262(2002).

- 120 **Horsch, C., Schulze, V. and Lohe, D.** Topography and microstructure of cavities obtained by micro-milling of tool steel. *Werkstoff Informationsgesellschaft mbH*, pp. 1-7, Frankfurt, 2003.
- 121 **Altintas, Y.** *Manufacturing Automation: Metal Cutting Mechanics, Machine Tool Vibrations, and CNC Design.* (Cambridge university press, 2000).
- 122 **Salgado, M.A., Lopez de Lacalle, L.N., Lamikiz, A., Munoa, J. and Sanchez, J.A.** Evaluation of the stiffness chain on the deflection of end-mills under cutting forces. *International Journal of Machine Tools & Manufacture*, 2005, **45**, 727-739.
- 123 **Rao, V.S. and Rao, P.V.M.** Tool deflection compensation in peripheral milling of curved geometries. *International Journal of Machine Tools & Manufacture*, 2006, **46**, 2036-2043.
- 124 **Uriarte, L., Zatarain, M., Santiso, G., Lopez de Lacalle, L.N. and Albizuri, J.** Evaluation of dynamic parameters of micromilling tools smaller than 0.3 mm in diameter. *Proceedings of the 1st International Conference on Multi-Material Micro Manufacture*, pp. 325-328, Karlsruhe, Germany, 2005.
- 125 **Uriarte, L., Herrero, A., Zatarain, M., Santiso, G. and de Lacalle, L.N.L.e.** Error budget and stiffness chain assessment in a micromilling machine equipped with tools less than 0.3mm in diameter. *Precision Engineering*, 2007, **31**, 1-12.
- 126 **Miyaguchi, T., Masuda, M., Takeoka, E. and Iwabe, h.** Effect of tool stiffness upon tool wear in high spindle speed milling using small ball end mill. *Precision Engineering*, 2001, **25**, 145-154.
- 127 **Mitsubishi Materials Corporation.** URL [www.mitsubishicarbide.com](http://www.mitsubishicarbide.com), 2009.
- 128 **Fehlmann AG.** URL [www.fehlmann.com](http://www.fehlmann.com), 2009.
- 129 **Georg Fisher AG.** URL [www.gfac.com](http://www.gfac.com), 2009.
- 130 **KERN Precision INC.** URL [www.kern-microtechnic.com](http://www.kern-microtechnic.com), 2009.
- 131 **Kistler Instrument AG.** URL [www.kistler.com](http://www.kistler.com), 2009.
- 132 **Taylor Hobson Ltd.** URL [www.taylor-hobson.com](http://www.taylor-hobson.com), 2009.
- 133 **Veeco.** URL [www.veeco.com](http://www.veeco.com), 2009.
- 134 **Keyence Corporation.** URL [www.keyence.com](http://www.keyence.com), 2009.
- 135 **JEOL Ltd.** URL [www.jeol.com](http://www.jeol.com), 2009.
- 136 **FEI Company.** URL [www.fei.com](http://www.fei.com), 2009.
- 137 **Olympus Corporation.** URL [www.olympus-global.com](http://www.olympus-global.com), 2009.
- 138 **Wilson Instruments.** URL [www.wilsoninstruments.com](http://www.wilsoninstruments.com), 2009.
- 139 **Özel, T., Liu, X. and Dhanorker, A.** Modelling and simulation of micro-milling process. *The 4th International Conference and Exhibition on Design and Production of Machines and Dies/Molds*, Cesme, Turkey, 2007.
- 140 **Solidworks Corp.** URL [www.solidworks.com](http://www.solidworks.com).
- 141 **Production Machining.** URL [www.productionmachining.com](http://www.productionmachining.com), 2009.
- 142 **Faassen, R.** Chatter prediction and control for high-speed milling: modelling and experiments. (Eindhoven University of Technology, Eindhoven, the Netherlands, 2007).
- 143 **Jun, M.B.G.** Modeling and analysis of micro-end milling dynamics. *Mechanical Engineering*, p. 193 (University of Illinois at Urbana-Champaign, Urbana, Illinois, 2005).

- 144 **Kweon, S.H., Lee, S.M., Lee, J.H. and Yang, S.H.** Chatter stability evaluation of a miniaturized machine tool using receptance coupling method. Proceedings of the euspen International Conference, pp. 514-517, Zurich, Switzerland, 2008.
- 145 **NIST/SEMATECH e-handbook of statistical methods.** URL [www.itl.nist.gov/div898/handbook/](http://www.itl.nist.gov/div898/handbook/), 2006.
- 146 **Montgomery, D.C.** Design and Analysis of Experiments. (John Wiley & Sons, INC., 2001).
- 147 **Petersen, R.G., ed.** Design and Analysis of Experiments. (Marcel Dekker, INC., New York, 1985).
- 148 **Vivancos, J., Luis, C.J., Ortiz, J.A. and González, H.A.** Analysis of factors affecting the high-speed side milling of hardened die steels. Journal of Materials Processing Technology, 2005, **162-163**, 696-701.
- 149 **Toh, C.K.** A study of the effects of cutter path strategies and orientations in milling. Journal of Materials Processing Technology, 2004, **152**, 346-356.
- 150 **Toh, C.K.** Cutter path strategies in high speed rough milling of hardened steel. Materials and Design, 2006, **27**, 107-114.
- 151 **The MathWorks INC.** URL [www.mathworks.com](http://www.mathworks.com), 2009.
- 152 **Diniz, A.E. and Filho, J.C.** Influence of the relative positions of tool and workpiece on tool life, tool wear and surface finish in the face milling process. Wear, 1999, **232**, 67-75.
- 153 **ISO 4287.** Geometrical Product Specifications (GPS) - Surface texture: Profile method - Terms, definitions and surface texture parameters, 1997.
- 154 **Van Hoorn Hardmetaal BV.** URL [www.hoorn-carbide.com](http://www.hoorn-carbide.com), 2009.
- 155 **Takeuchi, Y., Suzukawa, H., Kawai, T. and Sakaida, Y.** Creation of ultra-precision microstructures with high aspect ratios. Annals of the CIRP, 2006, **55(1)**, 107-110.
- 156 **Je, T., Lee, J., Choi, D., Lee, E., Shin, B. and Whang, K.** A study of the micro pole structure fabrication and application technology by micro end-milling processes. Engineering Materials, 2004, **257-258**, 453-458.
- 157 **Popov, K., Dimov, S., Pham, D.T. and Ivanov, A.** Micromilling strategies for machining thin features. Institution of Mechanical Engineers, Part C: Journal of Mechanical Engineering Science, pp. 1677-1684, 2006.
- 158 **Halevi, G. and Weill, R.D.** Principles of Process Planning: A Logical Approach. (Chapman & Hall, 1995).
- 159 **Fleischer, J., Deuchert, M. and Chlipala, M.** Development of a 5-axis micro-test-work piece for micro-milling machine tools. CIRP 3rd International Conference High Performance Cutting, pp. 795-804, Dublin, Ireland, 2008.
- 160 **Armarego, E.J.A., Wang, J. and Deshpande, N.P.** Computer-aided predictive cutting model for forces in face milling allowing for tooth run-out. Annals of the CIRP, 1995, **44(1)**, 43.
- 161 **Budak, E., Altintas, Y. and Armarego, E.J.A.** Prediction of milling force coefficients from orthogonal cutting data. Journal of Manufacturing Science and Engineering, 1996, **118**, 216-224.
- 162 **Gradišek, J., Kalveram, M. and Weinert, K.** Mechanistic identification of specific force coefficients for a general endmill. International Journal of Machine Tools & Manufacture, 2004, **44**, 401-414.



# Appendix A Measurement of the dynamic cutting radius of a micro endmill

As described in Chapter 3 the equipped tool setting system on the machine tools fails to measure accurately the cutting radius of a micro endmill when it is rotating. Therefore, a method was developed to measure the tool dynamic cutting radius manually; this manually measured value was used to replace the data in the tool table of the machine.

The developed method is summarized as follows:

- The geometrical cutting radius of the micro endmill is first measured by an optical microscope. This is the value by 'microscope' in Fig. A.3. It is a static measurement and used as a reference.
- Insert the micro endmill in a tool holder, and put the tool holder into the spindle. Warm up the spindle at the same rotational speed as used in machining.
- Measure the tool cutting radius at the aforementioned rotational speed by means of the BLUM laser tool setting system equipped on the machine. Read out the measured value from the tool table inside the machine control software. This is the dynamic tool cutting radius, by 'BLUM' in Fig. A.3.

The measurement has to be done at the same speed as testing because the dynamic cutting radius is spindle speed dependent.

- Clamp a piece of resin on the table of the machine, as shown in Fig. A.1, warm up the spindle, and drill a shallow hole on the top surface of the resin with the micro endmill under the same rotation speed.
- Measure the radius of the drilled hole on the resin by an optical microscope, as illustrated in Fig. A.2. This is supposed to be the real dynamic cutting radius of the micro endmill, represented by 'Drilled hole' in Fig. A.3.
- Compare the three measurements, namely the geometrical radius, the BLUM value, and the radius of the drilled hole, as shown in Fig. A.3. In this figure,

results of 5 tests with 5 different tools are shown. The result can be used to evaluate the accuracy of the BLUM system and to correct the tool data in the tool table inside the machine control software.

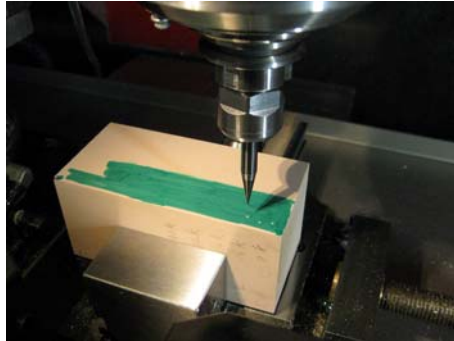


**Fig. A.1:** Drill a hole on a piece of resin by the micro endmill under the same rotational speed as used in machining.



**Fig. A.2:** Measure the radius of the drilled hole by an optical microscope.

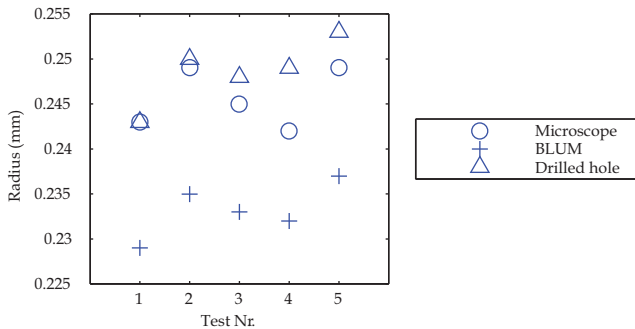


**Fig. A.3:** Comparison of the tool cutting radius measured by three methods. It is seen that the BLUM system gave smaller values than the other two methods.

## Appendix B Method to set up the workpiece coordinate in Z direction

The spindle is the main thermal source on the machine tool, it will elongate when warming up, which will result in a significant error in the depth of cut as described in Chapter 3. This error can be in the same magnitude as the applied depth of cut, therefore it has to be corrected when investigating the effect of machining parameters in micromilling.

Since the error is mainly in the Z direction and the error in the X and Y directions are relatively small and not critical for the experiments (because mainly slot milling and side milling are conducted), a method is developed to set up the Z coordinate manually. It is described as follows:

- Clamp the workpiece on the machine tool; mark the top surface of the workpiece with color for ease of observation, as shown in Fig. B.1.
- Warm up the spindle: the warming up time depends on the machine tool, a preliminary test is necessary to determine this property of the machine tool.
- Set up the workpiece coordinate (X, Y and Z directions) by means of the infrared touch probe equipped on the machine.
- Load the micro endmill into the spindle, and warm up the spindle again for about 10 minutes with the same rotation speed as used in machining.
- Move the cutting tool vertically towards the workpiece to a position 0.05 mm (suppose the error due to spindle thermal elongation is not bigger than 0.05 mm) above the workpiece.
- Move the cutting tool horizontally over the workpiece, lift the tool, and return the initial position. If the tool does not contact the workpiece, move the tool vertically down with a step of 2  $\mu\text{m}$ , as shown in Fig. B.2a.
- Repeat last procedure until the cutting tool touches the top surface of the workpiece.

- Set this new position to be  $Z=0$ .

Or the vertical step can be increased to 10 or 20  $\mu\text{m}$ , repeat the aforementioned procedures until the tool cuts the top layer of the workpiece material off, set new machined surface as  $Z=0$ , as shown in Fig. B.2b.

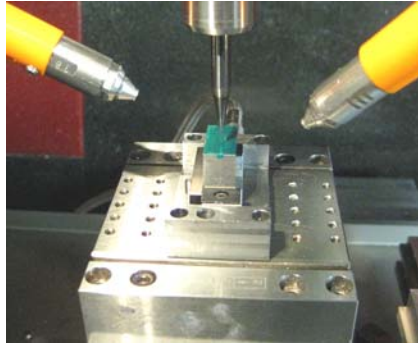
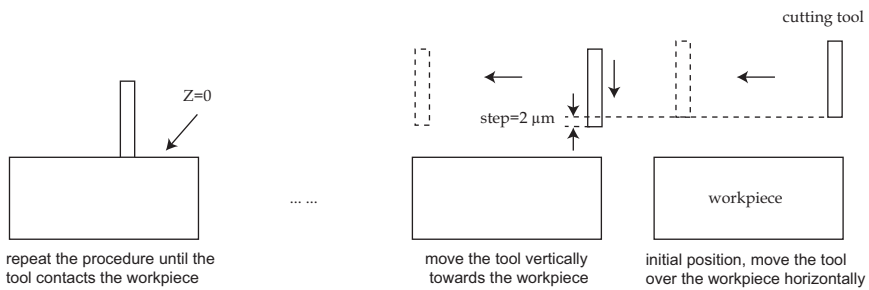
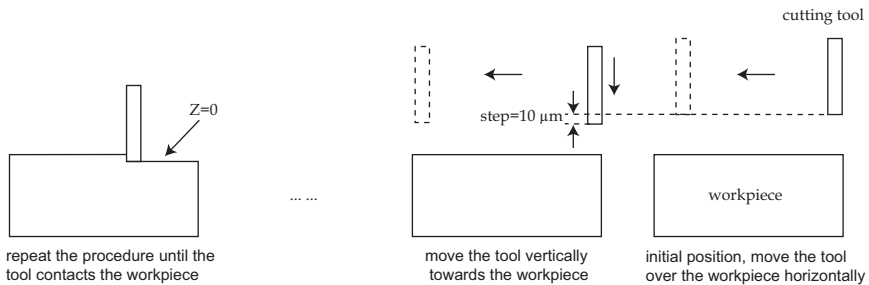


**Fig. B.1:** The top surface of the workpiece is colored for the setting of the Z coordinate.



(a) Use small steps until the tool contacts the workpiece. The advantages are the  $Z=0$  position can be set accurately and no damage to the tool; the disadvantage is time consuming.



(b) Use big steps until the tool removes some material. The advantage is it is quick and  $Z=0$  can be set accurately; the disadvantage is the cutting tool may be worn out, especially when the workpiece has a higher hardness.

**Fig. B.2:** Illustration of setting up the  $Z=0$  position manually. The sequence is illustrated from right to left.

## Appendix C Selection of spindle speed to minimize the motion error

The choice of the spindle speed in micromilling is constrained by many factors, such as the speed range of the spindle used, stability of the process (e.g. chatter), machinability of workpiece materials, desired productivity and production cost, and spindle motion error. Among all these factors, the spindle motion error becomes more important with the scaling down of the cutting tool, and it is seldom addressed in literature.

In this appendix, a test done at TNO Science and Industry Eindhoven is referred to illustrate how to learn the performance of the spindle and choose the right spindle speed to minimize the spindle motion error.

The basic principle of the test is to measure the spindle motion error under different rotational speeds by means of high precision capacitive sensors. In this test, three capacitive sensors were clamped on the table of the Mikron HSM 700; two sensors were in the X-Y plane to measure the radial motion error of the spindle, one sensor was in the Z direction to measure the axial error. A cylinder bar was inserted into the tool holder, and then to the spindle to replace the cutting tool. The measurement setup is illustrated in Fig. C.1.

The used sensor was capacitive C7-C; the bandwidth is 15kHz, applied range 250  $\mu\text{m}$ , and resolution 3.5 nm (rms). The following can be measured by this setup: the thermal drift of the spindle, synchronous motion error, asynchronous motion error, and revolutions per minute. The radial motion error is of the interest here, and the results of the test are shown in Fig. C.2.

The test results show clearly that the spindle has different magnitudes of motion errors under different rotational speeds. For the tested spindle, the speed with the smallest motion error is around 24000 rpm; the magnitude of the total error is about 0.57  $\mu\text{m}$ .

When the rotational speed is chosen to be the maximum speed for this spindle, 42000 rpm, the total motion error is about 7.50  $\mu\text{m}$ . If the cutting is done at this

speed for micromilling, there will be unavoidably uneven loads on the cutting edges of the micro endmill, which will speed up tool wear rate and shorten the tool life.

Therefore, it is important to take into account the motion error factor when choosing the spindle speed for micromilling.

An alternative method can be to drill holes on a piece of soft material under different rotational speeds, and measure and compare the radii of drilled holes afterwards.

However, it has to be pointed out that to choose the spindle speed with the smallest motion error does not necessarily mean that the runout at the tool tip will be the smallest. As discussed in Chapter 4 the spindle is only one of the components in the chain that will lead to a runout at the tool tip. In order to minimize the runout at the tool tip, all the components have to be set carefully.

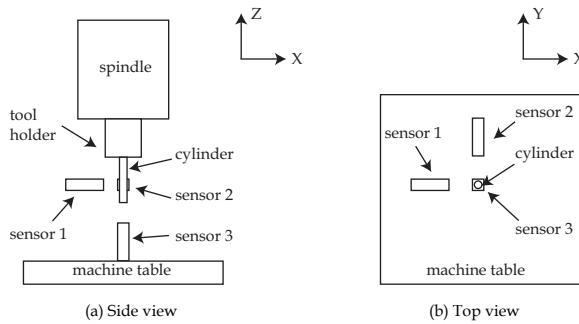


Fig. C.1: Illustration of the setup to measure the spindle motion error (not in scale).

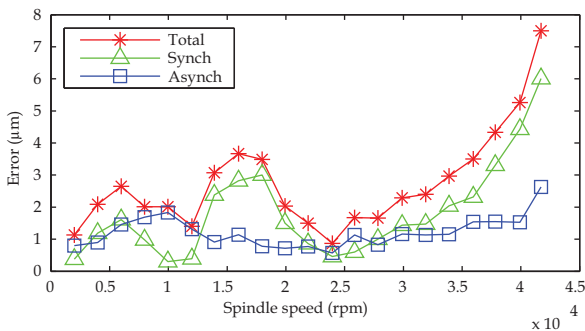
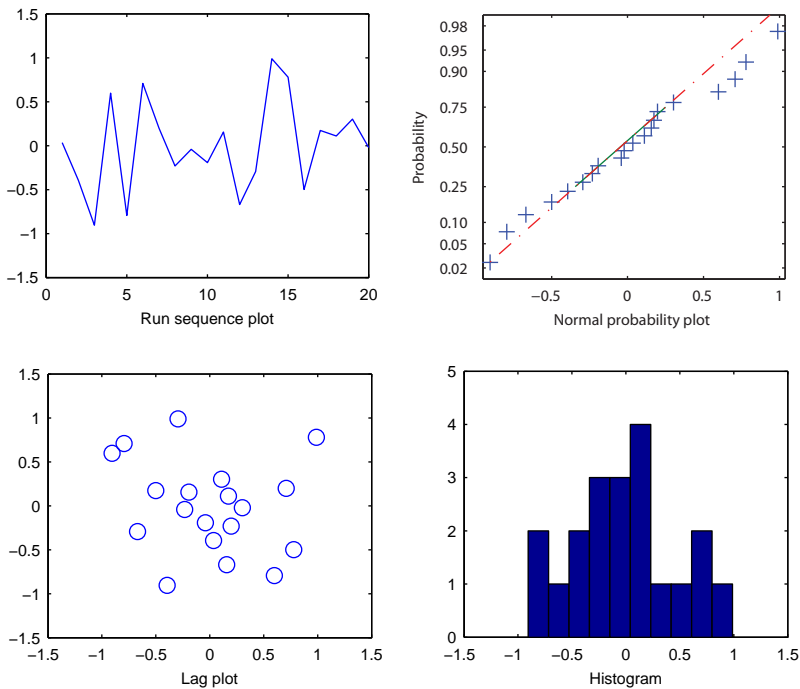


Fig. C.2: Measured radial motion errors of the spindle under different rotational speeds.

## Appendix D Checking of the tool wear data

As introduced in Chapter 5, 4-plot analysis was conducted on the measured tool wear to check the reliability of the collected data. The results are as shown in Fig. D.1.



**Fig. D.1:** Check of the reliability of the wear data by means of 4-plot.

The 4-plot revealed that the process had a fixed location (deterministic

component in the model) and fixed variation (random component, namely error). An approximately normal distribution can be seen. There is no obvious outlier in the data.

## Curriculum vitae

Peiyuan Li was born on May 4, 1975 in Jilin Province, China. After graduated from high school with excellence in 1994 he started his bachelor study in Mechanical Engineering at the Beijing Jiaotong University in Beijing, China. In 1998 he got Bachelor of Science degree with cum laude, and was awarded as Excellent Graduate Student in the Beijing Province due to the achievements both in academic study and extracurricular activities. From 1998 to 2003, he worked in the President Office at the Beijing Jiaotong University. During this period, his main responsibilities included the development of the Information Management System of the university, educational statistics, compilation of the university periodical and yearbooks, organization of university-level activities. In the year of 2000, he was awarded as Outstanding Staff of the university; in 2002, he got the second prize award from the Beijing Municipal Commission of Education for his paper about education analysis.

From 2003 to 2005, Peiyuan Li did his MSc study in Production Technology and Organization at Delft University of Technology in the Netherlands. This study was partly sponsored by the Delta Scholarship. During Sep. 2004 - Nov. 2004, he did internship at DAF Trucks Company in Eindhoven, the Netherlands on the topic of super-finishing technology. His graduation thesis was done at TNO Industrie & Techniek in Eindhoven, the Netherlands from Dec. 2004 to Aug. 2005. The topic was Influence of the Machining Parameters on the Lifetime of Endmills in the Micromilling Process.

Since Oct. 2005, Peiyuan Li started the PhD research on micromilling technology at Delft University of Technology. This project was sponsored by the Innovation Research Program (IOP) of the Dutch Government in the field of Precision Technology. This research itself was conducted in cooperation between TU Delft and TNO Industrie & Techniek in Eindhoven; the user committee included about 15 Dutch research institutes and industries. During the PhD period, Li did visiting research at Mondragon University in Spain (Nov. 2007) and Cranfield University in UK (Nov. 2008 - Jan. 2009). He was also partly involved in the European project Launch-Micro Project. Besides research work, he also gave lectures to MSc students (Evaluation of Engineering Surfaces) and

coached about 8 students' research assignments individually or together with other colleagues. In the last 4 years, Peiyuan Li published 10 international conference papers (including 2 collaborative papers) and 2 journal papers (being reviewed).